Department of Precision and Microsystems Engineering

A normally-open, wide-range, proportionally controlled 3D-printed microvalve using a piezo stack microactuator

Henrie Kramer

Report no : 2022.030
Coach : Gürhan Özkayar M.Sc.; Dr. Murali Ghatkesar
Professor : Prof. Dr. Ir. Joost Lötters
Specialisation : Micro- and Nano- Engineering
Type of report : Master's Thesis
Date : 23 July 2022

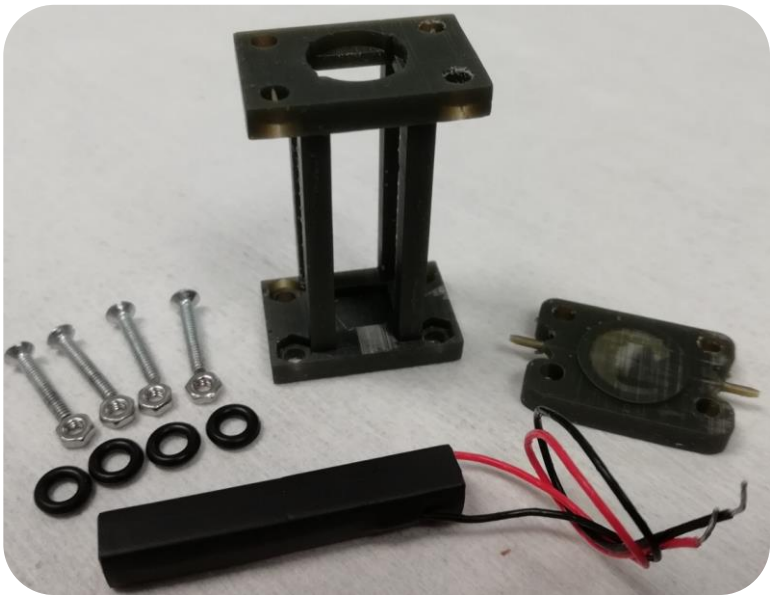

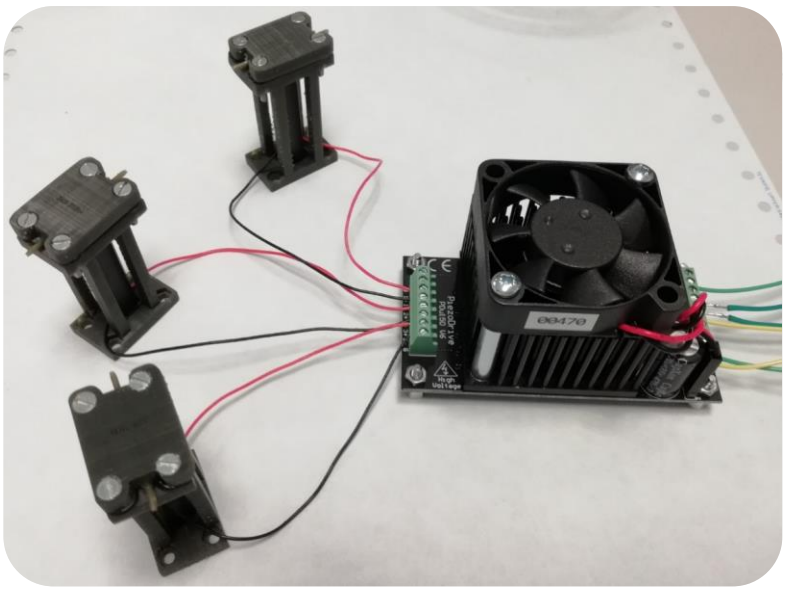

TU Delft Delft University of Technology

Challenge the future

A normally-open, wide-range, proportionally controlled 3D-printed microvalve using a piezo stack microactuator

by

Henrie Kramer

in partial fulfilment of the requirements for the degree of

Master of Science
in Mechanical Engineering

at the Delft University of Technology

Student number:	4299469	
Supervisor:	Gürhan Özkayar M.Sc.	TU Delft
Chair:	Dr. Murali Ghatkesar	TU Delft
Board:	Prof. Dr. Ir. Joost Lötters	University of Twente/TU Delft
	Dr. H. Bazyar	TU Delft

Date of submission: 21 July 2022

Contents

List of Figures

List of Tables

List of Acronyms

OOC	Organ-on-Chip
NO	Normally open
NC	Normally closed
SLA	Stereolithography
3D	Three dimensional
DLP	Digital Light Processing
IPA	Isopropyl alcohol
Di-water	Deionized water
PZT	Lead zirconate titanate
PDMS	Polydimethylsiloxane
FEM	Finite element method

1 Introduction

Organ-On-Chips (OOCs) technology is a promising application of microfluidics, where organ functions are mimicked in a multichannel or singular channel chip. The advantage of using OOC is that in vitro chips are replacing in vivo cell environments and reduces the time and cost of experiments like analyzing tissue architecture and diseases or drug studies[1]. Due to their well-tuned control of small volumes and the laminar flow in microfluidics, OOCs give a better simulation of the cell environment of organs than previous 2D cell cultures and 3D organ models[2]. An OOC consists of a main chamber for cells or tissue and an interacting micro-structural element (eg. a porous membrane for lung-on-chip) which mimics an organ functionality. The expectation on OOC technology is that when living cells or tissues are more accurately simulated and the culture media are better controlled the OOC will mimick the organ-function more accurately. Current OOCs include various organ functions such as: Lung-on-a-chip [3], OOC for cardiovascular psychology [4], Brain-on-a-chip [5], Liver-on-a-Chip [6], Kidney-on-a-chip [7], Gut-on-a-chip [8], Skin-on-a-chip [9] and Tissue-on-a-chip [10].

To control the culture media passage in the OOCs, functional components such as pumps, flow meters, valves and temperature sensors are needed. In order to achieve a control system which delivers the required flow-rate and controls the culture media a common practice is to build an experimental setup by combining off-the-self components. This way the desired simulation of the cell culture in the OOC is obtained. The main reason for using off-the-self components is the lack of standardization in making integrated microfluidic fluid handling platforms, which is a bottleneck in the goal for commercialization[11].

For controlling the culture media in OOCs a microfluidic platform can be used, which consists of pumps, flow-sensors, valves etc. These microfluidic platforms are aiming to miniaturize laboratory installations and provide better culture media dynamics[13]. An example of a microfluidic platform is developed by Zhu et al.[14] as shown in Figure 1A, were an integrated and portable microfluidic platform was build using off-the-shelf components. To further miniaturize the microfluidic platform to achieve even smaller dimensions and finer culture media control, the functional components are further miniaturized individually. One of the off-the-shelf-components to be miniaturized is the fluid selector (IDEX MHP7970-500-4) as shown in Figure 1B. The fluid selector selects one channel forward from one of the channels originating from the culture media reservoirs.

In this report, the device under exploration is the microvalve. Microvalves can be used independently or in combination, like in microfluidic multiplexers. Microvalves are known for their small volume, minimum dead volume, minimum power consumption and flow-rate control in the pico- to micro-liter range. Currently PDMS based microvalves (Quake valves) and Silicon micro-machined microvalves are the most used microvalve types in microfluidic applications. The major drawbacks of PDMS based microvalves are the required external pumps and valves, which are bulky and have a high power consumption. In addition PDMS is highly permeable so unsuitable for controlling gases. Silicon base microvalves use a rather complex fabrication process, where it is required to use manufacturing infrastructure which is not readily accessible.

The goal in this thesis report is to develop an easy to fabricate microvalve with flow characteristics suitable for OOCs applications. Next to that the microvalve will be the key component in miniaturizing and replacing the fluid selector in the presented microfluidic platform. This thesis report will first present a literature review on the state of the art microvalves and microfluidic multiplexers. A research gap is identified and target specifications are listed. Subsequently a paper is presented, where a proportionally controlled 3D-printed microvalve using a piezo stack

microactuator is designed, fabricated and tested. In this paper the replacement of the IDEX MHP7970-500-4 by a 3-to-1 fluid selector is also shown, whereby three microvalves in parallel actuated by a portable high voltage amplifier are used. In the subsequent chapters the conclusion and recommendations for future work are given. In the last chapter the author's reflection on the thesis project is given.

[a] 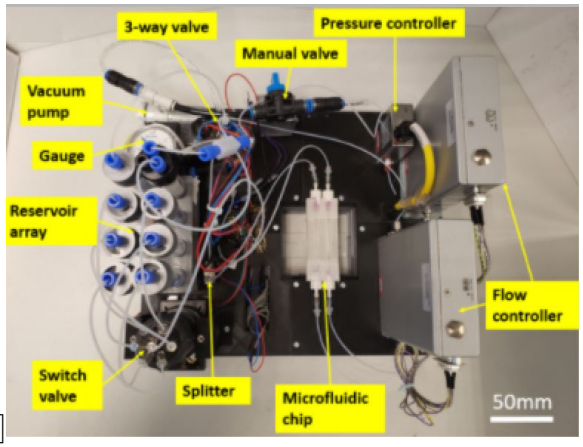

[b] 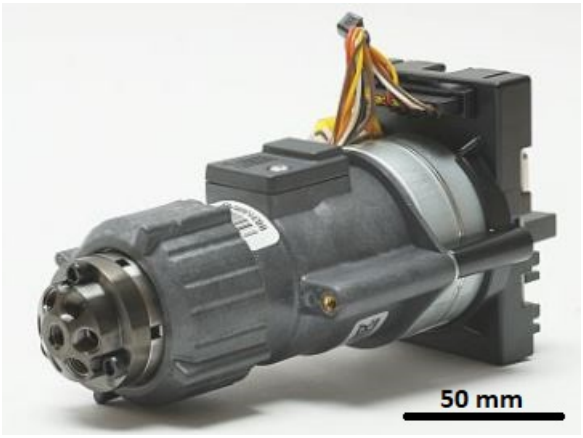

Figure 1: (a) Overview of the microfluidic platform developed by Zhu et al.[14] (b) Switch valve (IDEX MHP7970-500-4)

2 Literature review

In this chapter an exploration of existing literature regarding microvalves and microfluidic multiplexers is given. Subsequently a research gap is formulated that will be answered in a theses paper.

2.1 State of the art of Microfluidic Microvalves

In this chapter a state of the art study is conducted in microfluidic microvalves. Also the most promising actuation types are compared and their pros and cons are summarized.

2.1.1 Introduction to the Microfluidic Valve

Microfluidic microvalves manipulate the fluid flow in a micro channel in the pico- to milliliter range and are the functional elements of a microfluidic multiplexer. Microfluidic microvalves has some advantages over macrovalves like: low sample usage, high precision and small footprint [28]. A microvalve consist of the fluid inlet, a valving chamber and a fluid outlet. Most microvalves are manufactured by (soft) lithography techniques and are pneumatically actuated. The most used microvalve is the so called 'Quake valve', which is made of polydimethylsiloxane (PDMS) and uses a flexible membrane to obstruct the fluid flow when pneumatically actuated. The advantages of the 'Quake valve' are: the ease of fabrication, low costs and scalability[31].

Microvalves can have a passive operation or an active operation. In the passive operation microvalves are passively reducing the fluid flow by using surface friction, these microvalves do not require any external power source. In the active operation microvalves actively obstruct the fluid passage. These active operation valves can proportionally control or on-off control the fluid flow. Active microvalves are found with different actuation mechanisms, which can be divided in five groups based on their main actuation aspect, namely: electricity, gas, magnetism, material and biology and last surface acoustic wave (SAW), as shown in Figure 2.

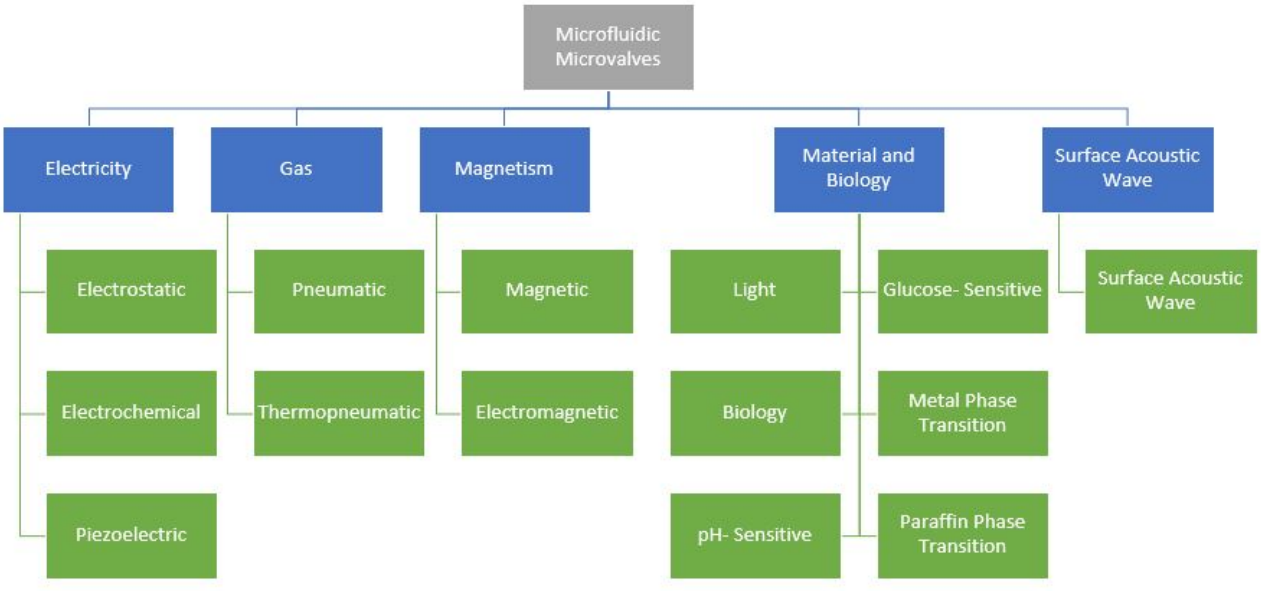

Figure 2: Active microfluidic microvalves actuation mechanisms divided in 5 groups based on their main actuation characteristic [28]

As shown in Figure 2. there are a variety of actuation mechanisms used in microvalves. For use in the multiplexer many of these actuation types are dropped beforehand due to limitations related to the project requirements, such as: long response times (Electrochemical,Light,pH-sensitive, Biology), high power consumption (Thermopneumatic,Paraffin phase transition, Metal phase transition) non controllable (Magnetic), toxicity (Electrochemical), complex structure (Glucose-sensitive) and leakage (Magnetic, SAW). The most promising actuation mechanisms, namely: electrostatic, piezoelectric, electromagnetic and pneumatic actuation will be further discussed in this chapter. At the end a comparison will be made and a selection is conducted to determine which actuation mechanism is the most promising to use in the microfluidic multiplexer.

Microvalves can further be categorized in normally-open (NO) and normally-closed (NC) initial states depending on their structures. In the NO microvalve, as shown in Figure 3a, the fluid flows freely initially without being obstructed, if the actuator is activated the membrane will deform as represented by the dashed lines, the microvalve will close and the fluid will stop flowing. NC microvalves, as shown in Figure 3b, are opposite to the NO microvalves, while the flow is initially obstructed. When the microvalve is actuated the membrane will deform, the microvalve will open and the fluid is free to flow. NC microvalves are preferred when dealing with culture media, because when the microvalve is not powered the microvalve stays closed and prevents contamination between different culture media [29].

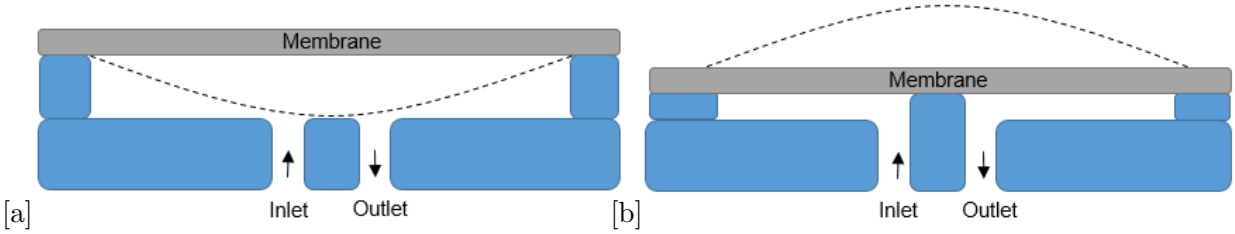

Figure 3: (a) NO microvalve configuration (b) NC microvalve configuration

The envisioned microfluidic multiplexer should be applied with both gasses and liquids. When dealing with gasses the multiplexer material shouldn't be gas permeable like PDMS. In the case of liquids it is important to prevent contact between the liquids and the actuation electrodes. Also the material shouldn't be permeable for liquids and needs to be bio-compatible for example, avoiding lead based materials that come in contact with liquids to avoid toxicity.

2.1.2 Actuation types

Electrostatic actuation Electrostatic actuated microvalves uses a force exerted by an electric field between two electrodes to deflect a membrane. This membrane can manipulate the fluid flow in a microchannel.

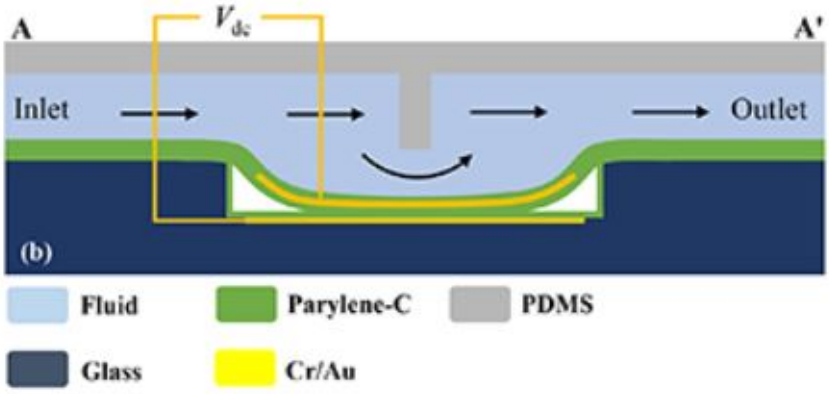

Figure 4: NC electrostatic actuated microvalve [35]

The example in Figure 4. is a NC electrostatic actuated microvalve [35]. When a voltage is applied at the electrodes (Cr/Au) the membrane is pulled downward with the result that the fluid can flow. The microvalve is build on a glass substrate and has a PDMS top layer. The 2 electrodes are covered with Parylene C which provides electrical insulation. In this example the membrane has a radius of 300 μm and a gap distance of 9.1 μm. To fully open the membrane a voltage of 221 V is needed, the response time is 370 ms. There are three forces acting on the valve membrane, as described in equation 1: the electrostatic force, as a result of the electric field which is characterized by equation 2, the stiffness force as a result of the rigidity of the membrane Fs and the force as a result of the fluid or gas flow Fa.

A force balance was performed on the membrane and can be represented by [28]:

$$Fe + Fs + Fa = 0 \tag{1}$$

The equation for the electrostatic force between two electrodes is given by [33]:

$$Fe = \frac{\varepsilon_0 \varepsilon_a A V^2}{2g^2} \tag{2}$$

Where ε_o is the vacuum permittivity, ε_a is the dielectric constant of the air between electrodes, A is the area of the electrode, V is the voltage across the electrodes and g is the total distance between the electrodes. Equation 2 shows that the electrostatic force increases exponentially as the distance between the electrodes decreases.

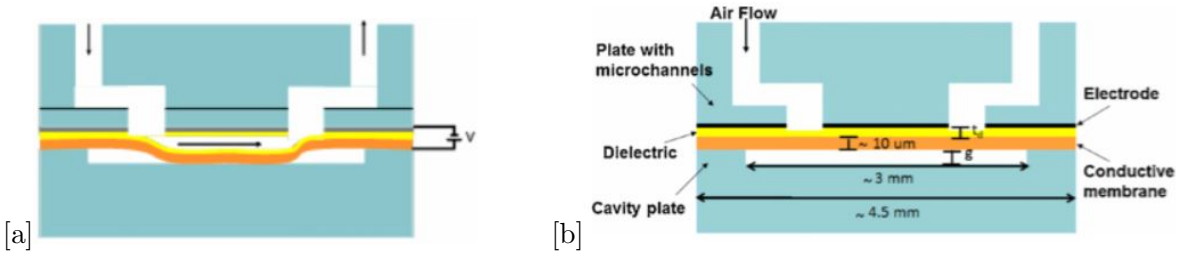

Figure 5: NO electrostatic actuated microvalve [34] (a) Open state (b) Closed state

An example of a NO electrostatic actuated microvalve, which is used for controlling gas, is shown in Figure 5 [34]. When no voltage is applied the microvalve is in the open state, when a

voltage is applied the electric field will pull the membrane upwards and closes the microvalve, as shown in Figure 5b. The microvalve is made of a poly(methylmethacrylate) (PMMA) substrate and has a copper foil which functions as a flexible membrane and as electrode. The other electrode is made of a thin chrome layer. Between the two electrodes a dielectric of Parylene C is applied to prevent shorting. A voltage of 680 V is needed to close the microvalve when a 40 kPa gas pressure is applied. The average gas flowrate is 1.05 mL/min and the microvalve needs 6s to close and 12s to open. This NO configuration brings a problem with the possibility of electrolysis of fluid flow, while the fluid flows between the electric field and non-spontaneous chemical reactions in the fluid flow can occur.

Piezoelectric actuation Piezoelectric actuated microvalves uses the inverse piezoelectric effect, whereby a deformation of the piezoelectric material takes place under the application of electric potential. Piezoelectric valves have a high power density, but a small stroke [38]. This problem is tackled by using piezostacks or piezobenders (unimorph/bimorph) configurations. Piezobenders are multilayer cantilever beams that include piezoelectric layers on one or both surfaces of the beam. Piezostacks utilize the direct in-line strain developed by piezoelectric material.

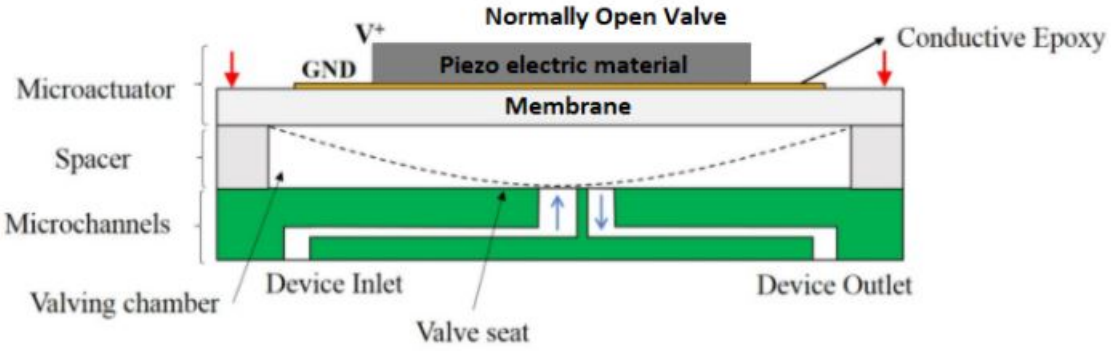

Figure 6: Unimorph NO piezoelectric microvalve [39]

An example of an unimorph NO piezoelectric microvalve by Gunda et al. is given in Figure 6.[39]. In this example the membrane is made of stainless steel on which PZT (piezoelectric material) was bonded by a conductive epoxy. By applying a voltage at the top of the PZT, the membrane will deform downwards into the valving chamber and closes off the inlet. The membrane radius is 5 mm and the PZT radius is 4 mm. By applying 150 V the membrane will fully close the valve, the membrane deflection in its center is 8.5 μm. The flow rate is in the range of 0-90 μL/min, with a leakage rate when fully closed of 0.8% open flow rate. The microvalve has a static power consumption of 37.5 μW.

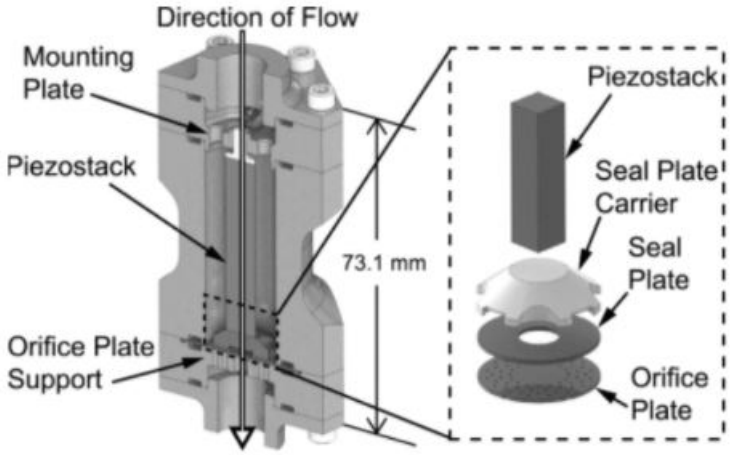

Figure 7: NO piezostack microvalve [41]

Hagstrom et al.[41] developed a NO piezostack actuated microvalve as shown in Figure 7. In this microvalve a single orifice is replaced by an array of orifices. The orifice plate is made of silicon and the orifice plate support is made of stainless steel. The piezostack has a stroke of 30.4 μm and it closes the orifice plate with a seal plate when a voltage of 75 V is applied. The dimensions are quite large for microvalves, namely: 73.1 x 44.0 x 38.1 mm. The piezostack can widthstand pressures up to 625 kPa, which shows the large forces a piezostack can produce. The microvalve has a static power consumption of 41.2 μW and a response time of 295 μs.

Electromagnetic actuation Microvalves which are electromagnetic actuated uses an electromagnetic field generated by a coil. This magnetic field can actuate a membrane in which a permanent magnet or ferrofluid is encapsulated.

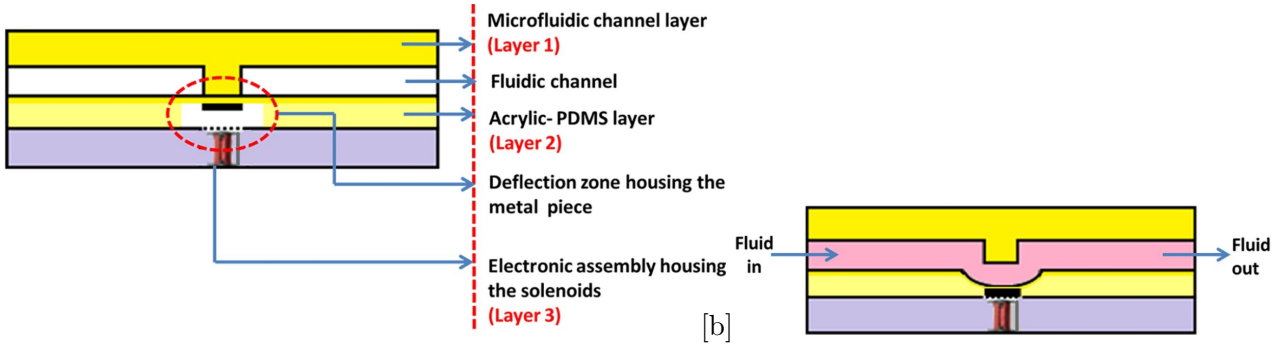

Figure 8: NC electromagnetic microvalve using a metal piece [43] (a) Closed state (b) Open state

A NC electromagnetic microvalve was developed by Pradeep et al.[43], whereby a metal piece is attracted by a solenoid, as shown in Figure 8. The valve consist of a PDMS microfluidic channel layer and an acrylic deflection zone. In the deflection zone the metal piece which is bonded to the PDMS membrane can deform downwards to open the valve, as shown in Figure 8b. Deflections of up to 1200 μm can be achieved with a 5V control and a response time of 3 ms. The valve dimensions are $4{\times}3 \times 21mm$.

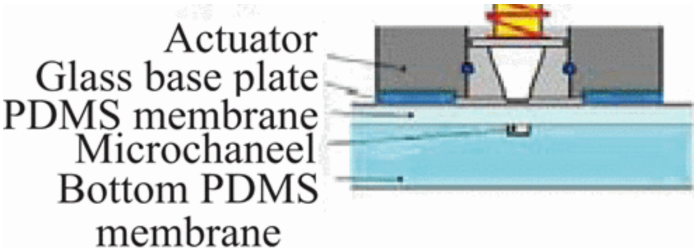

Figure 10: NC electromagnetic microvalve developed by Liu et al. [44]

An example of a NC electromagnetic microvalve without using a permanent magnet or ferrofluid is developed by Liu et al.[44], as visualized in Figure 10. The microvalve is made of PDMS, whereby a PDMS membrane can close the microchannel by deflection. In the closed state the microvalve is initially squeezed due to the stiffness of the deflected membrane. If the electromagnetic coil is actuated the coil will move up, due to the bonding of the coil and the PDMS membrane the membrane will move in the same direction. If the membrane moves up, the microchannel opens. The actuation voltage is 24 V with 1 W power consumption. The response time is 17 ms and the dimensions are $30 \times 17.5 \times 9.8mm$

Pneumatic actuation The most used microvalve actuation type is the pneumatic actuated microvalve. These pneumatic microvalves use pressurized air or vacuum to deform a membrane. As a result of the membrane deformation a flow passage can be closed or opened. In general the membrane is made of a PDMS layer. PDMS is bio compatible, but has the disadvantage of being gas-permeable. Pneumatic actuated microvalves use external equipments, a vacuum pump or a pressure pump in combination with a solenoid valve.

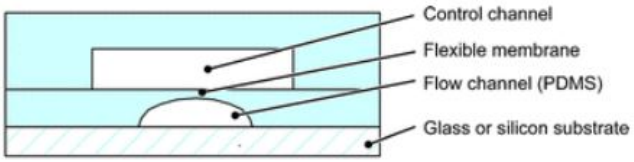

Figure 11: NO pneumatic microvalve [18]

A schematic of a NO pneumatic microvalve is shown in Figure 11. The microvalve made of PDMS is build on a glass or silicon substrate. On top of the flow channel the control channel is located. When a pressure is applied in the control channel the flexible membrane will deform and will shut off the flow channel. The pressure needed to close the channel is dependent on the thickness of the membrane, the membrane area and on the stiffness properties of the membrane material. In the NO microvalve made by Jiang et al.[47] the flow channels are 200 μm deep and have a width of 500 μm. The control channels have different widths of 500, 750 and 1000 μm in combination with a height of 200 μm. Closing pressures of 55, 34,5, 27,6 kPa are needed when control channel widths of 500, 750 and 1000 μm are used respectively. A flow rate of 60 μL/min can be achieved.

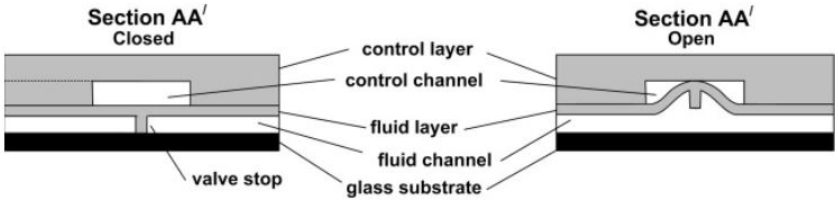

Figure 12: NC pneumatic microvalve [48]

Mohan et al. developed a NC pneumatic microvalve [48], as shown in Figure 12. In the closed position the fluid flow is blocked by the stiffness of the membrane and the adhesion between the valve stop and the glass substrate. When a vacuum is applied in the control channel the membrane deflects and the flow channel passage is opened. The vacuum pressure needed is dependent on the adhesion force between valve stop and glass substrate, the stiffness of the membrane and the area of the membrane. The vacuum pressure needed to open a NC microvalve is 13,8-20,7 kPa when the membrane thickness is 15-60 μm. The dimensions of the control channels are: height of 25-50 μm and a width of 50 μm. The flow channels have the dimension of: height of 25-50 μm and a width of 50-400 μm. Due to the NC configuration the microvalve is prone to leakage. In the closed position the fluid flow is blocked by stiffness and adhesion forces, because no actuation is available to further close off the channel leakage will occur.

Pneumatic actuated microvalves can be controlled by either a pressure in the NO configuration or vacuum pump in the NC configuration in combination with a solenoid valve. In Table 1. some commercial micro pumps and solenoid valves are presented with their characteristics.

Table 1: Commercial micro pumps and solenoid valves for use in pneumatic actuated microvalves

Pressure pump	**Power**	**Max Pressure**	**Dimensions**
Rs Pro D200	0.48 W	100 kPa	42 x 27 x 17 mm
Alldoo CMP-11G	0.9 W	50 kPa	17 x 26.5 x 35 mm
CH370-6A	2.28 W	66,6 kPa	27 x 26.9 x 60.4 mm
Smart Products AP-2P02A	0.96 W	46,6 kPa	33.04 x 10.01 x 16.51 mm
Vacuum pump			
AYNEFY JH 12-65	6 W	-65 kPa	80 x 70.1 x 80 mm
NW 9506	2,4 W	-60 kPa	64.5 x 24.4 x 24.4 mm
CHIHAI MOTOR CHP-030PUMP	0.9 W	-46,6 kPa	43.4 x 21 x 12 mm
3 way Solenoid valves			
DS-0520ST	1.2 W	46,6 kPa	37.1 x 15 x 13 mm
Fa0520F	1,68 W	46,6 kPa	38 x 13 x 15 mm
3V310-10-NO	3.0 W	0.8 MPa	109 x 66.7 x 22 mm

All devices in Table 1. use a voltage supply below 24 V dc. The switching time of the solenoid valves is around 30 ms.[50]. The deflation time, the time needed to degas the solenoid valve, is around 3-4 s.

2.1.3 Microfluidic valve comparison

In Table 2 some examples of the discussed actuation mechanisms are presented to give an indication of the characteristics of the actuation types. The pneumatic actuator examples are also presented in Table 2, despite of the lack of information in the literature on the power consumption and voltage supply. The main reason for this is that every researcher who designs pneumatic microvalves uses different pressure/vacuum pumps and solenoid valves, whereby the characteristics of these external equipment is not mentioned.

Table 2: Examples of different actuation mechanisms with their characteristics

Actuator type	Power	Voltage	Response time	Initial state	Pressure resistance	Flow rate	Leakage rate	Dimension
Electrostatic [35]		221 V	370 ms	NC	10 kPa			300 μm radius
[37]		60 V	0.3 s	NC	40 kPa	9.4 μL/min	9%	410 μm radius
[34]		640 V		NO	40 kPa	1.05 mL/min		
[36]	100 mW	217 V	0.2 s	NC	3 kPa			200 μm radius
Piezo electric [39]	37.5 μW	150 V	40 ms	NO	100 kPa	90 μL/min	0.8%	5 x 5 x 1.8 mm
[40]	48 mW	200 V	0.6 ms	NC	600 kPa	3100 mL/min		41.5 x 25 x 5 mm
[41]	41.2 μW	75 V	295 μs	NO	625 kPa			73.1 x 44.0 x 38.1 mm
[42]	2.5 mW	40 V	30 μs	NC	137 kPa	60.1 mL/min	0.002%	
Electro magnetic[44]	1 W	24 V	17 ms	NC	200 kPa	400 mL/min	0.06 %	30 $\times$ 17.5 $\times$ 9.8 mm
[45]				Bi-stable	50 kPa	0.684 mL/min	7%	7 $\times$ 7 $\times$ 21 mm
[46]	1.6 W	3.5 V	10 ms	Bi-stable	7.8 kPa	50 μL/min	1.6%	0.8 $\times$ 0.8 $\times$ 0.6 mm
[43]		5 V	3 ms	NC				4 $\times$ 3 $\times$ 21 mm
Pneumatic [47]				NO	55 kPa	60 μL/min		500 $\times$ 200 μm
[48]				NC	20,7 kPa			50 $\times$ 400 μm
[49]			1.67 ms	NO	80 kPa			50 $\times$ 100 μm

Using Table 2 a comparison between the actuation types is made in Table 3 on power consumption, actuation voltage, response time, pressure resistance and dimensions. Most values are given in a range to give a indication of the scale. The pneumatic actuated microvalves has a power consumption which is determined by using micro pump and solenoid valve properties

from Table 1.

Table 3: Comparison of the electrostatic, piezoelectric, electromagnetic and pneumatic microvalves on different parameters.

	Power	Voltage	Response Time	Pressure Resistance	Dimensions
Electrostatic	~ 100 mW	60-640 V	0.2-0.37 ms	3-40 kPa	200-410 µm radius
Piezoelectric	37.5 µW – 48 mW	40 – 200 V	30 µs – 40 ms	100- 625 kPa	39,9 × 25,7 × 15,0 mm
Electromagnetic	1-1.6 W	3.5 – 24 V	3 – 17 ms	7.8 – 200 kPa	10,5 × 7,1 × 13,1 mm
Pneumatic	0.48-6 W	3-24 V	~1.67 ms, 3-4 s deflation time)	20.7 – 80 kPa	350 × 233,3 µm

Good		Bad		Ok	

The advantages of electrostatic actuation are: low power consumption, low response time and small dimensions. The disadvantages are: high actuation voltages and low pressure resistances. Electrostatic actuation is mainly found in the NC initial state. This has the disadvantage that it is prone to leakage. In the NO initial state electrolysis of the fluid flow occurs, as discussed in Chapter 2.1.2.

Piezoelectric actuation has the advantages of: low power consumption, low response times, high pressure resistances. The disadvantages are: high actuation voltages and higher dimensions. To provide the high actuation voltages a piezodriver is needed, which increases the footprint and power consumption of the microvalve.

Electromagnetic actuation has the advantages of: low actuation voltages, low response times and good enough pressure resistances. The disadvantages are: high power consumption and larger dimension. The high power consumption and larger dimensions are the result of the coil which uses high power to create a magnetic field and takes up a lot of space.

Pneumatic actuated microvalves has the advantage of: low actuation voltages, small dimensions and good enough pressure resistances. The disadvantages are: high power consumption and high deflation times. The overall footprint of the pneumatic microvalves is also large, while the footprint of the micropump and solenoid valves needs to be accounted for which increases the overall size.

Using Table 3. the advantages and disadvantages of the 4 actuation types are summed up in Table 4.

Table 4: Advantages and disadvantages of the electrostatic, piezoelectric, electromagnetic and pneumatic actuation types

Actuation type	Advantages	Disadvantages
Electrostatic	+ Low power consumption	- High actuation voltages
	+ Low response time	- Low pressure resistance
	+ Small dimensions	
Piezoelectric	+ Low power consumption	- High actuation voltages
	+ Low response time	- Larger dimensions
	+ High pressure resistances	
Electromagnetic	+ Low actuation voltages	- High power consumption
	+ Low response time	- Larger dimensions
	+ Good pressure resistances	
Pneumatic	+ Low actuation voltages	- High power consumption
	+ Small dimensions	- High deflation times
	+ Good pressure resistance	

The overall most promising actuation type is the piezoelectric actuated microvalve, while it doesn't have insurmountable disadvantages. In the case of electrostatic actuated microvalves the pressure resistance is to low for use in the OOC microfluidic platform. This can have the consequence that there is to much leakage. Electromagnetic actuated microvalves are large and have a high power consumption as a result of the coils. The coils are a limiting factor in making smaller and more energy efficient microvalves. Pneumatic microvalves have bulky peripheral equipment with the consequence that the options in reducing the footprint and power consumption are limited. Also the deflation times are to high for use in the OOC microfluidic platform. The piezoelectric microvalves needs high actuation voltages, but this problem can be overcome by using a small, low power consuming piezo driver. Also the larger dimensions of the piezoelectric microvalves can be minimized by using better piezoelectric materials with higher piezoelectric coefficients and by optimizing the microvalve design.

2.2 State of the art of Microfluidic Multiplexers

Microfluidic multiplexers are devices with a high density of valves in combinatorial arrays which are controlled by control lines. By activating a combination of control lines the valves can close flow channels and forwards the selected flow channel to a single output. The microfluidic multiplexer is analogous to the electronic multiplexer, whereby a densely packed chip of transistors can binary control 2^n signal lines, whereby n is the amount of control lines. The valve is the building block of fluid controlling and is analogous to the transistor in electronics. By using a minimal number of inputs, which are binary controlled, the time needed for a process reduces while less time is needed to activate the control lines[17][18]. The goal in designing and fabricating microfluidic multiplexers is to get a large scale integrated device which is controlled by a minimum number of control lines. Examples of multiplexer applications include[19]: micro reactor technology [20], sanger sequencing of DNA [21], genetic analysis [22] and high-throughput sorting devices for drug delivery [23]. In this chapter a research will be done into the state of the art microfluidic multiplexers and a research gap is explored.

2.2.1 Complementary Binary Multiplexer

An example of a microfluidic multiplexer is the complementary Binary multiplexer as shown in Figure 13. [17][18]

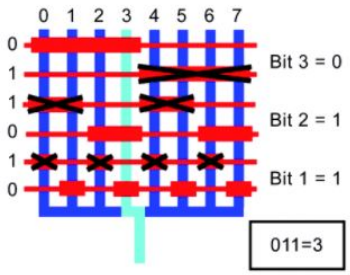

Figure 13: Schematic image of the Complementary Binary Multiplexer, where the blue lines represent the flow channels and the red lines the control lines. At the intersection of the control lines and the flow lines the bigger rectangular red blocks represents the locations of the microvalves. In this example flow channel 3 is selected forward. [17][18]

The blue lines are the flow channels which are connected to the fluid reservoirs at the inlet and can be selected forward to the outlet by the red lines which represent the control lines. The control lines can be actuated by applying a pressure. Due to the pressure build up, the valves which are located at the crossing of the control lines and flow lines will close off the fluid flows. The pressure build up deforms a membrane which in turn closes of the flow channel. The amount of pressure needed to close of a flow channel depends on the membrane stiffness and the distance between the membrane and the flow inlets. The control lines with the combination of valves is organized in complementary valve pairs to create a binary control. The combination of activated control lines determines which flow channels are selected forward, in the complementary binary multiplexer N flow channels can be controlled with 2 $\log_2$(N) control channels. In Figure 13 flow channel 3 is selected by activating the complementary control bit pairs 011. The complementary bit pairs are defined by 0 and 1, the bottom control line of each pair is defined by 0 and the top control lines as 1. If a bit is 1, the top control line of each pair is activated. If a bit is 0, the bottom line of each pair is activated.

2.2.2 High Radix Microfluidic Multiplexer

Another microfluidic multiplexer is the high radix microfluidic multiplexer, which uses different pressure levels to actuate the valve membrane [24]. In the earlier mentioned complementary binary multiplexer the valves all have the same threshold pressure level. In the high radix microfluidic multiplexer there are two and even three different threshold pressure levels, which are called the ternary and quaternary multiplexer respectively. In the ternary multiplexer N flow channels can be controlled with $2\log_3(N)$ control channels. In the quaternary multiplexer N flow channels can be controlled with $2\log_4(N)$ control channels. As can be seen in the above equations, the amount of control lines needed to control a number of flow channels reduces when more threshold pressure levels are used.

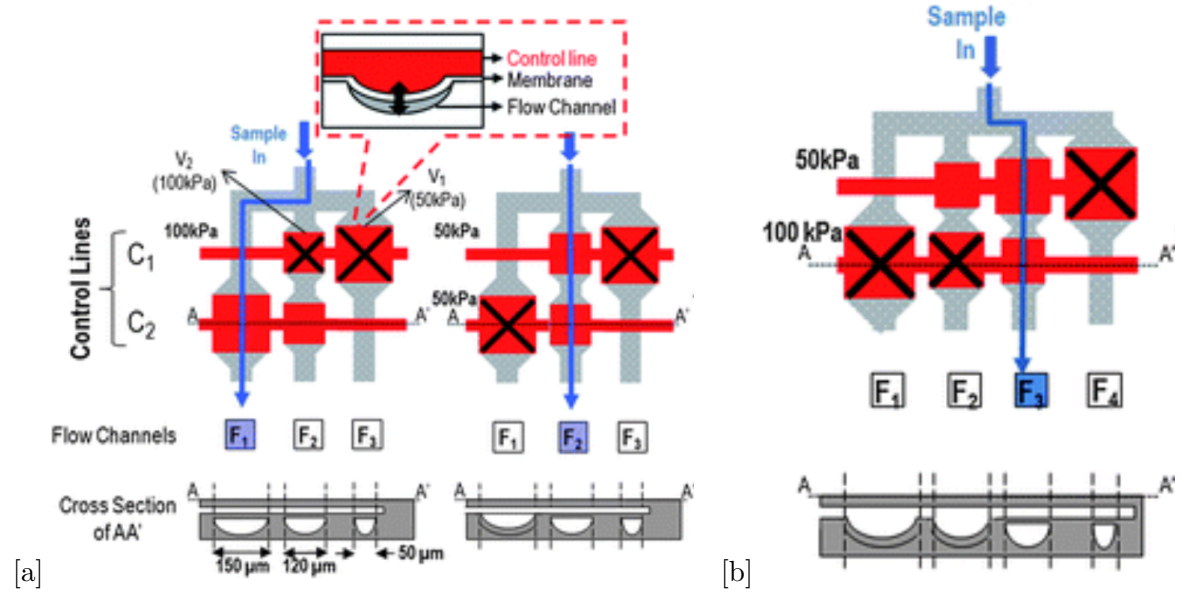

Figure 14: Schematic image of the high radix multiplexers, where the gray lines represent the flow channels and the red lines the control lines. The microvalves are represented as bigger rectangular red block, which when actuated are crossed, the associated actuation pressures are given at the left side of the control lines[24] (a) Ternary multiplexer (b) Quaternary multiplexer.

As shown in Figure 14a, the ternary multiplexer has 3 flow channels (F1,F2,F3), which are controlled by 2 control lines (C1, C2) with on each control line 2 different pressure threshold valves. The pressure levels are related with the dimensions as can be seen in equation 4, where P is the pressure, h is the maximum deflection of the membrane, t is the thickness of the membrane, a is the half width of the square membrane, E is the Youngs modulus of the membrane and C is a constant.

$$P = C\frac{tE}{a^4}h^3 \tag{3}$$

If a larger size of the membrane dimension is chosen the pressure will be less, while the pressure is inversely proportional with a^4. In this ternary multiplexer example the valve with the larger dimensions has a pressure threshold level of 50 kPa and the valve with the smaller dimensions has a pressure threshold level of 100 kPa. If flow channel F1 has to be selected forward to the output, flow channels F2 and F3 needs to be closed. This is done by activating control line C1 with a pressure of 100 kPa causing the valves with a pressure threshold of 100 kPa and 50 kPa to be closed, so closing flow channels F2 and F3. Control line C2 is not activated whith

a pressure, so no flow channel is closed by control line C2. Combining control lines C1 and C2 leaves only flow channel F1 open. In the second example of the ternary multiplexer flow channel F2 has to be selected forward to the output. Flow channels F1 and F3 needs to be closed. This is done by activating control line C1 with a pressure of 50 kPa causing the valve with a pressure threshold of 100 kPa to be closed, so closing flow channel F3. Control line C2 is also activated with a pressure of 50 kPa, causing the valve with a pressure threshold of 100 kPa to be closed, so closing flow channel F1. Combining control lines C1 and C2 leaves only flow channel F2 open.

As shown in Figure 14b, the quaternary multiplexer has 4 flow channels (F1,F2,F3,F4), which are controlled by 2 control lines (C1, C2) with on each control line 3 different pressure threshold valves. In this quaternary multiplexer example the valve with the largest dimensions has a pressure threshold level of 50 kPa, the valve with the medium size dimensions has a pressure threshold level of 100 kPa and the smallest valve has a pressure threshold level of 150 kPa. If flow channel F3 has to be selected forward to the output, flow channels F1, F2 and F3 needs to be closed. This is done by activating control line C1 with a pressure of 50 kPa, causing the valve with a pressure threshold of 50 kPa to be closed, so closing flow channel F4. Control line C2 is activated whith a pressure of 100 kPa, causing the valves with 100 kPa and 50 kPa to be closed, so flow channels F1 and F2 are closed by control line C2. Combining control lines C1 and C2 leaves only flow channel F3 open.

2.2.3 Multiplexed control system

Another way of multiplexing is done by not controlling the fluid lines, but instead controlling the control lines [25]. As shown in Figure 15 there are three kinds of lines used in this system. First of all the drive line (purple line color), which can close the on-chip valve with over pressure. Second the gate line (blue line color) which can close off the drive line and last the selective lines (green line color) which in turn control the gate lines with complementary binary selecting.

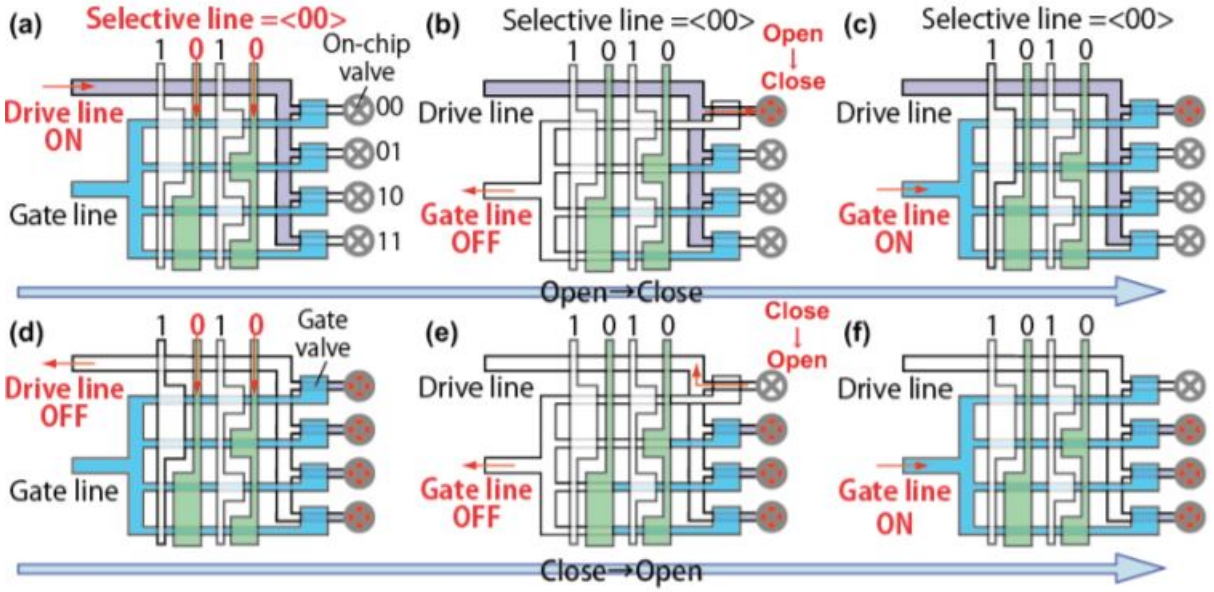

Figure 15: Schematic image of the working principle of the multiplexed control system. The working procedure from opening to closing a On-chip valve is presented in A-C, the working procedure from closing to opening is represented in D-F [25].

The working procedure for opening to closing a On-chip valve is as follow, A-C in the figure: The gate line is on and closes off the driver line, so the On-chip valves are open. Then the driver line and selective lines are pressurized. The selective line selects On-chip valve 0 (a). The gate line is turned off and the pressure in the On-chip valves 1,2 and 3 is latched by the selective lines (b). The gate line is turned on and latches the pressure in the On-chip valve 0 and the other On-chip valves which are still open (c). The working procedure from closing to opening On-chip valves is as follow, D-F in the figure: The gate line is on and closes off the pressure in the closed On-chip valves. Then the driver line is turned off and the selective lines are pressurized. The selective line selects On-chip valve 0 to be opened (d). The gate line is turned off and the pressure in the On-chip valves 1,2 and 3 is latched by the selective lines, so they stay closed. The pressure in On-chip valve 0 can escape, so the valve will be opened (e). The gate line is turned on again and latches the pressure in the On-chip valves (f). As can be seen the working mechanism is complex, while 3 steps are needed to actuate a On-chip valve. The number of on-chip valves can be controlled by $2\log_2(N)$ selective lines. The total number of control lines is $2\log_2(N)+2$, two extra because of the gate and drive lines.

2.2.4 Non-Pneumatic Microfluidic Multiplexers

The microfluidic multiplexers mentioned above are actuated with pneumatic valves and controlled by external solenoid valves. One example of a microfluidic multiplexer which doesn't use pneumatic actuation are pH-responsive hydrogel microspheres controlled by acid flows [26]. In Figure 16a a schematic of this mulitplexer is shown, whereby 4 flow channels are controlled by 3 buffer inlets.

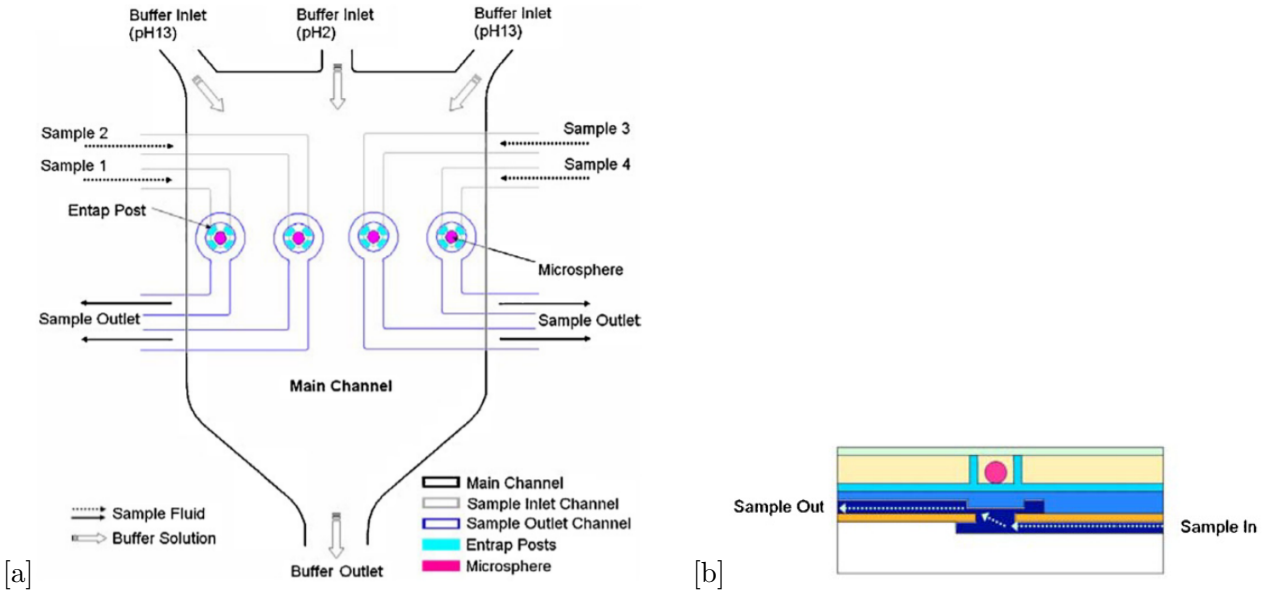

Figure 16: Schematic image of the pH-responsive multiplexer. (a) Gives an overview of the buffer inlets/outlets and the microvalves locations (b) Gives a cross section overview of the microsphere which is pH responsive and can deflect a membrane as a result of the pH responsive swelling [26].

In the flow channels sample fluid 1 to 4 can be controlled by the pH-sensitive hydrogels microspheres, which shrinks when a acid solution is applied and swells when a basic solution is

applied at the buffer inlets. As shown in the cross section of the multiplexer in Figure 16b when the pH-responsive hydrogel microspheres swells the membrane is preventing the sample to flow. So when a acid solution is applied the valve is opening and when a basic solution is applied the valve is closing. By controlling the pressure of the Buffer inlet solutions the widths of the sample flow can be changed. By changing the widths of the sample flow the valves that needs to be controlled can be selected. In theory an unlimited number of valves can be used in this system. The system has the disadvantages of having a very slow response time of 50 seconds and has buffer inlet waste.

Another example of a microfluidic multiplexer which isn't pneumatically actuated is the shape memory alloy (SMA) actuated multiplexer [27]. The benefit for using SMA actuation is that only an electric connection between the controller and the multiplexer is needed. As shown in Figure 17 SMA actuated control wires A,B,C and D are connected to the flow channels (1-6) by plungers which are represented as black blocks. When a current is applied at the SMA wires, resistive heating raises the temperature of the wire to transition temperature, shortening the shape memory wire's length, and squeezes the flow channels. When a combination of blocks are connected to the SMA wire complementary binary multiplexer can be achieved, so N flow channels can be controlled by $2\log_2(N)$ SMA control lines.A disadvantage is the high power consumption of 0.5 W for each SMA wire.

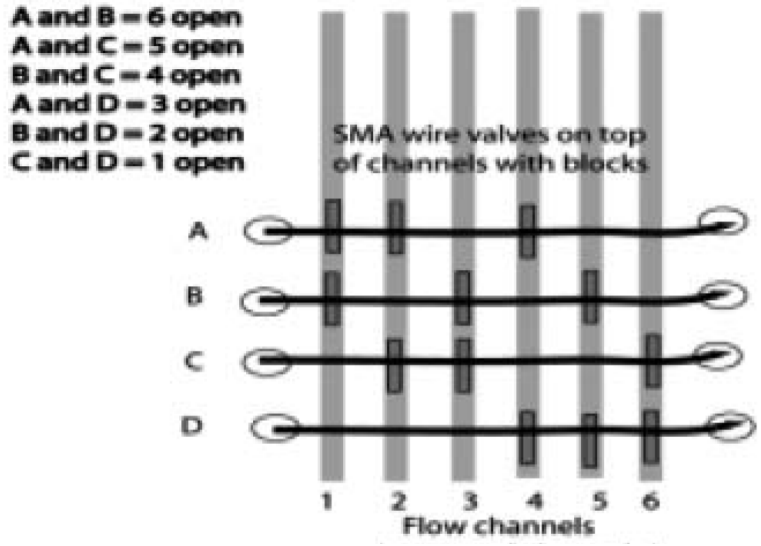

Figure 17: Schematic image of the Shape memory alloy multiplexer. The black lines represent the control lines A-D. the gray lines represent the flow channels. The black blocks on top of the flow channels are the plungers when actuated by the control lines can squeeze/close the flow channels [27].

2.3 Research Approach

In this chapter a research gap is explored based on the state of the art review of microfluidic multiplexers. Next to that a solution is presented to tackle the research gap. To check the viability of the proposed design a simulations study is performed. Finally a fabrication study is done to make clear which manufacturing steps are needed and which materials are going to be used.

2.3.1 Research Gap

An overview of the required number of control lines to control a certain amount of flow channels for every multiplexer type can be found in Table 5. If no multiplexers system were used and every flow channel is controlled by a single valve, 8 control lines are needed to control 8 flow channels and 1024 control lines are needed to control 1024 flow channels. When for example a complementary binary multiplexer is used, 6 control lines are needed to control 8 flow channels and only 20 control lines are needed when 1024 flow channels needs to be controlled. When multiplexed valve systems are used, the benefit becomes evident when looking at the number of control lines needed compared to the amount of flow channels that can be controlled. Multiplexers reduces the number of control lines needed extensively, especially if an order of hundreds or more flow channels needs to be controlled. Most of the current OOCs focus on preclinincal drug screening. In order to test the drugs an order of hunderd test samples can be applied to the OOCs, which is an opportunity for the microfluidic multiplexer [1].

Table 5: Number of control lines needed to control 8 or 1024 flow channels for every Microfluidic Multiplexer type

Multiplexer type	**8 Flow channels**	**1024 Flow channels**
Complementary Binary	6	20
Ternary	4	13
Quaternary	3	10
Multiplexed control system	8	22
Binary (proposed design)	3	10

The three main microfluidic multiplexing techniques are: complementary binary controlling, high radix multiplexing and multiplexing of the control system. Complementary binary multiplexing and the multiplexed control system uses one threshold pressure to close the valves. High radix multiplexing uses multiple pressure threshold valves, this technique reduces the need for control lines further compared to the complementary binary method and the multiplexed control system method. The big disadvantage of this technique is that regulatory equipment is needed to supply the valves with the correct threshold pressure [32]. Because of this and due to the complexity of the multiplexed control system, complementary binary multiplexing is the most used microfluidic multiplexing technique. When a closer look at the complementary binary multiplexer is taken in Figure 13, there is unused space on the control lines, meaning no valves are placed at every cross section of the flow channels and control channels. If the space on a control line can be fully optimized a large scale integrated device is created, which is controlled by a minimum number of control lines. The research gap lies in the need for a binary controlled multiplexer which uses all actuation space on the control lines, which leads to: less control lines, smaller dimension of the multiplexer, decrease of the processing time and a reduction of external equipment.

A proposed solution is to use a combination of NO- and NC valves as shown in Figure 18.

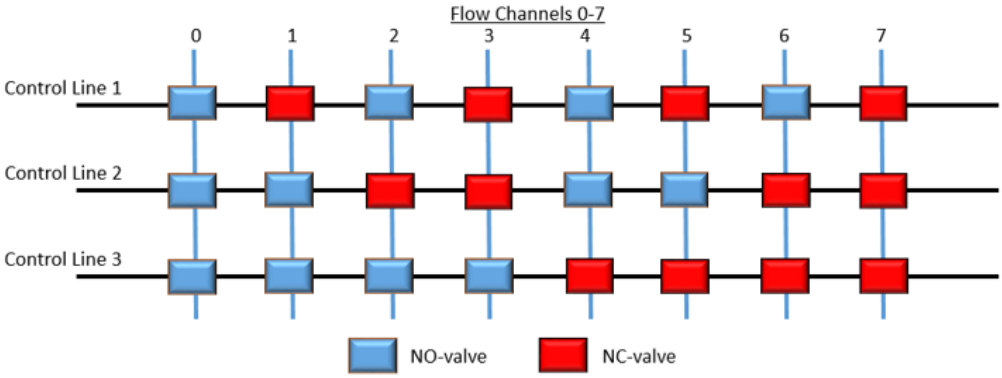

Figure 18: Schematic overview of the binary controlled multiplexer which uses a combination of NO- and NC microvalves. The blue lines represent the flow channels, the black lines represent the control lines.

At every cross section of a control line and a flow channel there is either a NO- or a NC valve. The combination of activated control lines determines which flow channels are selected forward, in this binary multiplexer N flow channels can be controlled with $\log_2(N)$ control channels. If for example flow channel 3 is selected, control lines 1 and 2 are activated causing the NC-valves to open. Control line 3 is not activated so the NO-valve stays open. The number of control lines needed in the binary multiplexer design compared to other multiplexer designs is also presented in Table 5. As shown in the table the binary and the quaternary multiplexer need the least number of control lines to control either 8 or 1024 flow channels. The binary multiplexer has the advantage over the quaternary multiplexer, while it only has 2 kinds of valves compared to 4 in the quaternary case making design and fabrication easier. Also regulatory equipment is needed to supply the valves with the correct threshold pressure[32].

2.3.2 Proposed design

As discussed in Chapter 2.1.3. the piezoelectric valve is the most promising microvalve. In order to use piezoelectric microvalves in the microfluidic multiplexer as depicted in the binary controlled multiplexer in Figure 18 NO- and NC configurations are needed. A simple design of a NO piezoelectric microvalve was developed by Gunda et al.[39]. This microvalve uses a unimorph design and has the advantages of having low power consumption, low response time, high enough pressure resistance, high flow rates, low leakage rates and small dimensions. Compared to other piezoelectric microvalves it stands out in having smaller dimensions and lower power consumption. The NC configuration can be made by changing the NO configuration whereby the poles are turned around and the spacer between the membrane and the microchannels is eliminated. In Figure 19a,b the NO- and NC configurations are presented respectively.

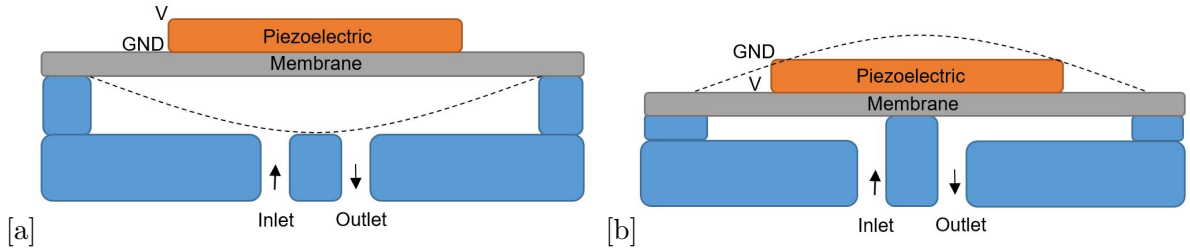

Figure 19: (a) NO piezoelectric actuated microvalve configuration (b) NC piezoelectric actuated microvalve configuration

The proposed design mentioned in Figure 18 of the piezoelectric microfluidic binary multiplexer with 8 inlets is depicted in Figure 20 where it is integrated into the microfluidic platform.

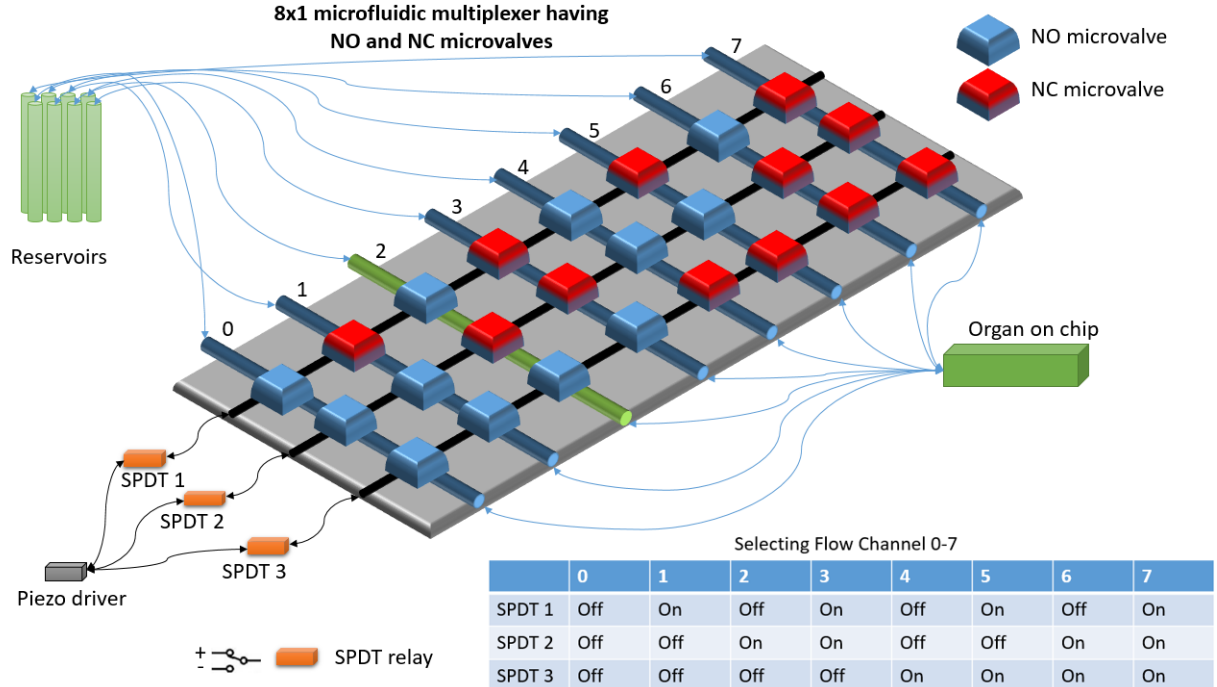

Selecting Flow Channel 0-7

	0	1	2	3	4	5	6	7
SPDT 1	Off	On	Off	On	Off	On	Off	On
SPDT 2	Off	Off	On	On	Off	Off	On	On
SPDT 3	Off	Off	Off	Off	On	On	On	On

Figure 20: Integration of the piezoelectric binary multiplexer in the OOCs platform

The culture media are stored in reservoirs and can be aspirated by a vacuum pump. Each reservoir is connected to a multiplexer channel. The required culture media can be selected by the control lines which are controlled by 3 SPDT relays. The SPDT relays are driven by an external Arduino board. SPDT relays stands for single pole double throw relay, which means there are one input and two outputs. In the integration of the binary multiplexer the SPDT relays is used in the reverse direction as shown in Figure 20. This means that there are two inputs, a negative and a positive delivered by the piezo driver, and one output. The positive inputs are used for opening the NC microvalves and for closing the NO microvalves. The negative inputs where used primarily for getting a closing force in the NC microvalve to achieve a leak tight valve. Using negative voltages is related to the disadvantage of using NC microvalves, while these microvalves are prone to leakage. This is a consequence of the fact that

only the stiffness of the membrane is withstanding the fluid to flow [30]. There is a trade off between the stiffness required to close the valve and flexibility to open the valve. The SPDT relays combination required to select a desired flow channel is shown in Figure 20.

When three SPDT relays are used, there is also the possibility to use it with one input and two outputs. This gives the opportunity to use a complementary binary piezoelectric actuated couple, as shown in Figure 21, whereby all actuation space is used and where only NO valves are needed. This leads to smaller dimensions and easier modeling and fabrication, because only one valve design is needed. Another advantage is that all the problems related to leakage and adhesion in the NC- microvalve design vanishes.

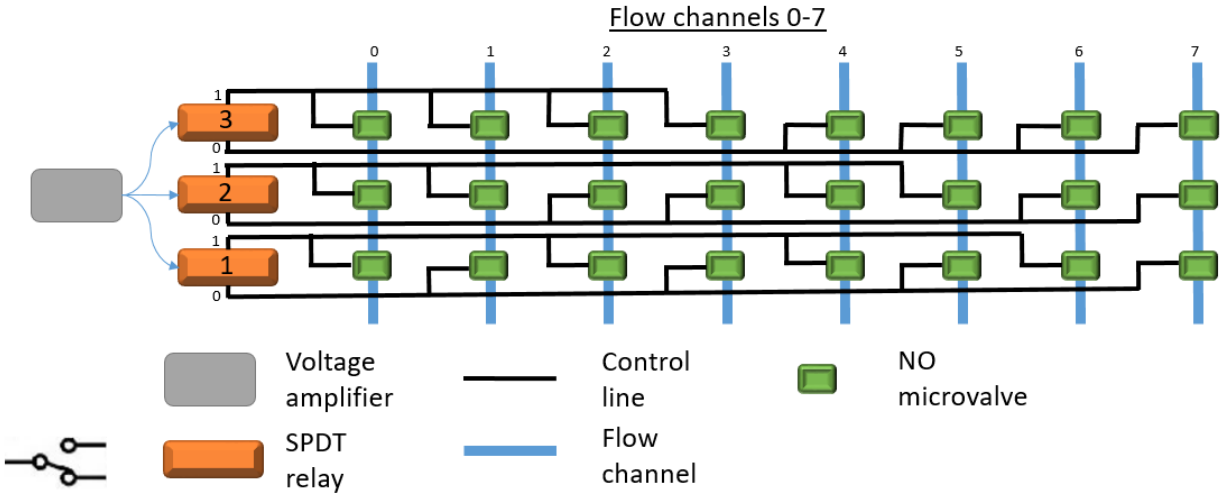

Selecting flow channels 0-7

	0	1	2	3	4	5	6	7
SPDT 1	0	1	0	1	0	1	0	1
SPDT 2	0	0	1	1	0	0	1	1
SPDT 3	0	0	0	0	1	1	1	1

Figure 21: New proposed design for the microfluidic multiplexer

The new proposed design shown in Figure 21 can be integrated the same way in the microfluidics platform as the old design. The SPDT relay combination required to select a desired flow channel is shown in the actuation table at the bottom of Figure 21. When flow channel 0 needs to be selected, SPDT relays 1,2 and 3 actuate output channels 0. When flow channel 3 needs to be selected, SPDT relays 1 and 2 actuate output channels 1 and SPDT relay 3 actuate output channel 0. To provide high voltages a DC voltage amplifier is needed. An example of a commercially available DC voltage amplifier and SPDT relay are shown in Table 6.

Table 6: Example of a DC voltage amplifier and of a SPDT relay

High voltage amplifier, EMCO		**SPDT relay, Phoenix contact**	
	• AG02 • 0-200 V range • 1.44 W • Input 24 V • 5.66 gram • 23.4 × 11.4 × 6.4 mm		• REL-MR-24DC • 250 V DC switching voltage • 0.17 W • 5.0 gram • 28 × 15 × 5 mm

The microfluidic multiplexer will be used in a OOCs platform, where it will replace the commercial Idex MHP7970-500-4 selector. Table 7 compares the Idex selector with the state of the art microfluidic multiplexer, namely the complementary binary pneumatic actuated multiplexer, and the new proposed complementary binary piezoelectric microfluidic multiplexer. The given values for power, footprint, pressure resistance, response time and costs for the microfluidic multiplexers are estimates when 8 flow channels needs to be controlled.

Table 7: Comparison between the commercial Idex MHP7970-500-4, the state of the art pneumatically actuated complementary binary multiplexer and the piezo electric actuated complementary binary multiplexer

	Idex MHP7970-500-4	**Complementary Binary**	**Complementary Binary Piezoelectric**
Number of flow channels	6	8	8
Power consumption	0.48 W off state 24 W on state	1 W (pump) + 4.5 W (3 solenoid valves) ≈ 5.5 W	1.44 W (Piezo driver) + 0.51 W (3 SPDT relays) ≈ 2W
Footprint	123,2 × 61,1 × 49,5 mm	Multiplexer 3 × 1.5 × 1 mm +Pump 44 × 35 × 29 mm +3 Solenoid valves 150 × 50 × 50 mm ≈ 197 × 86.5 × 80 mm	Multiplexer 40 × 15 × 2 mm +High voltage amplifier 23,4 × 11,4 × 6,4 mm +3 SPDT relays 84 × 45 × 15 mm ≈ 147,4 × 71,4 × 23,4 mm
Pressure resistance	41 MPa	≈ 50 KPa	≈ 100 KPa
Response time		3-4 s	40 ms
Costs	€ 2075.11	Pump + 3 solenoid valves €75 +Manufacturing multiplexer €100 ≈ €175	Piezo driver+ 3 SPDT relays €150 +Manufacturing multiplexer €350 ≈ €500

The proposed piezoelectric multiplexer can handle more flow channels, has lower power consumption, has a smaller footprint and lower costs compared to the Idex selector. The pressure resistance of the Idex selector is higher, but the ≈ 100 KPa of the piezoelectric multiplexer is sufficient enough for the OOCs platform.

Compared to the state of the art microfluidic multiplexer the proposed piezoelectric multiplexer has lower power consumption, this is primarily the consequence of the high power consumption of the three solenoid valves. Beside the proposed multiplexer has a smaller footprint, which is also primarily the consequence of the footprint of the solenoid valves. Another advantage of the piezoelectric multiplexer is the pressure resistance which is a fraction higher. The response time of the complementary binary multiplexer is high compared to the piezoelectric multiplexer due to the degassing of the control lines which is a disadvantage. The advantages of the complementary binary multiplexer are: the costs, the external equipment is cheap and widely available and the multiplexer device is manufactured by soft lithography which is a cheap manufacturing process. Another advantage are the small dimensions of the multiplexer device, but the overall footprint is large as a consequence of the large bulky external equipment. Overall the piezoelectric binary multiplexer is the most promising device to replace the Idex selector.

2.3.3 Simulation study

In this chapter the flow rate of three NO-microvalves in series and the membrane deflection of a single NO-microvalve are simulated using COMSOL Multiphysics. The dimensions used are preliminary and serve as a verification of the working principle of the microvalve designs and shows the design freedom to optimize the displacement and flowrate of the microvalve. The initial dimensions are based on the NO- microvalve developed by Gunda et al. [39] and are as follows: PZT radius= 2mm, PZT thickness= 127 μm , membrane radius= 2.5 mm, membrane thickness= 50 μm, epoxy thickness= 10 μm, voltage= 175 V, pressure = -55 kPa.

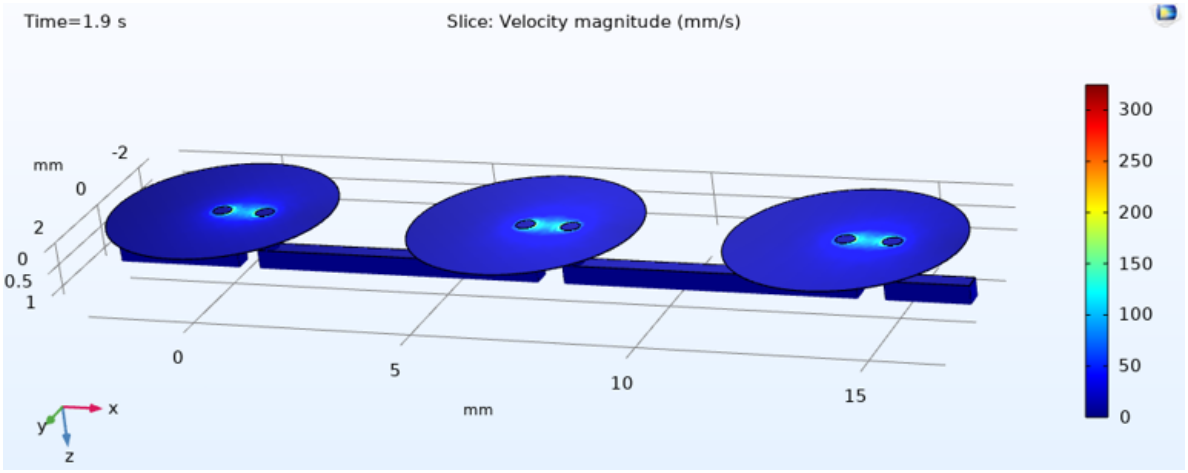

Figure 22: Flow simulation of three NO- microvalves in series

In Figure 22 three NO-microvalves in series are simulated. A valve chamber height of 7.5 µm is modeled and a flow rate of 74.4 µL/min is achieved. The flow rate can be calculated by integrating the velocity of the fluid over the surface area. This achieved flow rate is above the required flow rate of 68 µL/min used in the microfluidic platform.

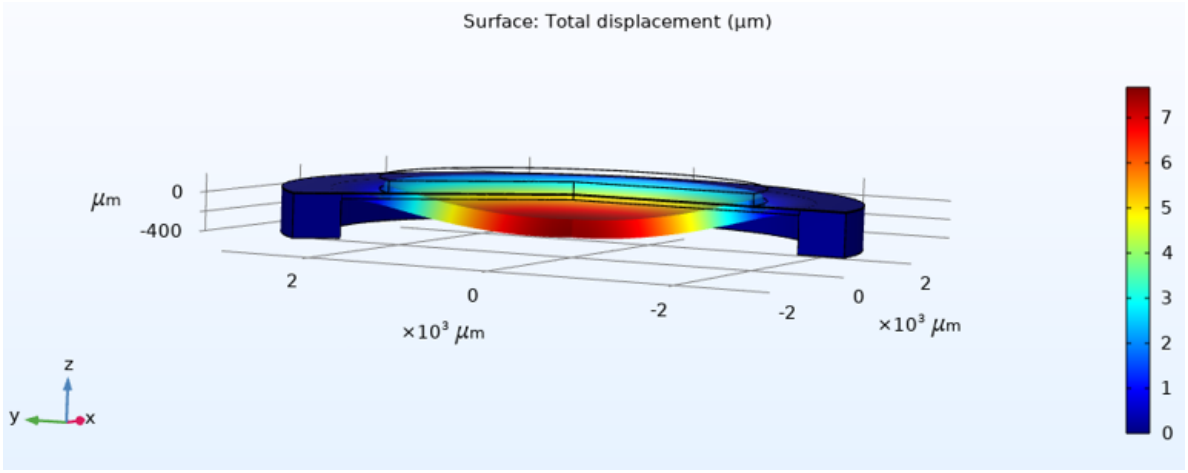

Figure 23: Membrane displacement of a NO- microvalve when 175 V is applied

In Figure 23 the microvalve deflection is shown. If a valve chamber height of 7.5 µm is used in the NO-design the membrane has to deflect at least 7.5 µm to close the inlet. In this simulation the achieved center displacement is 7.67 µm when a voltage of 175 V is applied. The displacements can be further optimized by changing the PZT radius, membrane radius and the voltage applied. The displacement has to be optimized to guarantee high enough flow rate capabilities and leak tight closing.

2.3.4 Fabrication study

To fabricate the NO piezoelectric microvalve laser cutting of a PZT -5H sheet is chosen to attain the required piezoelectric discs. At the beginning of the exploration of possible manufacturing steps concerning the piezoelectric discs there was the desire to inkjet print the piezoelectric discs on top of the valve membrane. This plan was not continued, because the sintering temperature is in the order of 1000 °C which would affect the membrane, also when inkjet printing is used the piezoelectric material solvent needs a low viscosity which is hard to attain. Another plan was to make PZT disks by screenprinting of PZT powder. Screenprinting brings additional steps such as: making the screenprinting substrate, sintering of the PZT powder and polarization of the PZT discs. Because there are no advantages compared to laser cutting of the PZT sheet, the latter fabrication step is chosen.

The fabrication of the microfluidic multiplexer is done in the following sequence:

1. Laser cutting of a PZT sheet
2. SLA printing of the microfluidic channels and multiplexer base
3. 3D printing of the multiplexer holder
4. Cutting of the spacer and placing it on the multiplexer base or monolithic SLA printing of the spacer and the valve seat base.
5. Cutting of the membrane. On top of the membrane the PZT disk is placed and bonded by conductive epoxy bonding or SLA printing of the membrane.
6. Clamping of the membrane on the spacer and multiplexer holder by using bolts, when a monolithic design is chosen this step is not needed.

The required materials and equipment to produce the microfluidic multiplexer are summarized in the inventory list Table 8.

Table 8: Inventory list

Material	Purpose
Resin	Multiplexer base/holder
Stainless Steel sheet 50 μm	Membrane
Stainless Steel sheet 5μm	Spacer
PZT sheet	PZT disc
Conductive epoxy	Bonding of PZT disc with the Membrane
Bolts	Clamping
3 SPDT relays	Switching of the voltage
Piezo driver	Voltage amplifier

2.4 Research Question

In this chapter the theoretical and experimental approach to answer the research (sub)questions are discussed. Further the risk and mitigations of the design and fabrication process will be explored.

2.4.1 Theoretical and Experimental approach

To tackle the research gap in finding a microfluidic multiplexer which is controlled by a minimum of control lines and uses all actuation space available, the following research question is asked:

How to design, fabricate and implement a modular, low-power, small footprint microfluidic multiplexer suitable for OOC applications? The microfluidic multiplexer has the following main requirements:

- Pressure withstanding of -55 kPa
- Footprint smaller than 123,2 $\times$ 61,1 $\times$ 49,5 mm
- Flow range of 1.5 – 68 L/min
- Power consumption with a maximum of 3.5 W

The following sub questions are asked:

1. What are the challenges on designing a microfluidic multiplexer?
2. Which manufacturing method is suitable for microfluidic multiplexer fabrication?
3. How to reach a leak tight microvalve?
4. How to clamp the membrane?
5. What are the achieved flow rates, leakage rates, response times, pressure widthstandings and power consumption?
6. How to implement the microfluidic multiplexer in the microfluidic platform?

The first step is modeling of the proposed microfluidic NO- microvalves. The theoretical approach starts with an analytical model to calculate the membrane deflection and the flowrate. Next step is to make numerical models using COMSOL. When the dimensions are optimized

the fabrication process can start. The question is of the microvalves can be made monolithic or must they be assembled using epoxy and clamping.

After fabrication the NO- microvalves can be tested on the requested parameters. The subquestion regarding getting a leak tight microvalve will be researched. The process cycle is repeated for the 4-to-1 multiplexer. The goal in manufacturing this device is to optimize the fabrication process for fabricating multiple microvalves. When the questions regarding how to reach a leak tight microvalve and what is the best way to fabricate multiple microvalves are researched the 8-to-1 multiplexer will be modeled and fabricated. After fabrication and testing it has to be implemented in the microfluidic platform, whereby attention must be paid to the tubing connections, electronic connections and the Arduino controlling.

2.4.2 Risks and Mitigations

One of the primary risks in the fabrication process is the bonding between the membrane and the PZT disk. For this purpose a conductive epoxy is used which has to be a thin layer, thinner than 20 μm. To achieve this a stencil with the required thickness is used which functions as a substrate for the epoxy layer. Another risk related to the epoxy is the PZT disk placement which has to be very accurate, this can be done by using vacuum tweezers. The goal is to place the PZT disk at the desired place, whereby a thin epoxy layer is equally spread. If epoxy is building up at one side of the PZT disk shorting is possible while the positive and negative voltages get in direct contact.

When the option of laser cutting of PZT disk is chosen above the option of screenprint the PZT disks a heat affected zone can arise. This can be prevented as much as possible by using the right laser parameters. In printing of the microchannels clogging of the channels can occur due to residue from the fabrication procces. This can be mitigated by flushing the microchannel with IPA and DI water regularly during the fabrication process.

A risk in the operation of the microvalves lies in the leakage that occurs due to insufficient closure between the membrane and the valve seat. This can be prevented by using a soft layer between the membrane and valve seat to guarantee that the valve is completely closed.

In Table 9. a summary of the risks and mitigations is given.

Table 9: Risks and Mitigations

Risks	**Mitigations**
Non uniformity of bonding layer thickness	Using of a 10 μm stencil
Misalignment of the PZT disk	Using vacuum tweezers
Shorting of the PZT disk	Equally spreading of the epoxy layer
Heat Affected Zone on the PZT disk	Using tuned laser parameters
Microchannels clogging	Regularly flushing
Leakage	Spin coating PDMS layer between membrane and valve seat

2.4.3 New research question

A new research question was proposed after the literature review presentation, namely:

How to design, fabricate and implement a modular, low-power, small footprint microvalve suitable for OOC applications?

The new research question now focuses on the microvalve instead of the microfluidic multiplexer. Next to that a implementation of the new microvalve in a microfluidic platform for OOC applications is presented in the paper, where it modular replaces the Idex MHP7970-500-4. The main requirements for the microvalve and fluid selector (replacement of the Idex MHP7970-500-4) are:

Table 10: Target specifications arising from OoC applications

Parameter	**Value**
Microvalve	
Flow range	0-100 $\mu l/min$
Leakage-rate	0% at 550 mbar
Pressure range	-600 mbar up to 600 mbar
Response time	100 ms at 500 mbar
Power consumption	50 mW
Dimension	61.1 × 49.5 × 20.5 mm
Costs	€ 345
Fluid selector	
Power consumption	3.5 W
Dimension	123,2 × 61,1 × 49,5 mm
Flow channels	6
Costs	€ 2075.1

The following sub questions are asked:

1. Which microactuator is able to deliver the force required to achieve zero leakage and is able to work with pressure ranges of -600 mbar to 600 mbar?
2. How to 3D print a single piece consisting of microfluidic connections, a membrane and not clogged internal channels?
3. How to design a portable fluid selector?

In the following chapter a paper is presented in which the research (sub)questions and target specifications are tackled.

3 Paper - A proportionally controlled 3D-printed microvalve using a piezostack microactuator

A normally-open, wide-range, proportionally controlled 3D-printed microvalve using a piezo stack microactuator

Henrie Kramer, 4299469
Department of Precision and Microsystems Engineering, TU Delft

***Abstract*—Microvalves are useful components for several microfluidic applications in which they control the fluid flow in a microfluidic system. Most microvalves to date are made by using silicon micro-machining, which is a complex manufacturing process, or soft lithography using Polydimethylsiloxane (PDMS) which has a high gas permeability. Next to that most microvalves in literature have small actuation forces resulting in small pressure ranges and large leakages at low pressure levels. In this paper, a normally open microvalve which is fabricated by only using 3D printing techniques with a bio-compatible resin is presented, making it more easy and accessible to manufacture. The novelty is the integrated micro-channels, membrane and microfluidic connections in a single 3D printed piece. The utilized actuator is a commercially available piezo stack, which has a displacement of** $34\ \mu m$ **at** $150\ V$**. Due to its large actuation force of** $900\ N$ **the microvalve can modulate fluids from** -600 **to** $2\ bar$**, with measured flow-rate levels between** $0-90\ \mu l/min$ **and projected flow-rate levels between** $0-410\ \mu l/min$**. In fully closed state the leakage-rate of the microvalve is** $1.67\ \mu l/min$ **at 600** $mbar$**, with a static power consumption of** $442.5\ mW$**. Subsequently it is shown that after using higher clamping torques (**$>0.7\ Nm$**) the microvalve can operate with zero leakage up to** $1.5\ bar$**. Additionally a 3-to-1 fluid selector is designed using three microvalves, which can be integrated into a portable microfluidic platform for Organ-on-Chip (OoC) applications.**

***Keywords*—** microvalve, monolithic, piezo stack, fluid-selector

I. Introduction

Microfluidics is a scientific research field with already promising achievements in several applications like: control cooling systems [1], spacecraft atmosphere monitors [2], OoC technology [3], bioreactors [4] etc. In microfluidics smaller sample usages with finer control of flow-rate can be achieved compared to macrofluidic experimental equipment [5].

Microvalves are one of the key components in microfluidic systems. They manipulate the fluid flow by actively or passively obstructing the fluid. Most microvalves consist of a fluid inlet, valving chamber and fluid outlet. Microvalves can proportionally control or on/off switch the fluids in the microfluidic system, where the typical range of fluid control is in the 10^{-9} to 10^{-18} litres range [6]. In developing new microvalves the main focus points are: achieving larger flow-rates, lower leakage rates, lower power consumption and less complex manufacturability [7]. A frequently used microvalve is the so called 'Quake' valve [8], which is manufactured by using soft lithography to make a bilayer polydimethylsiloxane (PDMS) structure. In this microvalve fluid flows in one channel, while in the other channel air is flowing which can be controlled by an external air system. The Quake valve is a check valve, so when enough pressure is build up in the air channel, the latter can squeeze the fluid channel and on/off switch the fluid passage.

Passive microvalves uses the back pressure or surface friction of the fixed structure to throttle the fluid flow. An example of a passive microvalve is the Tesla valve [9]. Most microvalves in literature use active operation to control the fluid flow, where a micro actuator obstructs the fluid passage when activated. The main advantage of active microvalves is the automated control, where microvalves are operated by external stimuli in an active way in contrary to passive microvalve where this is not possible. Also the valving efficiency of passive microvalves using the reverse flow direction to throttle the fluid flow is relatively poor, since the performance of these diode-like valves depends on input pressure [10]. The active microvalves can be classified by their actuation mechanisms. Many different actuation methods can be found in literature like: electrostatic [11], piezoelectric [12], thermal pneumatic [13, 14], electromagnetic [15] and pneumatic actuation [16]. Each actuation mechanism has their strengths and limitations in several microvalve characteristics like: power consumption, response time, force etc.

Thermal pneumatic actuation used in the microvalve designed by Takao et al. [13] achieves large strokes and reasonable actuation forces, but has a large power consumption and a slow response time which is typical for this actuation type. Electromagnetic actuation is used frequently in macro-scale valves, because of its ability to deliver large forces and strokes at a fast response time. The disadvantage is however their high power consumption. Yoshida et al. [11] applied electrostatic actuation in their desigend microvalve for portable fuel cell applications. It has the ability to deliver a fast response time at a low power consumption, however is characterized to have highly non linear behavior with a small stroke and actuation force, which is a general limitation of this actuation mechanism. Also it is actuated by high voltages. Piezoelectric actuation typically has a fast response time and low power consumption, however is operated at high voltages. Pneumatic actuation mechanisms uses polymer micro-structures for the fluid flow in combination with external control valves and pressure sources for the air channels control. A fast response time and a large actuation force can be achieved, however the drawbacks are the bulky external peripherals and high power consumption.

Because of the many merits of piezoelectric actuation compared to other actuation types like [17–20]: low power consumption (37.5 μW- 48 mW), high pressure resistances (1 bar - 6.25 bar) and fast response time (30 μs - 40 ms) a lot of research is done on this type of actuation. Two types of piezoelectric actuated microvalves can be found in literature: stack [21, 22] and disk type (unimorph [23] and bimorph [24]) microvalves. Piezoelectric stacks characteristically deliver large actuation forces, but small strokes. Piezoelectric disk type actuators on the other hand typically provide large displacements at moderate actuation forces. Most piezoelectric actuated microvalves in literature use complex fabrication processes like (silicon) micro-machining sacrificing time and costs [25]. An example in literature where rapid prototyping (3D printing and laser cutting) is utilized is the microvalve designed by Gunda et al. [20]. This microvalve can be proportionally controlled by using a piezoelectric unimorph. However it has small actuation forces (4.74 N) and a leakage rate of 0.8 open flow (at 1 bar), which is a limitation for OoC applications. Also this microvalve uses a stainless steel membrane and PZT disk, which needs to be laser cut causing heat affect zones at the membrane and disk.

Here in this work an active 3D-printed proportionally controlled microvalve using a piezo stack actuator is demonstrated. The microvalve

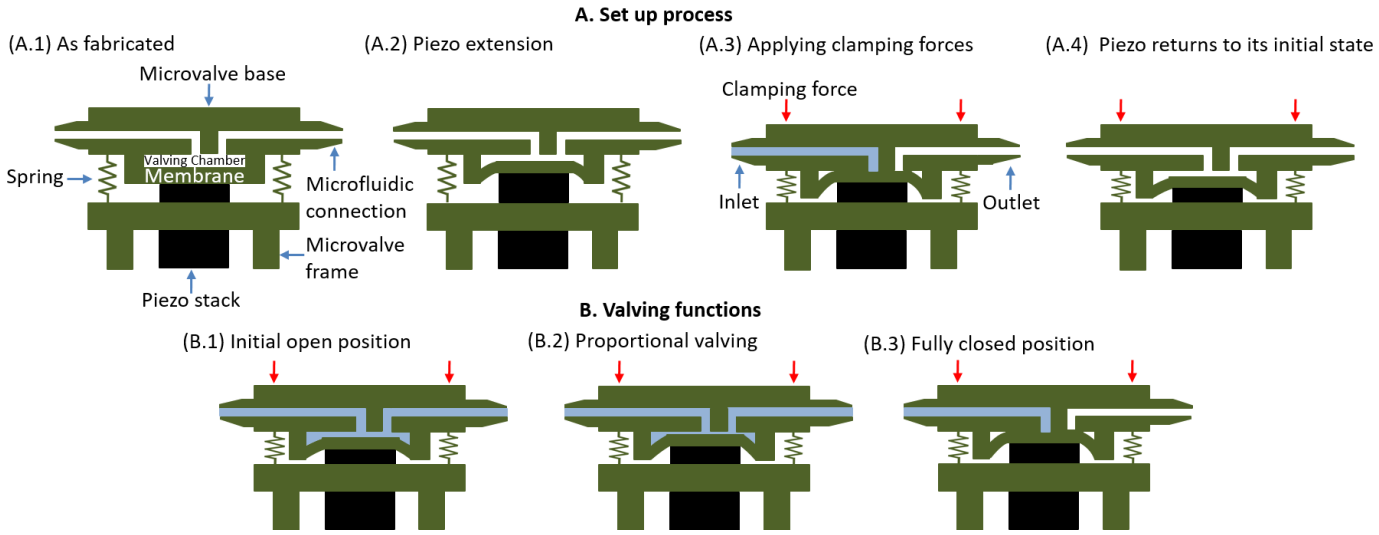

Figure 1: (A) Schematic overview of the microvalve set up process. (A.1) The microvalve consist of a microvalve base (which contains the micro-channels, membrane and microfluidic connections), a piezo stack, springs (O-rings in this work) and the microvalve frame. The microvalve base is placed on the microvalve frame as shown. (A.2) The piezo stack is actuated and expands, thereby deforming the membrane. (A.3) Clamping forces are applied to the microvalve base, thereby pressing the springs. This leads to an increasing force between the piezo stack and the membrane. The membrane is pressed on the valve seat leading to the closure of the valving chamber inlet. The clamping force direction is indicated by the red arrows. A fluid flow is applied at the inlet to check at the outlet if the microvalve is fully closed. (A.4) If the microvalve is fully closed the set up process is completed. The fluid flow is stopped and the piezo stack is not actuated anymore. (B) Schematic overview of the working positions (B.1) Microvalve in its inititial open position. A fluid is applied at the inlet and the fluid passage is not obstructed. (B.2) Microvalve in its proportionally controlled position. The piezo stack is partially expanded, but nevertheless creates a higher flow resistance which throttles the fluid flow. (B.3) Microvalve in its fully closed position. The fluid flow is obstructed by the fully expanded piezo stack.

is designed and fabricated for the requirements typical for microfluidic OoCs as shown in Table I [26]. A piezo stack actuator is selected while it provides large actuation forces resulting in wide pressure ranges and leakage reduction. While it is used for OoCs application the stroke of the piezo stack is of less importance while moderate flow-rates (0-100 $\mu l/min$) needs to be achieved. The microvalve is monolithically 3D-printed using a photo-polymerization manufacturing technique. No complex fabrication steps are needed and only one bio-compatible polymer material is used. Photo-polymerization is the most popular 3D printing method for fabricating finely machined structures, while this technique has the highest resolution compared to other 3D printing techniques like powder, extrusion and lamination techniques [27].

Table I: Target specifications arising from OoC applications

Parameter	**Value**
Microvalve	
Flow range	0-100 $\mu l/min$
Leakage-rate	0% at 550 mbar
Pressure range	-600 mbar up to 600 mbar
Closing time	100 ms at 500 mbar
Opening time	100 ms at 500 mbar
Power	50 mW
Dimension	61.1 × 49.5 × 20.5 mm
Costs	€ 345
3-to-1 fluid selector	
Power consumption	1.75 W
Dimension	61.6 × 61.1 × 49.5 mm
Costs	€ 1037.6

This work also shows an application of the designed microvalve where three microvalves are used in parallel to create a 3-to-1 fluid selector. A fluid selector can for example be used in the portable OoC platform designed by Zhu et al. [28] (the requirements for the 3-to-1 fluid selector are also listed in Table I). In this platform a vacuum range is used from -157 to -556 mbar, for sucking up culture media from fluid reservoirs to a microfluidic chip. Using vacuum minimizes the flow fluctuations and next to that it can be used for creating cyclic vacuum suction in order to mimick cyclic mechanical stretching of for example lungs [29] and guts [30]. The microfluidic platform uses a commercial available fluid selector, which selects one fluid forward selecting from six fluid reservoirs, functioning as a check valve with six inputs and one output. By replacing the commercial fluid selector by the proposed fluid selector the aim is to achieve a smaller device with less power consumption, less costs, leakage free characteristics and proportional control of the fluid. The following sections first give a introduction into the working principle of the microvalve. Thereafter the process of design and fabrication of the microvalve is described. Subsequently the experimental results are presented and discussed.

II. Design

In this chapter first a short explanation is given on the working principle of the designed microvalve. Next to that some design criteria are discussed.

A. Microvalve working principle

The designed microvalve is shown in Figure 1. The microvalve consists of two 3D printed parts (the microvalve base and the microvalve frame), springs (O-rings in this work) and a piezo stack. The microvalve base includes the micro-channels, membrane and the

microfluidic connections. In the valving chamber the membrane is deformed by the piezo stack and pressed on the valve seat. This leads to closing of the valving chamber inlet channel. To start using the microvalve first a set up process has to be completed after assembly of the microvalve. This set up process is shown in Figure 1A. In A.1 the microvalve is placed and aligned on the microvalve frame using bolts and nuts (not shown). The piezo stack is in contact with the membrane and is not actuated. In A.2 the piezo stack is actuated (more information on the working of piezoelectricity can be found in the supplementary material), resulting in piezo stack expansion, thereby deforming the membrane. Next to that in A.3 a clamping force is applied to the bolts and nuts causing a pressing force on the springs. Springs are used between the microvalve base and microvalve frame for fine tuning the distance between the membrane and valve seat. When a larger clamping force is used the springs will be pressed harder. The distance between the microvalve base and microvalve frame decreases, with the result that the membrane is pressed by the piezo stack on the valve seat. This leads to the closing of the valving chamber inlet. A fluid flow is applied at the inlet to check at the outlet if the microvalve is fully closed, if this is not the case a larger clamping force will be applied in order to increase the pressing force of the piezo stack on the membrane. If the microvalve is fully closed the set up process is finished. The applied fluid flow is stopped and the piezo stack is stopped being actuated as shown in A.4.
The microvalve has three working positions visualised in Figure 1B. In B.1 the microvalve is shown in its initial fully open state in which the piezo stack is not actuated and the fluid flow is not obstructed. In B.2 the piezo stack is partly expanded (depending on the applied voltage) resulting in a proportional throttling of the fluid flow. When the piezo stack is fully expanded the microvalve will obstruct all fluid passage as shown in B.3.

B. Design criteria

In this section the design criteria regarding the piezo stack, microchannels and membrane are discussed.

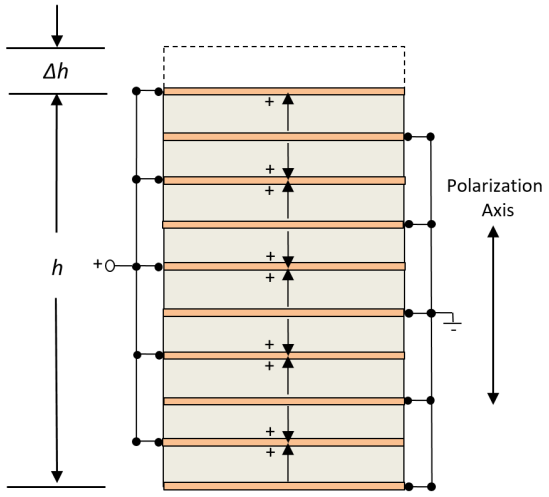

Figure 2: Schematic of the piezo stack. The grey layers represent the piezoelectric material and the orange layers represent the metal layers. The black arrows indicate the poling direction. The dashed lines show the expansion Δh of the piezo stack with original length h.

1) Piezo stack: Piezo stacks are multilayered actuators consisting of multiple layers of piezoelectric material and metal layers that function as electrodes. In Figure 2 a schematic of a piezo stack is shown. The piezoelectric material is represented by the grey layers, the metal layers are represented by the orange layers. The metal layers function as electrodes, where on the layers with a + sign 150 V is applied, while the other layers are connected to the ground. The voltage is applied in the poling direction of the piezoelectric material, which is represented by an arrow. The dashed lines show the expansion Δh of the piezo stack with original length h. The PZT and metal layers are glued together and are protected by an insulation sleeve.
The piezo stack expansion is a design criterion in defining the chamber height in the valving chamber as shown in Figure 1A. By varying the chamber height the flow resistance in a microfluidic system can be made larger or smaller, thereby controlling the flow-rate. The piezo stack expansion can be proportionally controlled by varying voltages and by adding more layers as in [34]:

$$\Delta h = n \cdot h_l \cdot d_{33} \cdot \frac{V}{h_l} \tag{1}$$

In Equation 1, Δh represents the actuator stroke, n represent the number of piezoelectric layers, d_{33} is the piezoelectric coefficient, h_l the thickness of the piezoelectric layer and V the actuation voltage. The capacitance of a piezo stack C as shown in Equation 2 is dependent on the number of piezo electric layers n, the dielectric coefficient ε_{33}^T, the cross-section of the piezo stack A and the thickness of a piezo stack layer h_l.

$$C = n \cdot \varepsilon_{33}^T \cdot \frac{A}{h_l} \tag{2}$$

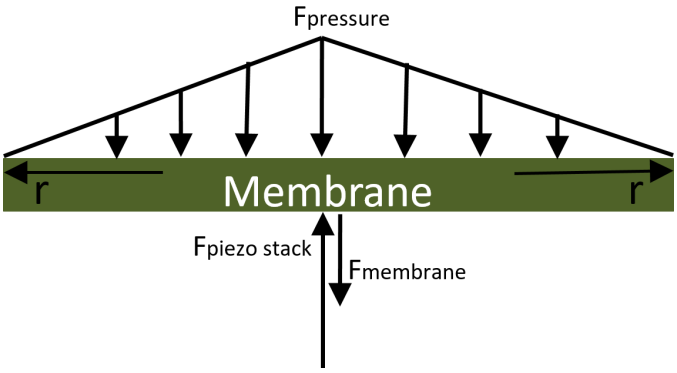

Figure 3: Forces working on the membrane. $F_{pressure}$ is represented as a triangular distributed load with P_1 as the static pressure at the center (valving chamber inlet) and 0 Pa at the corner. The force as a result of the stiffness of the membrane $F_{membrane}$ and the force as a result of the piezo stack $F_{piezostack}$ are represented as a point load.

To fully close the microvalve the force generated by the piezo stack has to provide a force to counterbalance the fluid pressure on the membrane and has to provide the force required to deform the membrane as shown in Figure 3. The force balance on the membrane is:

$$F_{pressure} + F_{membrane} = F_{piezostack} \tag{3}$$

To estimate the force on the membrane caused by the fluid pressure it is assumed that above the microvalve chamber inlet, with radius r_{ci}, there is a static uniform pressure working on the membrane when the valve is closed. When the valve opens the static pressure drops in the radial direction of the valving chamber [35]. The energy distribution can be estimated by using the Bernoulli equation for incompressible fluids as in [36]:

$$P_1 + \frac{1}{2}\rho v_1^2 = P_2 + \frac{1}{2}\rho v_2^2 \tag{4}$$

The pressure and kinetic energy per unit volume along a stream line with no height differences are in balance. Where P_1 and P_2 are the pressures at location 1 and 2 respectively and v_1 and v_2 are the fluid velocities at location 1 and 2 respectively. ρ is the density of the fluid (for water 997 kg/m^3). The force acting on the membrane can be represented as a triangular distributed load which reduces when the kinetic energy increases and the pressure energy decreases. This happens when the valve opens. The maximum force as a result of the fluid pressure can be estimated with the following equation:

$$F_{pressure} = r_{ci}^2 P_1 \pi + \int_{r_{ci}}^{r_m} 2\pi r^2 P(r) dr \tag{5}$$

Where r_{ci} is the microvalve chamber inlet, r_m is the membrane radius and P_1 is the static pressure at the microvalve chamber inlet and $P(r)$ is the distributed pressure load. The force required to deform the membrane can be estimated by the tensile forces in the membrane during deflection, so when the piezo stack is in its fully extended position [37]:

$$F_{membrane} = \frac{d_m D}{0.0056 c_m^2} \tag{6}$$

Where d_m is the membrane deflection (stroke of the piezo stack), c_m is the circumference of the membrane and D is the flexural rigidity which can be calculated by:

$$D = \frac{t_m E}{12(1-\nu^2)} \tag{7}$$

Where t_m is the thickness of the membrane, E is the Young's modulus of the membrane material and ν is the Poisson's ratio of the membrane material.

The minimal total force needed to be delivered by the piezo stack can be estimated by:

$$F_{total} = F_{pressure} + F_{membrane} \tag{8}$$

2) Microfluidic resistance: Microfluidic systems typically consist of fluid channels, valve chambers and other fluidic elements with sizes in the order of the micrometer to millimeter range. The Reynolds number is low for water in microfluidic systems (Re$<$ 100) when characteristic dimensions of ($l < 50\ \mu m$) and fluid velocities of ($v < 1\ m/s$) are used, leading to laminar flows. To achieve flow-rates between 0-100 $\mu l/min$ at pressure levels between -600 to 600 mbar as required in Table I, the flow resistances in a microfluidic system needs to be calculated. When a pressure is applied to a microfluidic circuit, for instance with a pressure controller, the flow-rate can be calculated using Hagen–Poiseuille's law:

$$\Delta P = Q R_t \tag{9}$$

This is analogous to Ohm's law, where R_t is the total flow resistance in a microfluidic circuit, ΔP is the pressure difference between inlet and outlet and Q is the achieved flow-rate. In this analogy the assumption is made that the fluid flow is laminar, viscous and incompressible [31].
The flow resistance for common channel shapes with a specific length is estimated using the following equations [32]:

$$R_r = \frac{12 l \mu}{w h^3 (1 - 0.63 \frac{h}{w})} \tag{10}$$

$$R_c = \frac{8 l \mu}{\pi r^4} \tag{11}$$

Equation 10 is used for rectangular shaped channels, where l, w and h are the channel length, width and height respectively, μ is the dynamic viscosity. Equation 11 is used for circular shaped channels, where r is the radius of the channel. The first step in designing the microfluidic system is to estimate the piezo stack expansion, which defines the chamber height in the valving chamber and creates a variable flow resistance. To calculate this variable flow resistance Equation 10 is used, whereby the height h is represented by the piezo stack expansion. After calculating the variable flow resistance the total flow resistance in the microfluidic system can be calculated. Subsequently the flow-rates at varying pressure levels can be calculated using Equation 9. If the flow-rates are too low or too high the dimensions of the static flow resistances can be adapted taking into account the 3D printer resolution. In addition to the analytic calculations a FEM model is created in which the flow-rates are calculated at different pressure levels using the same micro-channel dimensions that are possible to print with the 3D printer.

3) Membrane: Other design criteria are the membrane parameters. Next to the flow-resistances, as already discussed, the membrane is dependent on the ability of the 3D printer to print an intact membrane. The membrane has the following design parameters:

1) The radius of the membrane needs to be large enough, so the piezo stack has enough space and is able to deform the membrane.
2) The thickness of the membrane.
3) The valving chamber height of the microvalve. The membrane is printed at a certain height above the microvalve inlet. The space between the inlet and membrane defines the valving chamber.

After successfully printing an intact membrane and micro-channels a monolithically printed part consisting of micro-channels, microfluidic connections and membrane is created.

III. Materials and Methods

In this section first the utilized piezo stack is introduced. Subsequently the 3D printing and assembly of the microvalve is explained. Lastly the experimental setup used to characterise the microvalve is discussed.

A. Piezo stack

As micro actuator a commercially available piezo stack (PiezoDrive SA050536) is used, while it provides enough stroke and force to meet the design requirements. The piezoelectric material in the piezo stack is similar to PZT-5H and Navy type VI. In the following table the stroke and other parameters of the piezo stack (supplied by the manufacturer) are listed.

Table II: Piezo stack parameters [33]

Parameter	**Symbol**	**Value**
Length	h	36 mm
Cross section	A	5x5 mm
Mass	m	7.1 g
Stroke	Δh	42 μm $\pm$10%
Blocking force	F	900 N
Stiffness	k	28$\cdot$ 10^6 N/m
Piezoelectric coefficient	d_{33}	600$\cdot$ 10^{-12} m/V
Capacitance	C	4.3 μF
max. Temperature	T	85°C

As shown in Table II the blocking force is 900 N. The minimum required total force, F_{total}, of the piezo stack to fully close the microvalve is 37.2 mN using Equation 8. The estimated $F_{pressure}$ is 17.8 mN and the estimated $F_{membrane}$ is 19.4 mN, using the boundary conditions as shown in Table III.

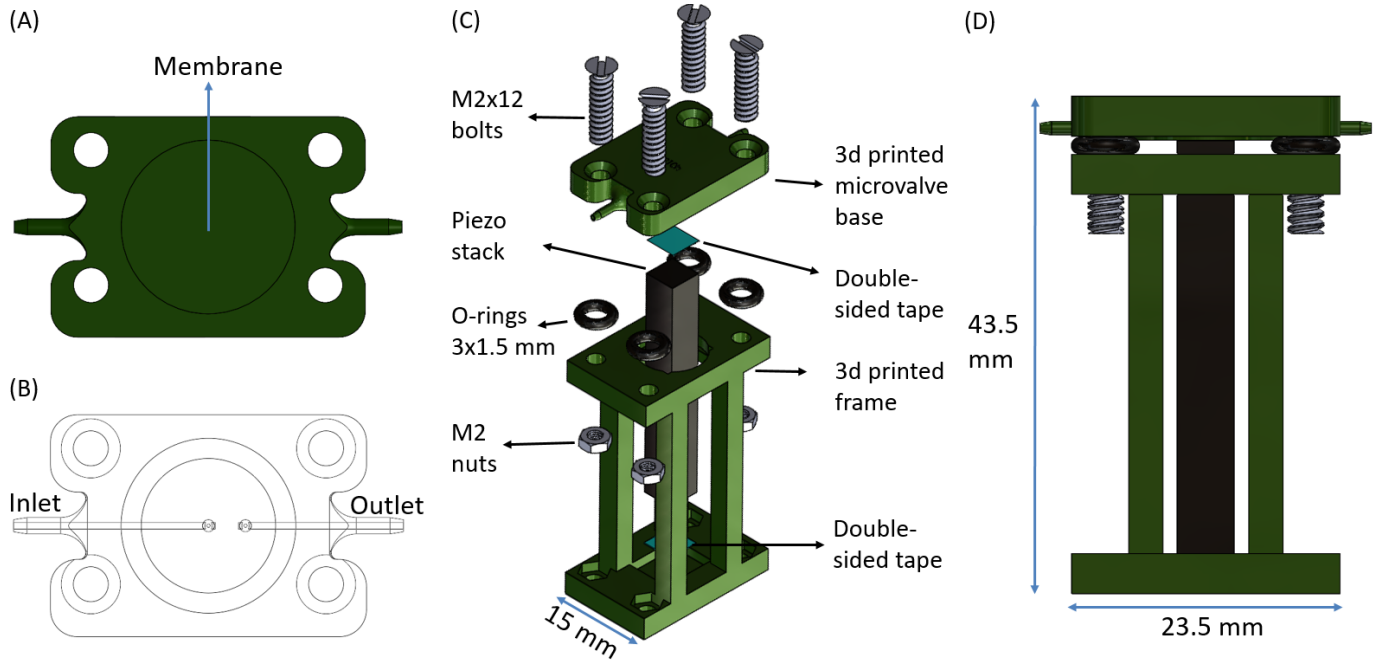

Figure 4: (A) Top view of the microvalve base. The membrane is indicated. (B) Transparent view: internal channels of the microvalve are visible. The inlet and outlet of the microvalve are shown. (C) Exploded view of all the components used during assembling the microvalve. (D) Front view of the assembled microvalve. Also the dimensions are presented.

Table III: Forces working on the membrane

Parameter	Value
$F_{pressure}$	17.8 mN
r_{ci}	105 μm
r_m	5 mm
P_1	60000 Pa
$P(r)$	60000-12257406r
$F_{membrane}$	19.4 mN
d_m	42 μm
c_m	0.031 m
t_m	245 μm
E	1.8553 GPa
ν	0.33
F_{total}	37.2 mN

Concluding, the force generated by the piezo stack can easily close the microvalve. Due to the large actuation force compared to the forces generated by the fluid and stiffness of the membrane, proportional control of the flow rate can be achieved. In contrast to electromagnetic and electrostatic actuation types with their non-linear behaviour characteristics, which are a disadvantage in proportional control [18].

The stiffness of the membrane is estimated to be 461.9 N/m using:

$$k_{membrane} = \frac{F_{membrane}}{d_m} \tag{12}$$

B. 3D printing of the microvalve

The microvalve base and frame are printed using Direct Light Processing (DLP) printing, which is a photo-polymerization technique. (More information on this printing technique is found in the supplementary material) For fabricating the microvalve base and frame a desktop DLP printer (Envision-TEC GmbH. Micro Plus Hi-Res) is used. This printer has a XY resolution of 30 µm × 30 µm. The Z resolution is material dependent, if a higher Z resolution is obtained the layer thickness will be smaller. For achieving the finest 3D structures the resin with the lowest layer thickness was used, namely HTM 140 V2. First the 25 µm layer thickness was tested, but it turned out that with the 35 µm layer thickness better quality models could be made. HTM 140 V2 is a green bio-compatible resin, with a Young's modulus of 1855.3 MPa ± 62.1 [38]. More properties of the resin are presented in the supplementary material.

The microvalve base shown in Figure 4A has microfluidic connections which functions as inlet and outlet. Further the microvalve base consists of micro-channels (Figure 4B) and a membrane (see Figure 8 for design parameters). A membrane is spaced at a certain distance (h_3) above the valving seat. The monolithic design proposed in this study has the advantage of using an in-built membrane. This prevents leakages occurring at clamping regions while using separate membranes. Further there will be no misalignment between structures and the number of fabrication steps will be reduced. The frame shown in Figure 4C functions as the piezo stack holder. The frame and microvalve base have M2 openings to clamp the two parts.

After printing the microvalve base it is important to flush the micro-channels and valving chamber with isopropyl alcohol (IPA) to remove all uncured HTM 140 resin. The first step is to immerse the microvalve base in an ultrasonication bath. Thereafter a syringe with IPA is put on the microfluidic inlet, after which all left behind resin is removed under high pressure. After this step the micro-channels and valving chamber are cleaned with DI-water using the syringe again. For the microvalve frame it is only needed to immerse it in an ultrasonication bath of IPA.

The flow-rates can be analytically and numerically estimated. Using the parameters in Table IV the flow resistances are calculated by using Equation 10 and Equation 11. When a certain pressure level is applied in a microfluidic circuit the analytic flow-rate can be estimated using Equation 9. For the numerical estimation a COMSOL Multiphysics

(v5.6) study was used. A creeping flow study was conducted and the flow path of the microvalve was recreated as shown in Figure 5A. The smallest feature is the valving chamber height which varies between $0-34$ μm. A close up of the valving chamber height is shown in as shown in Figure 5B. Water at room temperature was selected as the building material. At the inlet a pressure was applied, which creates a pressure difference between the inlet and outlet. A stationary simulation was made and the flow-rate estimated using a physics controlled mesh.

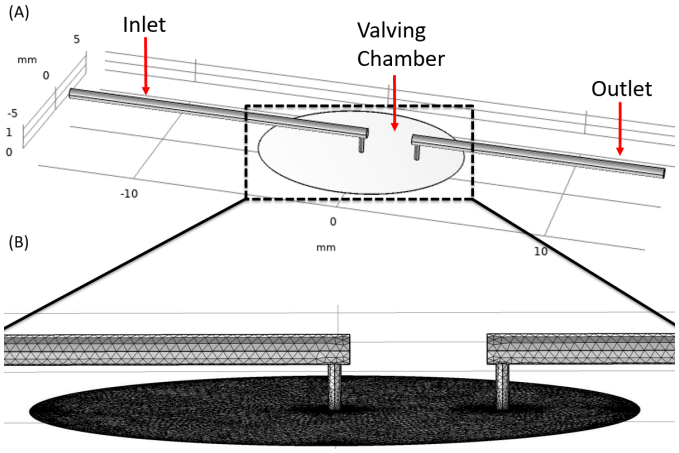

Figure 5: (A) Schematic of the flow path of the microvalve. Indicated are the inlet (where the pressure is applied), the valving chamber and the outlet. (B) Close up of the valving chamber. Also shown is the fine meshing of this feature

C. Assembly

After printing the microvalve base and frame the microvalve needs to be assembled (Figure 4D). The microvalve base is used for connecting the microvalve to the outer world. The microfluidic connections have an outer radius of 0.61 mm and can be used with Tygon tubings having an inner radius of 0.5 mm. The frame holds the piezo stack and contains M2 nuts, the microvalve base can be clamped on the frame using M2 bolts.

All components used in the assembly are shown in Figure 4C. The first assembly step is to bond the piezo stack to the frame using double-sided tape. The second step is to glue the four M2 nuts in the frame, so they stay in place. The third step is to place the four O-rings (3x1.5mm) on top of the frame, aligned with the bolt openings. This O-rings function as springs between the microvalve base and frame. The fourth step is to put double-sided tape on top of the piezo stack, this tape provides bonding ($\sim$7.2 N) between the piezo stack and the membrane of the microvalve. Subsequently the microvalve base is placed on top of the piezo stack and aligned with the frame using the M2 openings in the frame and microvalve base. The last step is moving the bolts through the M2 openings of the microvalve base and frame and align them into the fixed nuts. By turning the bolts the piezo stack can be pressed on the membrane and the set up process can start as described in subsection II-A.

D. Experimental setup

The main experiments that were conducted are related to the piezo stack displacement measurement, the flow-rate measurement of the microvalve and the characterization of the fluid selector.

1) Piezo stack: To measure the displacement of the piezo stack at different voltages a high voltage generator (Stanford research systems Inc. PS310) is used in combination with a laser displacement sensor (Keyence LC-2420 sensor-head with a Keyence LC-2400W laser displacement meter), which has a working range of $\pm$200 µm with a resolution of 0.01 µm. For measuring the creep and response time a data-acquisition device (National Instruments NI-DAQ USB-6211) was used with which displacement data can be collected over time.

2) Flow-rate: The flow-rates in the microvalve are measured using the setup in Figure 6. A pressure source (Elveflow OB1 Mk3+), which is connected to reservoir 1 has a pressure range from -650 mbar to 6 bar. The pressure builds up (also negative pressure) in reservoir 1 and causes a fluid flow to reservoir 2 or in the reverse direction (dependent on the pressure difference). The fluid passes the thermal flow-sensor (Elveflow MFS3), which has a maximum flow-rate limit of 90 µl/min (accuracy: 5% of measured value). The next stop is the microvalve, which is connected to a high voltage generator (Stanford research systems Inc. PS310). The applied voltages ranges from 0 to 150 V. The applied pressure and the achieved flow-rates are controlled and visualised in the Elveflow smart interface (ESI) software. The flow resistances in the experimental setup are negligible compared to the flow resistance in the microvalve.

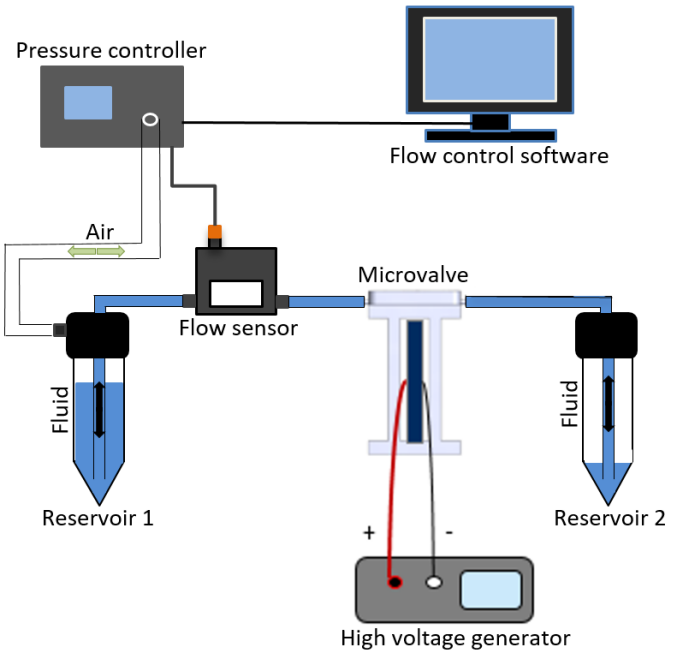

Figure 6: Schematic of the test setup used for measuring the flow-rate. Pressure is applied by the pressure controller to reservoir 1 creating a fluid flow. The flow-sensor measures the flow-rate and the high voltage generator applies voltage to the microvalve. The microvalve can control the fluid flow by adjusting the flow-resistance. The applied pressure and the achieved flow-rates are controlled and visualised in the flow control software.

3) Fluid selector: In this setup a portable 3-to-1 fluid selector is created using three microvalves in parallel. A fluid selector selects one fluid forward from three reservoirs by opening only one microvalve, while the other two microvalves are closed. To control three microvalves a 3-channel high voltage amplifier (Piezo Drive, PDu150) is used. The 3-channel high voltage amplifier is powered by a power supply (Delta Elektronika ES 030-5), where a 24 V output is used. To control the output voltage to the microvalves a power supply (Delta Elektronika EST 150) is connected to the control inputs of the 3-channel high voltage amplifier with voltages ranging from 0 to 7.5 V. The setup is shown in Figure 23A.

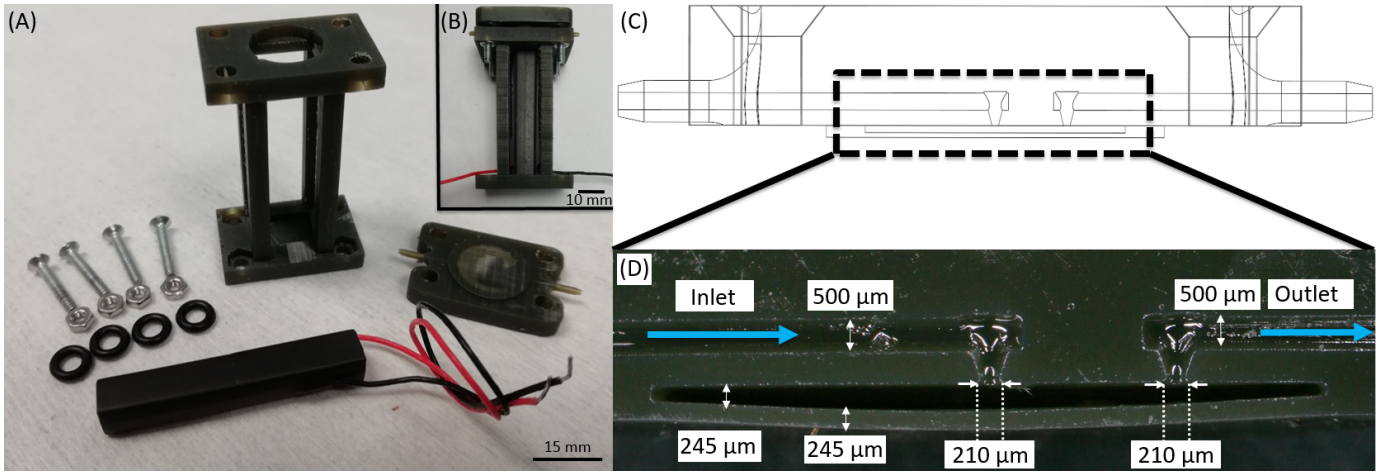

Figure 7: (A) Overview of all the components used in assembling the microvalve. Shown are: the piezo stack, the O-rings, the bolts, the nuts and the 3D-printed microvalve base and frame. (B) The assembled microvalve. (C) Cross-section of the internal channels of the microvalve. A close-up of the valving chamber is indicated. (D) Close-up of the fabricated valving chamber. Visible are d_1 and d_5 with diameter 500 μm, d_2 and d_4 with diameter 210 μm, h_3 with a height of 245 μm and M_t with a thickness of 245 μm.

IV. Results

In the first section of this chapter the fabrication results are discussed. Subsequently the piezo stack displacement, microvalve behaviour and fluid selector are characterised.

A. Fabrication

The microvalve is designed to operate within a flow-rate of 0-100 $\mu l/min$ at a pressure range of -600 to 600 mbar as discussed in subsubsection II-B2. To achieve this performance the first step is to conduct an optimization study. The achieved flow-rates in the microvalve depend on the applied pressure and the flow resistances as described in Hagen-Poiseuille's law Equation 9. The inlet and outlet channels (flow resistances R_1 and R_5) are defined by design parameters L_1, d_1, L_5 and d_5 and connect the outer world to the chamber inlet and outlet (flow resistances R_2 and R_4), which are defined by design parameters L_2, d_2, L_4 and d_4 (See Figure 8 for design parameters). Because of the relative large lengths of R_1 and R_5 their diameter is chosen to be larger to prevent clogging of the channels. Channel resistances R_2 and R_4 are optimized to have smaller diameters to achieve the wanted total static resistance of the microvalve in order to obtain the required flow-rates at the desired pressure levels. Also a small diameter of chamber inlet diameters d_2 and d_4 lead to better closing behavior, while a smaller area has to be closed off. The analytic and numerical models show that a chamber inlet diameter for both, d_2 and d_4, of 37.8 μm and 47.4 μm is needed respectively, when a desired flow-rate of 100 $\mu l/min$ at a pressure of 600 mbar and a valving chamber height h_3 (piezo stack expansion) of 34 μm is assumed. To fabricate such small channel diameters an experimental study is conducted, where the boundary condition is the 3D printer resolution. In this study the channel radii were increased until a microvalve was created without clogged internal channels. It turned out that a conical shaped channel, with a chamber inlet/outlet diameter (d_2 and d_4) of 210 μm on one side and on the other side of the cone a diameter of 900 μm, created the smallest not clogged internal channels. In Table IV the set of smallest manufacturable parameters are given.

Another experimental study was performed to search for the minimum dimensions needed to achieve an intact membrane at a minimum chamber height as discussed in subsubsection II-B3. The limit is again the 3D printer resolution, in addition the membrane was constrained to a radius of 5 mm in order to have enough space for the piezo stack placement.

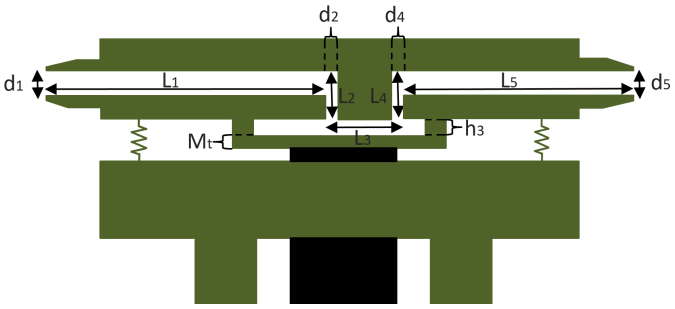

Figure 8: Cross-section of the microvalve base. The design parameters are: Inlet channel length (L_1), Inlet channel diameter (d_1), Chamber inlet length (L_2), Chamber inlet diameter (d_2), Chamber length (L_3), Valving Chamber height (h_3), Chamber outlet length (L_4), Chamber outlet diameter (d_4), Outlet channel length (L_5), Outlet channel diameter (d_5), Membrane thickness (M_t).

Table IV: Microvalve design parameters

Parameter	Value
Inlet channel length (L_1)	15 mm
Inlet channel diameter (d_1)	500 μm
Chamber inlet length (L_2)	1 mm
Chamber inlet diameter (d_2)	210 μm
Chamber length (L_3)	3 mm
Valving Chamber height (h_3)	245 μm
Chamber outlet length (L_4)	1 mm
Chamber outlet diameter (d_4)	210 μm
Outlet channel length (L_5)	12.25 mm
Outlet channel diameter (d_5)	500 μm
Membrane thickness (M_t)	245 μm
Membrane radius	5 mm

The parameters to be optimized in this study were the valving chamber height (h_3) and the membrane thickness (M_t). Ideally the chamber height is 34 μm (the piezo stack displacement as discussed in subsection IV-B) with minimum membrane thickness, but the layer thickness (3D printer resolution) is 35 μm. A gradual increase of 35 μm was used for both parameters. This made clear that at least a membrane thickness of 245 μm at a valving chamber height of 245 μm is needed to fabricate an intact and robust membrane.

As mentioned the fabricated valving chamber height (h_3) is 245 μm and the piezo stack displacement is 34 μm. This means that the piezo stack is not able to fully close the microvalve. To solve this a clamping force is applied that adjust the distance between the microvalve base and frame by pressing more or less on the O-rings, which functions as springs as discussed in subsection II-A. As a consequence the piezo stack is pressed onto the membrane, this way the distance between the membrane and valve seat decreases. The variable valving chamber resistance R_3 is defined by design parameter L_3 and the valving chamber height after the set up process and piezo stack expansion. To clamp the microvalve base to the frame, bolts and nuts are used. The maximum clamping torque is ~0.7 Nm measured with a torque screw driver. The final assembly is shown in Figure 7B. The 3D printed microvalve base and frame plus all other components used in the microvalve are shown in Figure 7A. After printing, the microvalve base and frame are flushed with IPA. Next to that a syringe is connected to the microvalve base inlet and IPA is pressed into the micro-channels. As a result green resin residue is observed. As a final step DI-water is used to flush the micro-channels. In Figure 7C the internal channels of the microvalve are shown. In Figure 7D a close up of the fabricated microvalve cross-section is presented. Clearly visible are the inlet and outlet channels with a diameter of 500 μm, the conical shape of the inlet and outlet to the valving chamber with diameter 210 μm, the valving chamber height and membrane thickness of 245 μm. The surface roughness of the membrane and valve seat is measured to be 3.69±1.32μm.

B. Piezo stack

The piezo stack displacement measurement is done by placing the piezo stack under the laser displacement sensor. In Figure 9 the displacement for the voltage-up path and for the voltage-down path are plotted using a voltage range from 0 to 150V.

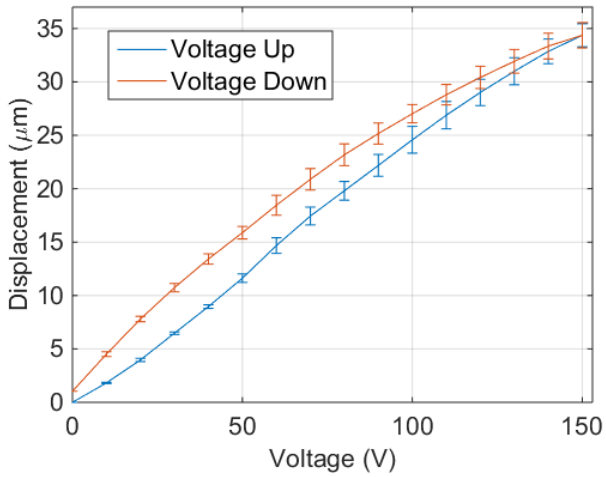

Figure 9: Displacement plot of the piezo stack. The blue curve is measured during voltage-up path and the red curve during voltage-down path. Error-bars indicate one standard deviation of three measurements.

Hysteresis is clearly observed for voltage-displacement graph of the piezo stack. At 0V a remnant polarization causes the voltage-down path to be in a slightly extended position compared to voltage-up path.

The response time of the piezo stack for the start position to the extended position (on the left) and for the extended position to the begin position (on the right) is shown in Figure 10. From begin position (0V) to fully extended position (150V) the response time is 337±4 ms. From fully extended position to begin position the response time is 1.86±0.13 s.

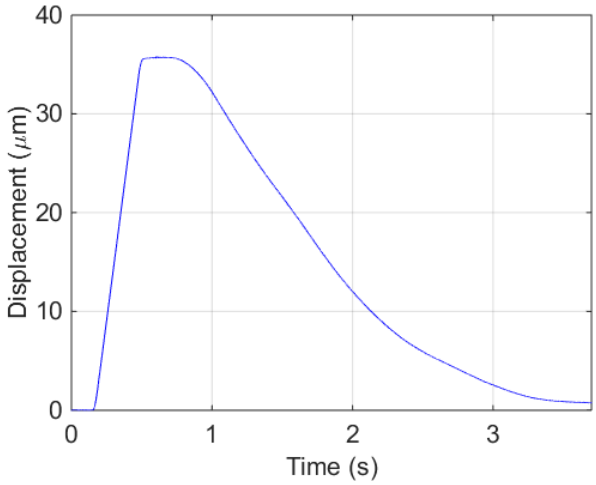

Figure 10: Response time of the piezo stack during elongation (on the left) and compression (on the right).

For different actuation voltage levels the creep rate is shown in Figure 11. At higher voltage levels the extension over time is higher compared to lower voltage levels, which means that more dipoles are polarized when higher voltages are used.

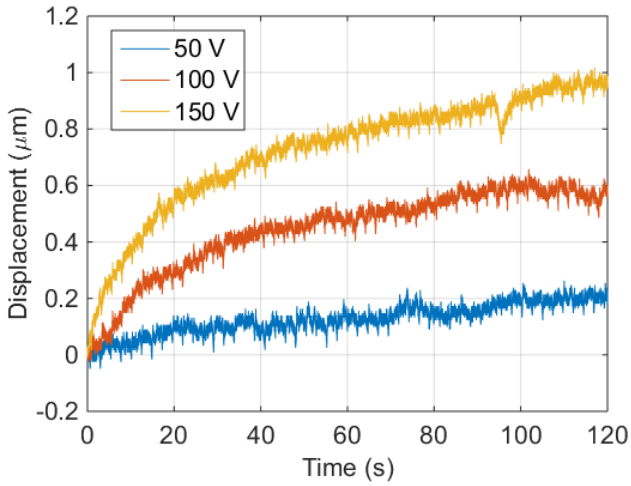

Figure 11: Displacement of the piezo stack over time when the actuation voltage is constant. Different actuation voltages show the corresponding creep rate.

C. Microvalve

Characterisation of the valving behaviour of the microvalve is done using the experimental setup as shown in Figure 12. De-ionized water at room temperature was used in the experiments.

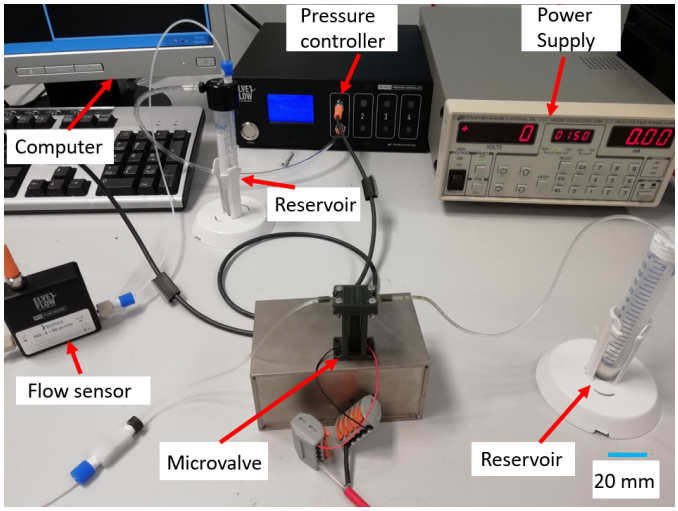

Figure 12: Microvalve test-setup. The microvalve is placed in the centre on a stage to compensate for the height differences with the fluid levels in the reservoirs.

1) Flow rate: As a result of the setup process as discussed in subsection II-A, the maximum distance between the membrane and valve seat is in the range of 34 μm. Otherwise the piezo stack is not able to fully close the chamber inlet. The estimated numerical and analytic flow-rates, using the design parameters of Table IV with varying valving chamber heights (after piezo stack actuation) at 600 mbar, is shown in Figure 13. The flow-sensor limit of 90 $\mu l/min$ is reached when a valving chamber height of around 7 μm is used.

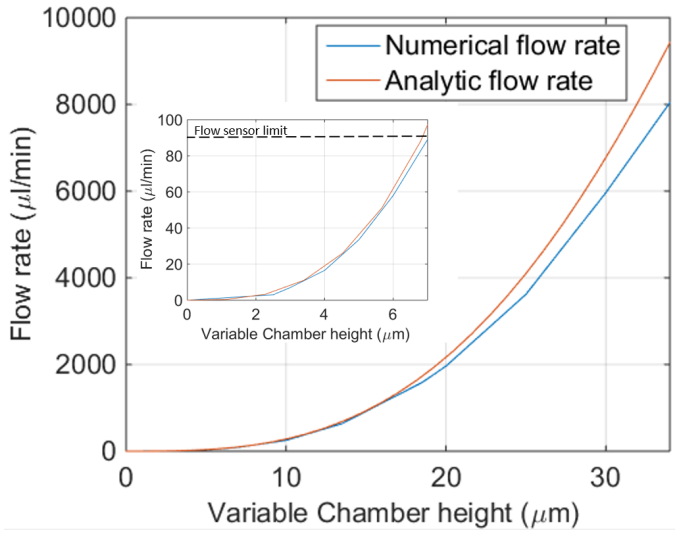

Figure 13: The predicted numerical and analytical flow-rates with varying chamber heights at 600 mbar. The zoom-in plot shows the variable chamber height region with the related flow-rates within the flow-sensor limit of 90 $\mu l/min$.

After the set up process the microvalve behaviour is characterised. The validity of the analytic and numerical models are checked by comparing them with the experimental results. In Figure 14 the results are plotted alongside each other. In this plot the microvalve is fully open and the flow-rate is observed at different pressure levels. The flow sensor limit is 90 $\mu l/min$, so the experimental flow-rate values above this level cannot be measured.

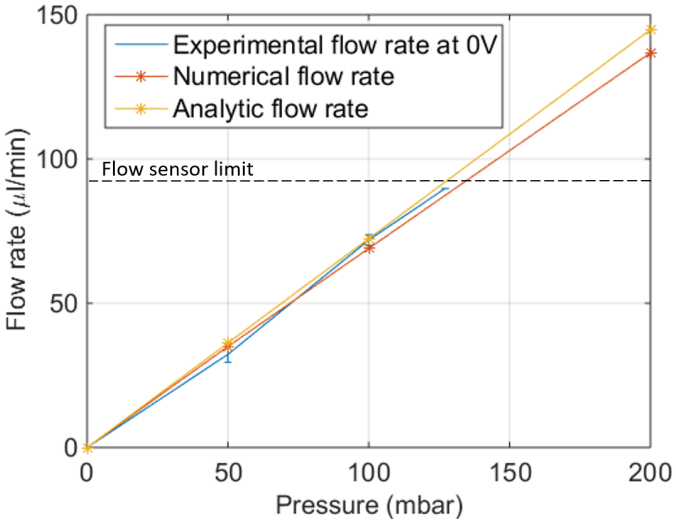

Figure 14: Comparison of the predicted numerical and analytical flow-rates to the measured flow-rates in the microvalve at different pressure levels. The numerical and analytic models assume a valving chamber height of 11.6 µm. Indicated is the flow-sensor limit of 90 $\mu l/min$.

The estimated flow resistances of the micro-channels used in the analytic model are tabulated in Table V, the used design parameters can be found in Table IV. Flow resistances R_1,R_2, R_4 and R_5 are calculated using the equation for circular shaped channels Equation 11 as discussed in subsubsection II-B2. The flow resistance in the valving chamber R_3 is modeled using the equation for rectangular shaped channels Equation 10, while the piezo stack creates a rectangular shaped channel between the membrane and valving seat The numerical and analytic models assume a chamber height after finishing the set up process of 11.6 μm.

Table V: Flow resistances

Resistance	**Value** [Pas/m^3]
R_1	8.7028×10^{9}
R_2	1.8645×10^{10}
R_3	8.2347×10^{12}
R_4	1.8645×10^{10}
R_5	7.1073×10^{9}

When the voltage level is increased from 0 to 150V at pressure levels ranging from 50 to 600 mbar, the valving behaviour shown in Figure 15 is observed. For pressure levels of 200 mbar and above the maximum observed flow-rate is 90 $\mu l/min$. The valving behaviour shows that the microvalve is able to proportionally control the fluid flow, with a precision of $<$3.63 $\mu l/min$.

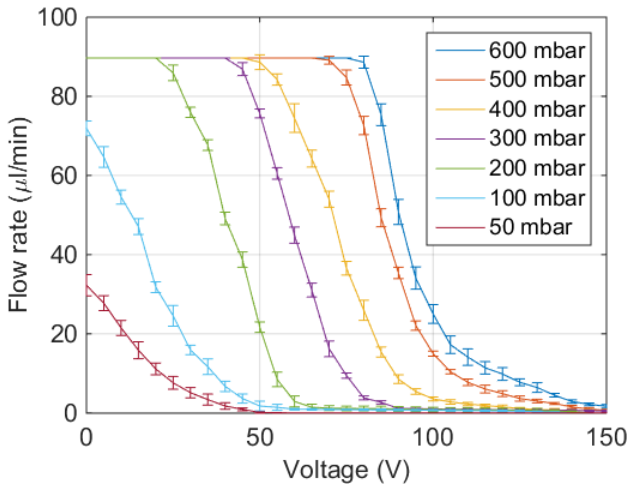

Figure 15: Proportional control of flow-rate at different pressure levels and actuation voltages. Error-bars indicate one standard-deviation of three measurements, with a precision of $<$3.63 $\mu l/min$. Clearly visible is the flow-sensor limit of 90 $\mu l/min$.

For vacuum regions from -50 to -600 mbar the valving behaviour as shown in Figure 16 is observed. The same valving behaviour was expected compared with the 50 to 600 mbar pressure range. The precision of the microvalve in the vacuum region was found to be $<$4.66 $\mu l/min$.

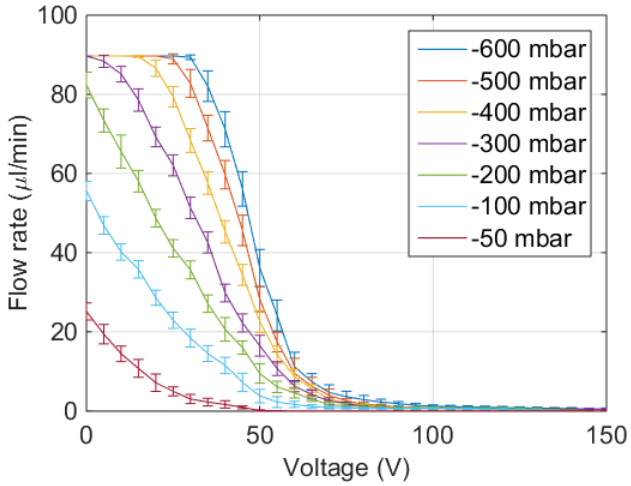

Figure 16: Proportional control of flow-rate at different vacuum levels and actuation voltages. Error-bars indicate one standard-deviation of three measurements, with a precision of $<$4.66 $\mu l/min$.

The stability of the microvalve is characterised in Figure 17. The microvalve is fully closed in each subplot and the measured flow-rate deviation is plotted against time. When a pressure level of -600 mbar is used the flow-rate is stable with some large deviation peaks. At a pressure level of -300 mbar the deviation peaks disappear, but there are still some small deviations. At a pressure level of 600 mbar the deviations are even smaller.

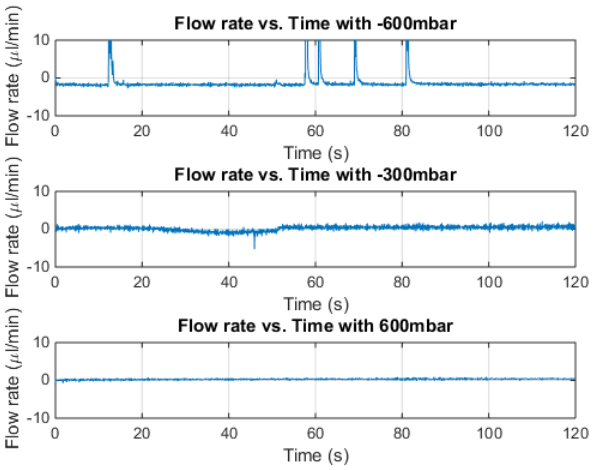

Figure 17: Microvalve stability after being fully closed at different pressure levels.

2) Reproducibility: The reproducibility plot for five fabricated microvalves is shown in Figure 18. After the set up process the chamber height can be calibrated by applying a larger or smaller clamping force, resulting in a varying pressure force of the piezo stack on the membrane. This results in a smaller or larger chamber height causing a change of flow-resistance R_3. The calibration process is sensitive, while too much force results in a low flow-rate and too little force results in a high leakage rate. To replicate the same valving behaviour for each produced microvalve, a calibration point is used. To achieve the best microvalve characteristics the calibration point used in this work is $\pm$70 $\mu l/min$ at 100 mbar when fully opened. The accuracy of the microvalve was found to be $<$17.89 $\mu l/min$.

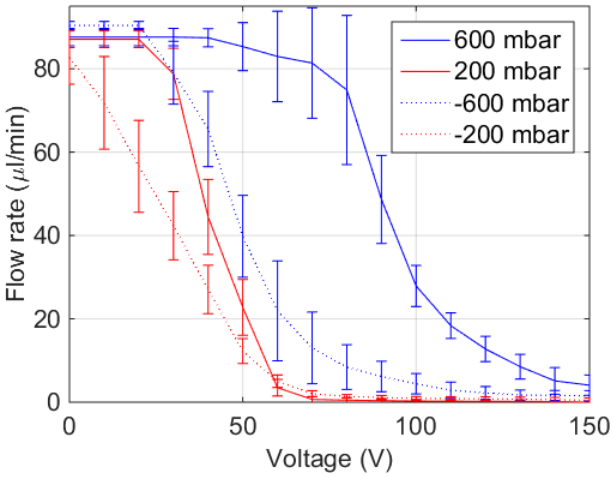

Figure 18: Reproducibility plot for five fabricated microvalves. Each line represents a pressure level and the error bars represent the standard-deviation for five microvalves, with an accuracy of $<$17.89 $\mu l/min$. The microvalves are calibrated on $\pm$70 $\mu l/min$ at 100 mbar when fully opened.

3) Leakage: An important characteristic of microvalves is the leakage rate. In Figure 19 the flow-rates at different pressure levels are plotted for the fully open and fully closed situation. Zero leakage

is achieved for pressure levels up to 200 mbar. The leakage rates are mentioned in the caption.

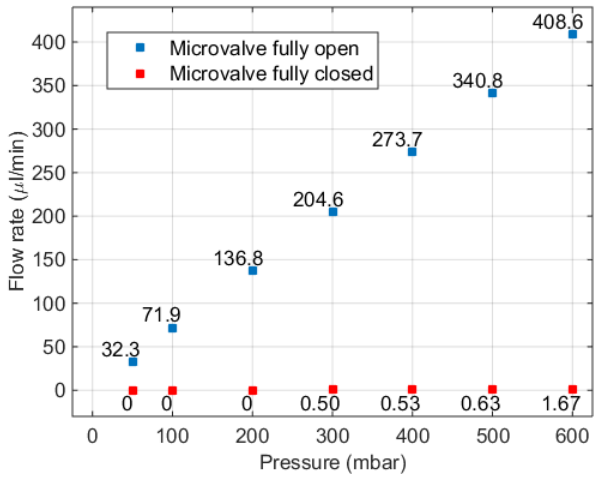

Figure 19: Flow-rate of the microvalve in the fully open and in the fully closed position at different pressure levels. The numbers indicate the flow-rates at the data points. Leakage-rates: 0% (50 mbar), 0% (100 mbar), 0% (200 mbar), 0.24% (300 mbar), 0.19% (400 mbar), 0.18% (500 mbar), 0.41% (600 mbar).

When a larger clamping torque is used (>0.7 Nm) in calibrating the microvalve, the piezo stack is pressed harder on the membrane. This results in a better leakage performance. The results are shown in Figure 20. With this calibration process zero leakage is achieved at a pressure level up to 1.5 bar. Also using the same calibration a small leakage of 0.67 $\pm$0.15 $\mu l/min$ is achieved at a pressure level of 2.0 bar.

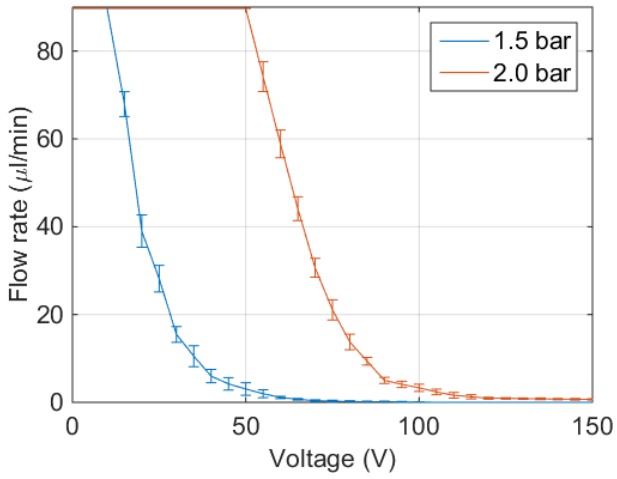

Figure 20: Closing behaviour of the microvalve after using a larger clamping force. Error-bars indicate one standard-deviation of three measurements.

4) Response time: The closing behaviour of the microvalve at 500 and -500 mbar is shown in Figure 21. The closing time for the 500 mbar pressure level is 45.0 $\pm$5.8 ms and for the -500 mbar pressure level 47.8 $\pm$6.8 ms. The closing time is defined as the time needed to reach 10% of the begin flow-rate. The acquisition frequency of the flow-sensor is limited, therefore the acquired data is not smooth. A fit curve is fitted to the acquired data to make a smooth closing curve.

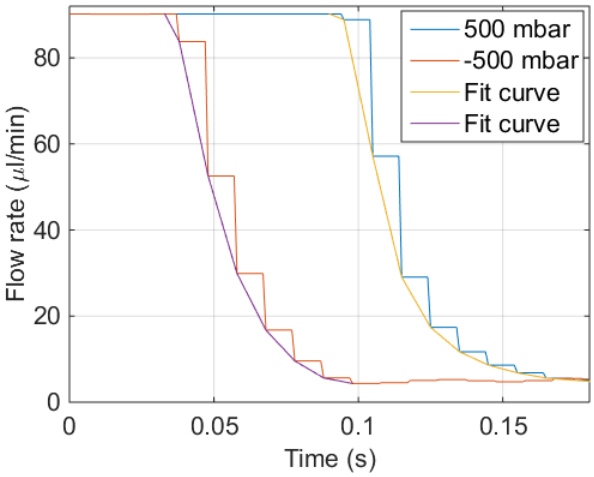

Figure 21: Closing time of the microvalve at 500 and -500 mbar. A fit curve is used to make a smooth closing curve. The closing times are 45.0 $\pm$5.8 ms (500 mbar) and 47.8 $\pm$6.8 ms (-500 mbar).

In Figure 22 the opening behaviour of the microvalve is presented for 500 and -500 mbar. The opening time for the 500 mbar pressure level is 0.79 $\pm$0.25 s and for the -500 mbar pressure level 0.86 $\pm$0.05 s. The opening time is defined as the time needed to reach 90% of the final flow-rate. At the -500 mbar pressure level small deviation peaks are observed.

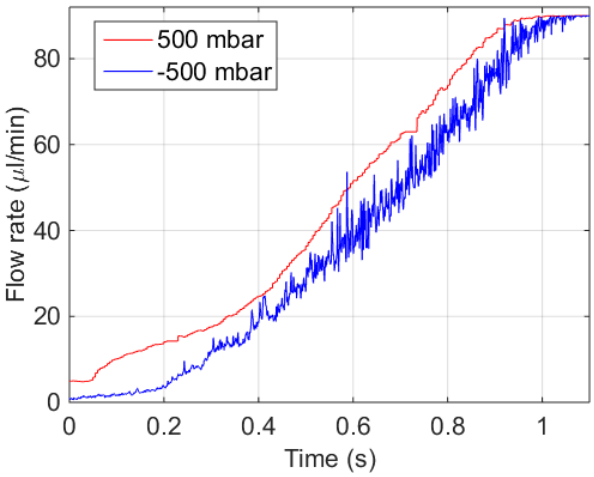

Figure 22: Opening time of the microvalve at 500 and -500 mbar. At 500 mbar vacuum small devation peaks are observed. The opening times are 0.79 $\pm$0.25 s (500 mbar) and 0.86 $\pm$0.05 s (-500 mbar).

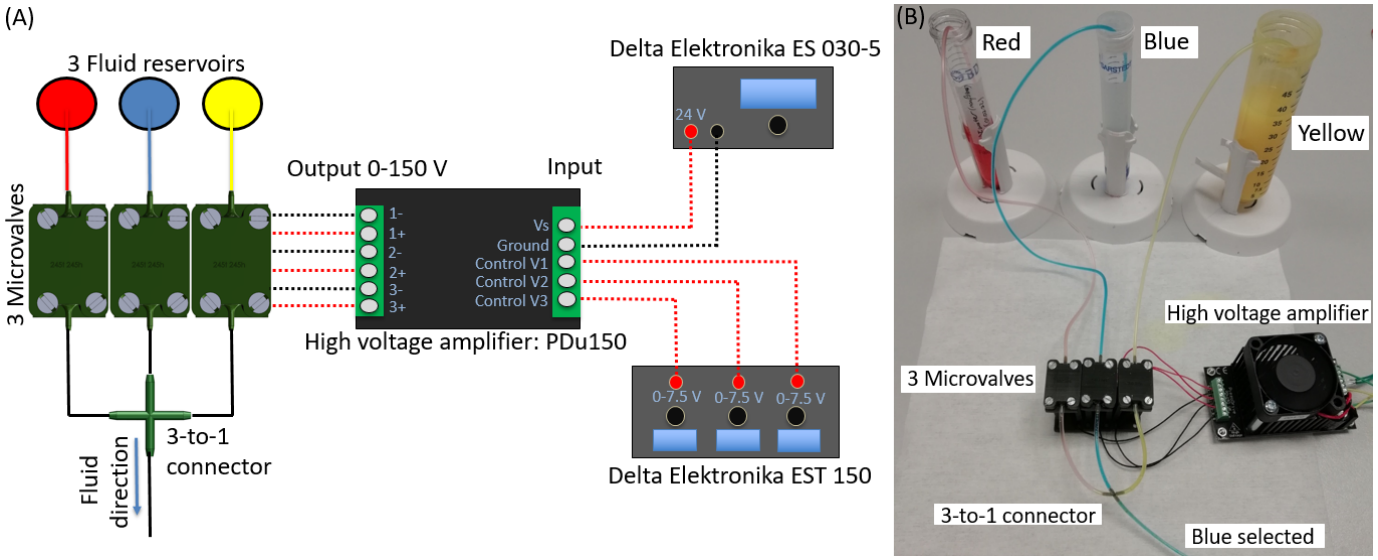

Figure 23: (A) Schematic of the fluid-selector experimental setup (B) Setup of the 3-to-1 fluid selector using three microvalves in parallel. The microvalves are proportionally controlled by the high voltage amplifier. The reservoirs with different colours are connected to the microvalves using a Tygon tubing (ID 1mm). At the output the microvalves are connected with tubings to a 3-to-1 connector. One fluid can be selected forward (blue colored fluid in this Figure).

D. Fluid selector

When multiple microvalves are placed parallel to each other they can function as a fluid selector. A fluid selector selects one fluid forward to the output selecting from multiple reservoirs. An example where a fluid selector can be found is the portable OoC microfluidic platform designed by Zhu et al. [28]. The used commercial available fluid selector (IDEX MHP7970-500-4) selects one reservoir and channels the desired culture medium forward to a mircrofluidic chip. In this OoC platform a vacuum range is used from -157 to -556 mbar, with flow-rate levels between 1.5 to 68 $\mu l/min$. The presented microvalve in this work meets these requirements. To show that the microvalve can be implemented as a portable fluid selector in a system like the OoC platform, a 3-to-1 fluid selector is designed as shown in Figure 23A. Also a small high voltage amplifier (dimensions: 80.0 $\times$ 44 $\times$ 40.4 mm) with low power consumption and with output voltages between 0-150 V is included in the design to present all components needed when a 3-to-1 fluid selector is implemented in a portable system.

In the shown setup three microvalves are placed parallel to each other. The piezo stacks are connected to a portable high voltage amplifier (Piezo Drive, PDu150). This high voltage amplifier has three output channels, with an output ranging from 0-150 V. The output voltage can be proportionally controlled by a control input voltage and the high voltage amplifier is powered by an external power supply of 24 V as discussed in subsubsection III-D3. The microvalves are connected at the input side to the reservoirs by a Tygon tubing (ID 1mm). At the output side the microvalves are connected to a 3-to-1 connector also using Tygon tubings. In the 3-to-1 connector the outputs converge to one output. During experiments the fluid reservoirs are filled with three fluid colors (Red, Blue and Yellow). As shown in Figure 23B, from the three fluid colors the blue fluid is selected forward. In the case the 3-to-1 fluid selector is used in an OoC platform application, the blue fluid can be put forward to a microfluidic Organ-on-Chip.

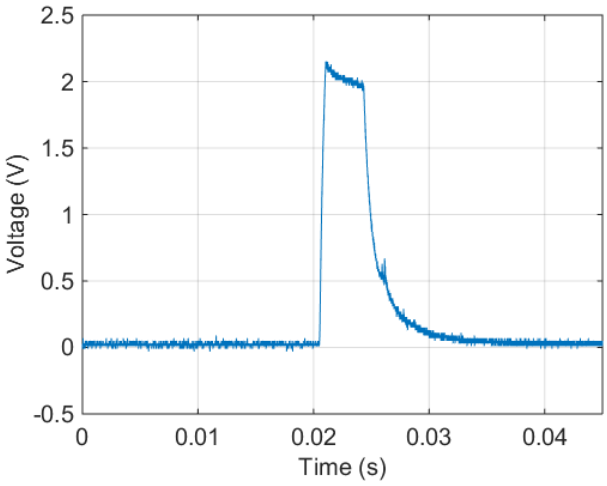

Figure 24: Applied voltage by the portable high voltage amplifier across a resistor connected in series with the piezo stack. Visible are the peak voltage of ∼2.15 V and the stabilized voltage of 53 mV after charging the piezo stack. The time needed to charge the piezo stack is ∼15 ms

The high voltage amplifier has a 24 V input and a 0-7.5 V control voltage for each channel. The measured power consumption for the high voltage amplifier is 3.84 W, when all three channels are used. To measure the power consumption of an individual microvalve, a resistor of 18 ohm is placed in series with the piezo stack output and the ground of the high voltage amplifier. When the voltage is applied to the piezo stack the voltage across the resistor is measured, the measurement results are shown in Figure 24. After a peak voltage of $\sim$ 2.15 V, the voltage across the resistor is stabilized at 53 mV. This voltage is a result of the 'leakage' current. This 'leakage' current transfers in the electric circuit, which consists of the piezo stack connected in series with the resistor. The leakage current is (using

Ohm's law) 53/18=2.95 mA. This means that the power consumption of the piezo stack is 150 $\times$ 2.95 = 442.5 mW. Also from Figure 24 it can be observed that the response time of the amplifier to charge the piezo stack is measured to be $\sim$15 ms. The output noise of the high voltage amplifier is 89.9 mV RMS.

V. Discussion

In this section the fabrication and experimental results are discussed. Also recommendations for further research are presented. Subsequently a comparison is made between the requirements and the measured results.

A. Fabrication

During fabrication of the micro-channels the chamber inlet and chamber outlet were chosen to be conical shaped with a diameter (d_2 and d_4) of 210 μm on one side and at the other side of the cone a diameter of 900 μm. The smallest channel was fabricated using this shape, while cylindrical shaped channels were clogged when a diameter of 210 μm was used. As discussed in subsection IV-A the analytic and numerical models show that a chamber inlet diameter for both, d_2 and d_4, of 37.8 μm and 47.4 μm is needed respectively, when a desired flow-rate of 100 $\mu l/min$ at a pressure of 600 mbar and a valving chamber height h_3 (piezo stack expansion) of 34 μm is assumed. The desired flow-resistance could not be fabricated, which means that higher flow-rates are achieved. In addition it turned out that the valving chamber flow resistance was much higher than the other flow resistances in the microvalve as shown in Table V. This makes that the dimensions and shape of the chamber inlet/outlet doesn't have a lot of influence on the flow-rate. This doesn't mean that minimizing the chamber inlet/outlet diameter is not important, while it can be used to minimize leakage. If a smaller area needs to be closed by the membrane a better leakage performance can be achieved.

The fabricated membrane has a thickness of 245 μm and a chamber height of 245 μm. In the experimental study also intact membranes with a thickness of 210 μm and a chamber height of 210 μm were fabricated, but they were less robust. So to be safe, membranes with a thickness of 245 μm and a chamber height of 245 μm were preferred during the experiments.

Ideally the chamber inlet/outlet diameter, valving chamber height and membrane thickness are smaller, but they are limited by the 3D printer resolution and the resin quality. In further research microvalves with smaller dimension can be explored using better 3D printers with resins of higher quality.

It is important to flush the micro-channels first properly with IPA to remove all the resin residue. Thereafter the IPA needs to be flushed with DI-water in order to be used in experiments.

The assembly process of the microvalve is manual, meaning that there is an introduction of the human error. The main step where uncertainty is introduced is during the clamping of the microvalve base to the frame. This can result in a too large/small clamping force and in misalignment of the piezo stack on the membrane. The maximum torque on the bolts to clamp the microvalve base was $\sim$0.7 Nm, measured using a torque screw driver. To further minimize the components used in the microvalve it can be examined in future research if the O-rings can be replaced by 3D printed compliant mechanisms. This way a single 3D printed part is fabricated where the microvalve base and frame are connected by a 3D printed compliant mechanism. In addition the misalignment will be smaller.

B. Piezo stack

To validate the working principle of the designed microvalve, an available piezo stack was used to make the first prototypes of the microvalve. Manufacturer data indicated that the displacement of the piezo stack will be in the range of 42 μm $\pm$10%, but from experiments the displacement was found to be 34 μm.

The piezo stack displays non linear behaviour like hysteresis and creep. Hysteresis and creep causes positioning inaccuracies, which can be solved by a feedback loop. An example is found in blood pressure waveform monitoring, where a capacitive displacement sensor can proportionally control the flow-rate in a microvalve using a feedback controller [40]. Another method to solve the non linear behaviour is to use charge control instead of voltage control [41]. There is a linear relation between charge across the piezo stack and the displacement, hence controlling the charge can eliminate non linear behaviour.

The closing time of the piezo stack (45.0$\pm$5.8 ms at 500 mbar) is quite large compared to other piezo stacks in literature. The reason for this lies in the large capacitance of 4.3 μF of the used piezo stack. For example one piezo stack in literature has a response time of 700 μs, with a capacitance of $\sim$700 nF [39]. Another example has a response time of 0.6 ms, with a capacitance of 983 nF [17]. To have a faster charging and discharging of the piezo stack, which result in a faster response time, a lower capacitance of the piezo stack is needed in future work. If smaller n is used in Equation 2 the capacitance will decrease accordingly, resulting in a faster response time. This can be achieved by for example using a smaller piezo stack.

To scale down the dimensions of the piezo stack, without losing the stroke, mechanical amplification can be used. The amplification mechanisms augment the displacement of the piezo stack using a leverage structure. A commercial available mechanical amplification mechanism is used in a microvalve designed by Fazal et al. [35], where a stroke is achieved of 80 μm $\pm$10% using a piezo stack (including amplification mechanism) with a dimension of 8 x 10 x 17 mm.

C. Microvalve

1) Flow-rate: The predicted flow-rates in Figure 13 using different chamber heights at 600 mbar indicate that the wanted flow-rate of 100 $\mu l/min$ can easily be achieved when the chamber height is 34 μm. The minimum required chamber height to achieve this flow-rate is $\sim$7.1 μm. This also show that in future research smaller piezo stacks can be used.

The numerical and analytic models match closely with the experimental results. The measured values have a limit of 90 $\mu l/min$, as a result of which the flow-rates at higher pressure levels could not be measured. The predicted flow-rate of the microvalve at 600 mbar, using the numerical model, is 408.6 $\mu l/min$. For calculating the flow resistances in Table V it is assumed that flow resistances R_2 and R_4 are cylindrical shaped resistances, while they are in fact conical shaped. This assumption doesn't have major influence on the total flow resistance of the microvalve. Another assumption made was to model flow-resistance R_3 as a rectangular shape. The piezo stack creates due to its high stiffness and its shape a rectangular shaped channel between the membrane and the valve seat. For both the numerical and analytic model the valving chamber height of flow resistance R_3 was chosen to be 11.6 μm. It turned out from the experimental results that the chamber height was 11.6 μm. Ideally a chamber height of 34 μm is obtained, the same value as the stroke of the piezo stack. During the set up process the valving chamber height was reduced. Due to human errors it is impractical to achieve a perfect chamber height of 34 μm.

Proportional control of the flow-rate in the microvalve is clearly observed in Figure 15 and Figure 16. In both figures it is shown that

first the flow-rate decreases fast, after which the flow-rate seems to asymptotically decrease to zero. During asymptotically decreasing of the flow-rate the membrane flattens on the valve seat. In the experiments the pressure range from -600 to 600 mbar was explored. The projected maximum blocking pressure is $900/2.5 \cdot 10^{-5}$ = 360 bar (the blocking force divided by the cross section of the piezo stack). It was expected that Figure 15 and Figure 16 had the same valving behaviour, but it turned out that using vacuum caused problems. Leakages appeared at the connections between the tubings and flow-sensor and between the tubings and reservoir. Due to the leakages air is sucked into the circuit creating air bubbles, which caused vacuum fluctuations in the microfluidic system. Although the leakages were minimized and resolved were possible, it still had an effect on the obtained results. When using positive pressure it turned out that the remaining leakages didn't cause problems, however in the vacuum regime it still remained an issue. This is also visualised in Figure 17 where the pressure fluctuations create peaks in the flow-rate plot in the vacuum regime. When a lower vacuum level is used the flow-rate peaks gets smaller. In contrary to the vacuum levels the positive pressure doesn't have large pressure fluctuations, as a result of which there are only small flow-rate deviations

When a vacuum source is used as fluid flow control mechanism like in the OoC microfluidic platform designed by Zhu et al. [28] a negative pressure in the valving chamber of the microvalve is created. This can influence the flow-rate in a microvalve, while the vacuum can pull downward the moving membrane and possibly close the inlet or reduce the valving chamber volume. Especially low stiffness membranes can have this problem when using vacuum. The presented microvalve in this work is tested for pressures at vacuum level up to -600 mbar.

2) Reproducibility: The microvalve was relatively easy to reproduce. In Figure 18 five microvalves are used to characterise the standard deviation of the flow-rate at different pressure levels. The manual calibration causes a reproducibility accuracy of <17.89 $\mu l/min$. In each microvalve a slightly different clamping force was used, which resulted in small differences in the microvalve characteristics. The used calibration flow-rate is experimentally determined, with which the best flow-rate characteristics were obtained. A solution to the manual calibration could be bonding of the microvalve base to the frame.

3) Leakage: In Figure 19 the flow-rates at pressure levels above 200 mbar are estimated using the numerical model, because experimental data is not available due to the flow-sensor limit. The numerical model is used, while it gives a more conservative estimation of the flow-rate compared to the analytical model.

The main causes of leakage are the surface roughness and the manual assembling. The surface roughness is determined to be 3.69 $\pm 1.32 \mu m$, which means that when the microvalve is closed fluid can slip through imperfections. The manual assembling can cause tilting of the membrane on the valve seat, through which some areas of the membrane are touching the valve seat with higher forces than other parts. When higher contact forces are used, less leakage is expected while more material pressing is created. This material pressing flattens out the surface roughness, preventing fluid passage. A method to decrease the leakage is using valve seat trenches [42]. With this method the contact area between the valve seat and membrane is decreased. This results in higher contact pressures causing surface defects to flatten out.

When a higher clamping force is used, the leakage performance improves as shown in Figure 20. The microvalve has in this case leakage free closing characteristics up to 1.5 bar. The designed microvalve is leakage free at high pressure levels, in contrary to some microvalves in literature where this is a problem. For example a microvalve designed by Groen et al. [24] has a leakage of 370 $\mu l/min$ at 1 bar. Another microvalve, designed by Gunda et al [20], has a leakage of 0.76 $\mu l/min$ at 1 bar. Leakage free operation of microvalves is a key requirement for OoC application, this prevents contamination of culture media when one culture medium is selected forward to the OoC.

4) Response time: The closing time of the microvalve (Figure 21), is smaller than the time it needs to fully expand (Figure 10). This faster response time is evidence for a smaller chamber height than the 34 μm of the piezo stack displacement. The closing time for 500 mbar and -500 mbar are closely matched, as expected. On the other hand in Figure 22 the opening times of the -550 mbar pressure level is larger than the 550 mbar pressure level. This is probably related with the vacuum problem, where due to small leakages in the experimental setup the pressure built up fluctuates. This also explains the small deviation peaks.

D. Fluid selector

The power consumption of the microvalve is 442.5 mW, which is high compared to other piezo stack actuated microvalves in literature. For example the microvalve designed by Yang et al. [43] uses 3 mW in stationary state and another microvalve designed by Zhang et al. [17] uses 48 mW. To reduce the power consumption of the microvalve the 'leakage' current has to decrease. The leakage current is a consequence of humidity, surface contamination or other potential charge paths. Charge transport in a capacitor is given by:

$$I = \frac{dQ}{dt} = C\frac{dV}{dt} \tag{13}$$

This means that the produced current I is linearly related with the capacitance C of the piezo stack. When reducing the capacitance, less 'leakage' current will flow, resulting in a lower static power consumption. Another way to reduce the static power consumption is to use a microvalve with a normally closed (NC) initial state instead of a normally open (NO) initial state like the microvalve presented in this work. When for example the 3-to-1 fluid selector is used, one microvalve is open while the other two needs to be closed. This means that two microvalve consumes power. When the microvalves are NC, only one microvalves needs to be actuated. Also the NC microvalves have the advantage, when used in OoC applications, that when there is no power (for whatever reason) the microvalves are closed and not wanted culture media is obstructed to flow to the OoC.

The power consumption of the microvalve is 442.5 mW, but when it is implemented in a portable OoC platform the total power consumption will also include the power of the high voltage amplifier. This means that the total power consumption will be 3.84 W in the case of 3 implemented microvalves, instead of 3×442.5 = 1.328 W. In literature this is not mentioned, while it is important to take into account. It also emerged during experiments that the charging and discharging of the portable high voltage amplifier (Piezo Drive, PDu150) is faster than the high voltage power supply (Stanford research systems Inc. PS310). This can influence results when time is a factor, for example in determining the response time. It turned out that the opening time for the microvalve, when the high voltage power supply is used, is $\sim$10x higher than when the portable high voltage amplifier is used. For the experiments in this work the portable high voltage amplifier is used, so the charge and discharge influence is minimized.

E. Achieved results

In Table VI a comparison is made between the target specifications and the measured performance of the microvalve.

Table VI: Target values compared to measured values

Parameter	Target Value	Measured Value
Microvalve		
Flow range	0-100 $\mu l/min$	0-410 $\mu l/min$ (tested till 90 $\mu l/min$)
Leakage	0% at 550 mbar	0% until 200 mbar* 0.41% at 600 mbar* 0% until 1.5 bar **
Pressure range	-600 mbar up to 600 mbar	-600 mbar up to 2 bar
Closing time	100 ms at 500 mbar	45 ms at 500 mbar
Opening time	100 ms at 500 mbar	0.79±0.25 s at 500 mbar
Power	50 mW	442.5 mW
Dimension	61.1 × 49.5 × 20.5 mm	43.5 × 23.5 × 15 mm
Costs	€ 345	€ 151.1
3-to-1 fluid selector		
Power	1.75 W	3.84 W
Dimension	61.6 × 61.1 × 49.5 mm	70.5 × 45 × 43.5 mm High voltage amplifier: 80.0 × 44 × 40.4 mm
Costs	€ 1037.6	€ 789

* Calibrated at 100 mbar ** Calibrated at 1.5 bar

The microvalve meets the target requirements on design parameters like flow-rate range, leakage-rate, pressure range and costs. Next to that it is shown that a microvalve can be fabricated using 3D printing. On design parameters like opening time and power consumption the microvalve doesn't meet the requirements. The limits are found in the large capacitance of the piezo stack, which results in longer discharging and higher 'leakage currents' of the piezo stack. This can be solved by using smaller piezo stacks. The drawback of using a smaller piezo stack is the smaller stroke, but this can be solved by using the piezo stack in combination with a displacement amplification mechanism if larger strokes are required. In future work if a 3D printer is available with higher printing resolution in combination with a better resin, smaller dimensions can be printed. This allows printing of smaller unclogged micro-channels, resulting in better design of flow-rates below 100 $\mu l/min$. Next to that smaller valving chamber heights can be printed, so no set up process is needed. Additionally smaller membrane thicknesses can be printed allowing more flexibility of the membrane if desired. Regarding the 3-to-1 fluid selector it meets the target requirements on costs and on portability, which makes it implementable in microfluidic platforms. On design parameters like power consumption and dimension the targets are not achieved. The limits are found in the high voltage amplifier, which increases the overall dimension and the total power consumption significantly. In future work it should be taken into account that when designing microvalves for portable devices using piezo electric actuation the high voltage amplifier has a negative impact on power consumption and footprint.

Compared to the state of the art microvalves, the presented microvalve in this work can be further improved on the flow-rate range, the pressure range, power consumption and dimensions. See the conclusion chapter for a comparison table between the designed microvalve and the state-of-the-art microvalves. The microvalve was designed and fabricated for the requirements typical for microfluidic OoCs, in contrary to the state-of-the-art microvalves which are mostly used in high pressure gas applications. The fabricated microvalve in this work has a projected fluid flow-rate range of 0-410 $\mu l/min$, while for example the Bürkert type 6724B has a fluid flow-rate range of 0-166.7 ml/min using solenoid actuation. The pressure range of the microvalve in this work is -600 mbar up to 2 bar, while for example the silQflo® Silicon Servo Valve has a pressure difference range of 0-34.5 bar using electro thermal actuation. This actuation type however has the disadvantage of a high power consumption of 5 W, but the advantage of small dimensions 10.8×4.83×2.23 mm. The microvalve in this work stands out in 3D printing of the microfluidic connections, micro-channels and membrane in one single piece, thereby preventing misalignment and leakages at clamping regions. In contrary to existing microvalves which use different pieces to assemble the same one single printed piece, thereby increasing fabrication steps. The presented microvalve in this work was specifically designed on monolithically printing the microvalve structures and on meeting the OoC requirements. In future work the performance boundaries of the designed microvalve can be explored further especially focusing on the weak spots in comparison with the state-of-the-art microvalves.

VI. Conclusion

In this work a 3d printed proportionally controlled microvalve is presented actuated by a commercially available piezo stack. The microvalve is monolithically printed with a bio compatible resin using an easy to use 3D printer. Using 3D printing is a benefit, while most microvalves in literature use silicon micro-machining, which is a rather complex manufacturing process. The micro-channels, membrane and microfluidic connections are printed in one part which is novel compared to existing microvalves.

The microvalve is designed for OoC applications. During experiments the microvalve was tested with Di-water. The measured flow-rate range is 0-90 $\mu l/min$ and the projected flow-rate range is 0-410 $\mu l/min$. The used piezo stack is controlled within a voltage range of 0-150 V. It has a dimension of 5×5×36 mm and a measured displacement of 34 μm. The large actuation force of the piezo stack ensures a wide pressure range of -600 mbar to 2 bar. In addition the microvalve can operate leakage free after calibration up to 1.5 bar and has a closing time of 45 ms at 500 mbar. In Table VII the measured results of the microvalve are shown.

Next to characterising the microvalve an experimental study is performed in which the optimal chamber inlet/outlet channel parameters are explored. Subsequently the minimum thickness of the membrane is found to print an intact membrane at a certain chamber height and membrane radius. Recommendations are made to decrease the response time and power consumption. Also further research opportunities are provided on increasing the piezo stack displacement, leakage reduction and fabrication improvements.

Table VII: Measured results

Parameter	Value
Microvalve	
Flow range	0-410 $\mu l/min$ (tested till 90 $\mu l/min$)
Leakage	0% until 200 mbar* 0.41% at 600 mbar* 0% until 1.5 bar **
Pressure range	-600 mbar up to 2 bar
Closing time	45.0 ms at 500 mbar
Opening time	0.79±0.25 s at 500 mbar
Operating Voltage	0-150 V
Initial state	Normally open
Power consumption	442.5 mW (static state)
Power consumption	3.6 W (Including high voltage amplifier)
Precision	<4.66 $\mu l/min$
Accuracy	<17.89 $\mu l/min$
Dimension	23.5 × 15 × 43.5 mm
Costs	€ 151.1
3-to-1 fluid selector	
Power consumption	3.84 W
Dimension	70.5 × 45 × 43.5 mm High voltage amplifier: 80.0 × 44 × 40.4 mm
Costs	€ 789

* Calibrated at 100 mbar ** Calibrated at 1.5 bar

A portable 3-to-1 fluid selector is designed, which can be used in a microfluidic platform for OoC applications. In this 3-to-1 fluid selector three microvalves are connected in parallel and are actuated by a high voltage amplifier. The fluid selector selects one culture medium from three fluid reservoirs and channels the culture medium forward to the output. The total power consumption of the 3-to-1 fluid selector is 3.84 W. The piezo stack consumes 442.5 mW in stationary state. In Table VII also the measured results of the 3-to-1 fluid selector are shown. Due to its versatility in manufacturability, wide pressure range and leakage performance there are a lot of opportunities for the presented microvalve in future work.

REFERENCES

[1] Zhang, C., Xing, D., Li, Y. (2007). Micropumps, microvalves, and micromixers within PCR microfluidic chips: Advances and trends. Biotechnology advances, 25(5), 483-514.

[2] M. B. Coskun et al., "A MEMS Microvalve Array For Gas Flow Control," 2022 IEEE 35th International Conference on Micro Electro Mechanical Systems Conference (MEMS), 2022, pp. 466-469, doi: 10.1109/MEMS51670.2022.9699667.

[3] Zhu, J. (2020). Application of organ-on-chip in drug discovery. Journal of Biosciences and Medicines, 8(3), 119-134.

[4] Teworte, S., Malcı, K., Walls, L. E., Halim, M., Rios-Solis, L. (2021). Recent advances in fed-batch microscale bioreactor design. Biotechnology advances, 107888.

[5] Qian, J. Y., Hou, C. W., Li, X. J., Jin, Z. J. (2020). Actuation mechanism of microvalves: A review. Micromachines, 11(2), 172.

[6] Whitesides, G. M. (2006). The origins and the future of microfluidics. nature, 442(7101), 368-373.

[7] Lu, H. T., Qin, Y., Gianchandani, Y. (2021). A Microvalve Module with High Chemical Inertness and Embedded Flow Heating for Microscale Gas Chromatography. Sensors, 21(2), 632.

[8] Team, E. (2021). PDMS Quake valves and co: a review. Elveflow.

[9] Shi, H., Cao, Y., Zeng, Y., Zhou, Y., Wen, W., Zhang, C., ... Chen, Z. (2022). Wearable tesla valve-based sweat collection device for sweat colorimetric analysis. Talanta, 123208.

[10] Oh, K. W., Ahn, C. H. (2006). A review of microvalves. Journal of micromechanics and microengineering, 16(5), R13.

[11] Yoshida, K., Tanaka, S., Hagihara, Y., Tomonari, S., Esashi, M. (2010). Normally closed electrostatic microvalve with pressure balance mechanism for portable fuel cell application. Sensors and Actuators A: Physical, 157(2), 290-298.

[12] Li, H. Q., Roberts, D. C., Steyn, J. L., Turner, K. T., Yaglioglu, O., Hagood, N. W., ... Schmidt, M. A. (2004). Fabrication of a high frequency piezoelectric microvalve. Sensors and Actuators A: Physical, 111(1), 51-56.

[13] Takao, H., Miyamura, K., Ebi, H., Ashiki, M., Sawada, K., Ishida, M. (2005). A MEMS microvalve with PDMS diaphragm and two-chamber configuration of thermo-pneumatic actuator for integrated blood test system on silicon. Sensors and Actuators A: Physical, 119(2), 468-475.

[14] Aravind, T., Kumar, S. P., Raj, G. K. F., Prasanth, P., Gobinath, P. S. (2013, March). A novel thermopneumatic based micropump and microvalve using phase change liquid. In INTERNATIONAL CONFERENCE ON SMART STRUCTURES AND SYSTEMS-ICSSS'13 (pp. 66-69). IEEE.

[15] Liu, T. G., Wu, J., Xia, C., Qian, Z. H. (2012). A microvalve driven by a ferrofluid-based actuator. In Advanced Materials Research (Vol. 433, pp. 3767-3772). Trans Tech Publications Ltd.

[16] Thuillier, G., Malek, C. K. (2005). Development of a low cost hybrid Si/PDMS multi-layered pneumatic microvalve.

[17] Zhang, D.; Lv, J.; Jiang, Y.; Chen, H.; Fu, J. A piezoelectric microvalve with a flexure- hinged driving frame and microfabricated silicon sealing pair. Mechatronics 2014, 24, 511–518.

[18] Hagstrom, N. P., Fikru, N., Hargus, A. M., Chase, T. R. (2019). A novel piezoelectrically driven miniature proportional pneumatic control valve utilizing a microfabricated orifice array. IEEE/ASME Transactions on Mechatronics, 24(5), 1931-1941.

[19] Lee, C., Yang, E. H., Saeidi, S. M., Khodadadi, J. M. (2006). Fabrication, characterization, and computational modeling of a piezoelectrically actuated microvalve for liquid flow control. Journal of microelectromechanical systems, 15(3), 686-696.

[20] Gunda, A., Özkayar, G., Tichem, M., Ghatkesar, M. K. (2020). Proportional microvalve using a unimorph piezoelectric microactuator. Micromachines, 11(2), 130.

[21] Choonsup, L., Eui-Hyeok Y., Saeidi S. M. and Khodadadi J. M. (2006), Fabrication, characterization, and computational modeling of a piezoelectrically actuated microvalve for liquid flow control (vol. 15, no. 3, pp. 686-696). Journal of Microelectromechanical Systems. doi: 10.1109/JMEMS.2006.876783.

[22] Dibon, M., Pautasso, G., Griener, M., Herrmann, A., Mertens, V., Neu, R., Ploeckl, B. (2017). Piezo-driven valve for disruption mitigation studies in tokamaks. Fusion Engineering and Design, 123, 797-801.

[23] Chen, S., Lu, S., Liu, Y., Wang, J., Tian, X., Liu, G., Yang, Z. (2016). A normally-closed piezoelectric micro-valve with flexible stopper. Aip Advances, 6(4), 045112.

[24] Groen, M. S., Brouwer, D. M., Lötters, J. C., Wiegerink, R. J. (2015). Miniature proportional control valve with top-mounted piezo bimorph actuator with millisecond response time. Journal of micromechanics and microengineering, 25(10), 105008.

[25] Kim, J. H., Na, K. H., Kang, C. J., Jeon, D., Kim, Y. S. (2004). A disposable thermopneumatic-actuated microvalve stacked with PDMS layers and ITO-coated glass. Microelectronic engineering, 73, 864-869.

[26] Özkayar, G., Lötters, J. C., Tichem, M., Ghatkesar, M. K. (2022). Toward a modular, integrated, miniaturized, and portable microfluidic flow control architecture for organs-on-chips applications. Biomicrofluidics, 16(2), 021302.

[27] Low, Z. X., Chua, Y. T., Ray, B. M., Mattia, D., Metcalfe, I. S., Patterson, D. A. (2017). Perspective on 3D printing of separation membranes and comparison to related unconventional fabrication techniques. Journal of membrane science, 523, 596-613.

[28] Zhu, H., Özkayar, G., Ghatkesar, M. K.(2020). Portable and Integrated Organ-On-Chip Platform Using Off-the-shelf Components.

[29] Huh, D. (2015). A human breathing lung-on-a-chip. Annals of the American Thoracic Society, 12(Supplement 1), S42-S44.

[30] Kim, H. J., Huh, D., Hamilton, G., Ingber, D. E. (2012). Human gut-on-a-chip inhabited by microbial flora that experiences intestinal peristalsis-like motions and flow. Lab on a Chip, 12(12), 2165-2174.

[31] Oh, K. W., Lee, K., Ahn, B., Furlani, E. P. (2012). Design of pressure-driven microfluidic networks using electric circuit analogy. Lab on a Chip, 12(3), 515-545.

[32] Bruus, H.(2008). Theoretical Microfluidics. Oxford. Oxford University Press.

[33] "Piezo stack SA050536 Data sheet". Accessed on 15-07-22. https://www.piezodrive.com/actuators/150v-piezo-stack-actuators-2/

[34] Schmidt, R. M., Schitter, G., Rankers, A. (2014). The design of high performance mechatronics-: high-Tech functionality by multidisciplinary system integration. Ios Press, 428.

[35] Fazal, I., Elwenspoek, M. C. (2007). Design and analysis of a high pressure piezoelectric actuated microvalve. Journal of micromechanics and microengineering, 17(11), 2366.

[36] Qin, R., Duan, C. (2017, October). The principle and applica-

tions of Bernoulli equation. In Journal of Physics: Conference Series (Vol. 916, No. 1, p. 012038). IOP Publishing.
[37] Timoshenko, S., Woinowsky-Krieger, S. (1959). Theory of plates and shells (Vol. 2, pp. 240-246). New York: McGraw-hill.
[38] Dixon, P. G., Muth, J. T., Xiao, X., Skylar-Scott, M. A., Lewis, J. A., Gibson, L. J. (2018). 3D printed structures for modeling the Young's modulus of bamboo parenchyma. Acta biomaterialia, 68, 90-98.
[39] Park, J. M., Taylor, R. P., Evans, A. T., Brosten, T. R., Nellis, G. F., Klein, S. A., ... Gianchandani, Y. B. (2007). A piezoelectric microvalve for cryogenic applications. Journal of Micromechanics and Microengineering, 18(1), 015023.
[40] Groen, M. S., Wu, K., Brookhuis, R. A., van Houwelingen, M. J., Brouwer, D. M., Lötters, J. C., Wiegerink, R. J. (2014). A piezoelectric micro control valve with integrated capacitive sensing for ambulant blood pressure waveform monitoring. Journal of micromechanics and microengineering, 24(12), 125020.
[41] Zhong, J., Nishida, R., Shinshi, T. (2021, June). Digital charge control for reducing nonlinearity in fast steering mirrors driven by piezoelectric actuators. In 2021 IEEE 30th International Symposium on Industrial Electronics (ISIE) (pp. 1-6). IEEE.
[42] Durasiewicz, C. P., Güntner, S. T., Maier, P. K., Hölzl, W., Schrag, G. (2021). Piezoelectric Normally Open Microvalve with Multiple Valve Seat Trenches for Medical Applications. Applied Sciences, 11(19), 9252.
[43] Yang, E. H., Lee, C., Mueller, J., George, T. (2004). Leak-tight piezoelectric microvalve for high-pressure gas micropropulsion. Journal of Microelectromechanical systems, 13(5), 799-807.

4 Conclusion and Recommendations

4.1 Conclusion

This report starts with a literature review on the state-of-the art microvalves and the state-of-the-art microfluidic multiplexers. A research question was proposed with the goal to design, fabricate and implement a modular microvalve suitable for OOC applications. In the subsequent paper a monolithically 3D printed microvalve actuated with a piezo stack was presented. In this paper the focus is on simplifying the manufacturing process, resulting in only using a 3D printer for fabricating all main components of the microvalve. This fabrication technique is a less complex method compared to Silicon-micromachining, which is used by most microvalves in literature and industry. Next to simplifying the manufacturing process the goal was to achieve the targets arising from OOC applications as shown in Table 11. The main requirements are the leakage-rate, flow-rate and pressure range. The microvalve achieved a leakage of 1.67 $\mu l/min$ at 600 mbar (calibrated at 100 mbar), but it was also shown that after using higher clamping forces zero-leakage could be reached up to 1.5 bar (calibrated at 1.5 bar). The microvalve was tested at pressures of -600 mbar up to 2 bar and a flow-rate range of 0-90 was measured with a projected flow-rate range of 0-410 $\mu l/min$. The achieved specifications are also shown in Table 11. In addition to the design and fabrication of the presented microvalve an application of the microvalve is shown, where a fluid selector with three channels is designed and tested.

Table 11: Target values compared to measured values

Parameter	**Target Value**	**Measured Value**
Microvalve		
Flow range	0-100 $\mu l/min$	0-410 $\mu l/min$ (tested till 90 $\mu l/min$)
Leakage	0% at 550 mbar	0% until 200 mbar* 0.41% at 600 mbar* 0% until 1.5 bar **
Pressure range	-600 mbar up to 600 mbar	-600 mbar up to 2 bar
Closing time	100 ms at 500 mbar	45 ms at 500 mbar
Opening time	100 ms at 500 mbar	0.79±0.25 s at 500 mbar
Power	50 mW	442.5 mW
Dimension	61.1 × 49.5 × 20.5 mm	43.5 × 23.5 × 15 mm
Costs	€ 345	€ 151.1
Fluid selector		
Power	3.5 W	3.84 W
Dimension	123,2 × 61,1 × 49,5 mm	70.5 × 45 × 43.5 mm High voltage amplifier: 80.0 × 44 × 40.4 mm
Flow channels	6	3
Costs	€ 1037.6	€ 789

* Calibrated at 100 mbar ** Calibrated at 1.5 bar

In Table 12 some commercial available microvalves are compared with the fabricated microvalve presented in this report. The microvalve in this work distinguishes itself by the ease of fabrication, compared to the commercial microvalves which use complex fabrication techniques

like micro-machining and laser cutting. The microvalve in this work stands out in 3D printing of the microfluidic connections, micro-channels and membrane in one single piece, thereby preventing misalignment and leakages at clamping regions. The microvalve presented in this work can further be improved on the flow-rate range, the pressure range, power consumption, and dimensions. The microvalve was designed and fabricated for the requirements typical for microfluidic OOCs, so in future work the performance boundaries of the designed microvalve can be explored further especially focusing on the weak spots in comparison with the state-of-the-art microvalves. The leakage-rates of the commercial microvalves are not mentioned in the data sheets, so a comparison could not be made.

Table 12: State-of-the-art microvalves

Valve	**Type**	**Principle**	**Flow-rate range**	**Pressure range**	**Power**	**Voltage**	**Dimensions**
Memetis Series09 [57]	NC proportional	Shape memory alloy	0-90 ml/min (water)	0-2 bar	0.3 W	-	20.0 × 8.0 × 5.0 mm
Bürkert type 6724B [58]	NO proportional	Solenoid	0-166.7 ml/min (water)	-2 - 3 Bar	1 W	12 V	41.9 × 26 × 8.9 mm
Staiger VP204-502 [59]	NC proportional	Solenoid	0-90 l/min (air)	0-8 bar	-	12 or 24 V	31 × 15 × 15 mm
silQflo® Silicon Servo Valve [60]	Proportional	Electro thermal	0–60 ml/min (hydraulic oil)	0-34.5 bar	5 W	12 or 24 V	10.8 × 4.83 × 2.23 mm
Fabricated microvalve	Proportional	Piezo electric	0-410 $\mu l/min$ (tested till 0-90 $\mu l/min$ with water)	-600 mbar up to 2 bar	442.5 mW (static state)	0-150 V	23.5 × 15 × 43.5 mm

4.2 Recommendations and Future Work

This report showed a monolithically 3D printed microvalve, however during assembly it still uses additional parts like bolts, nuts and O-rings. In future work it may be possible to get rid of these parts, so assembling isn't needed anymore. A possible way to achieve this is by 3D printing a microvalve which includes a displacement amplification mechanism. If a mechanism is designed with a displacement equal to the 3D printed chamber height doing the set up process and calibration of the microvalve isn't required anymore. In addition the O-rings, bolts and nuts become obsolete while no associated clamping forces are needed. Another advantage is a further simplification of the fabrication process, while only the piezo stack needs to be placed in the displacement amplification mechanism. This also ensures that no misalignment occurs between the two clamped 3D printed part. Next to that it is recommended to change the initial state from NO to NC, this reduces power consumption and is saver when a power disruption occurs.

To further reduce leakage it is recommended to use valve seat trenches. These trenches results in higher contact pressures causing surface defects to flatten out. In future work great caution has to be taken when working in the vacuum range. The smallest leakages in the microfluidic circuit causes pressure fluctuations.

Concerning the piezo stack it is advised to use smaller dimensions. This leads to a lower capacitance resulting in faster response time, while the piezo stack has a faster charging and discharging. Next to that when a lower capacitance is obtained, less 'leakage' current will flow, resulting in a lower static power consumption. Using smaller piezo stack doesn't cause foreseeable problems concerning the pressure withstanding, especially when used in the pressure range from -600 mbar to 600 mbar the piezo stack will most likely be strong enough to deliver the required closing force. When larger strokes are required than the piezo stack can provide a displacement amplification mechanism can be considered.

In further projects the microvalve can be used not only as a fluid selector (as shown in the paper), but also as a micro-pump (using three microvalves in series) and as a micro-controller (using a microvalve in series with a sensor). For proportionally controlling the flow-rate it is recommended to use a feedback loop to compensate the hysteresis and creep.

5 Reflection

In the following chapter I try to reflect on the thesis project and on the achieved results. I will elaborate on what went well and what could be done better in future research.

The initial approach was to develop a microfluidic multiplexer, which modular replaces a commercial fluid selector in a microfluidic platform for OOC applications. After my literature review it was advised to focus on developing a microvalve first. The proposed microfluidic multiplexer consists of 24 microvalves and is able to control 8 flow channels. In practice it is hard to fabricate a functioning microvalve, let alone 24 microvalves. Next to that there is no clear advantage of using a microfluidic multiplexer. For example for controlling 8 flow channels 24 microvalves are needed, while the job also can be done by 8 microvalves in parallel. Microfluidic mulitplexers start to make sense when an order of hunderd test samples can be applied to the OOCs. Most of the current OOCs focus on preclinincal drug screening which uses this order of test samples, so this is an opportunity for microfluidic multiplexers [1].

The starting point of the thesis project was the piezoelectric unimorph microvalve designed by Gunda et al. [39]. This microvalve is fabricated using a combination of laser cutting and 3D printing. The main goal was to improve the manufacturing process by reducing the number of manufacturing steps. Next to that the microvalve needed to fulfill requirements arising from OOC applications like obtaining zero leakage and achieving flow-rates between 0-100 $\mu l/min$ at pressure ranges varying from -600 mbar to 600 mbar. The proposed designs can be found in Appendix B. Some problems were encountered, which made it impossible to create a microvalve that met the requirements. Problems like: buckling of the membrane during clamping of the unimorph, unequally spreading of the conductive epoxy and leakage between the membrane and microvalve base. By researching literature in gaining new insights, a new idea came up. The idea was to use a piezo stack instead of a unimorph design. Piezo stacks have the advantage of producing large forces and moderate actuation strokes with fast response time. For the first prototypes an available piezo stack at the PME department was used to check the working principle and to save time. In combination with the monolithic design, which was already explored during the unimorph designs, a novel microvalve was created. In the new design the fabrication is simplified, while only 3D printing is used. In addition a wide pressure range and leakage reduction is achieved due to the large piezo stack forces.

Different resins were considered, like 3DM tough, HTM 140 V2 and E-Glass V2 using the Envisiontec Hi-res and the Prusa SL1. It turned out that with printing HTM 140 V2 using the Envisiontec Hi-res printer the best results were achieved. After printing and assembling the two microvalve parts (microvalve base and frame) are clamped during the set up process. The best possible microvalve characteristics were explored during calibration. These microvalve characteristics were pursued during reproducing the microvalve. In the paper it shown that when higher clamping forces are used during calibration, better leakage performance is achieved. The reproducibility of the microvalve is limited by human errors (misalignment and too much/few clamping force).

The O-rings used in the microvalve function as springs. O-rings were used, while they are widely available and easy to implement (Bolt fits in the O-rings inner diameter). A new microfluidic connection was used (designed by Pieter van Altena) to replace threaded design connections which have larger dimensions. To bond the piezo stack to the membrane it was first considered to use vacuum grease, while it is a non permanent bonding technique contrary to glue. It was expected that the vacuum grease could deliver enough bonding force, but it turned out that it

didn't. Lab technicians advised me to use double-sided tape instead, which turned out to be a good choice.

The available testing equipment in the lab was used during experiments. A drawback is the flow-sensor limit of 90 $\mu l/min$, this prevented to explore the full flow-rate range. Also leakage in the test setup turned out to be a problem. The leakage was minimized as far as possible, but still had influence on the obtained results when using vacuum. The microvalve is tested with Di-water in future work it also can be tested for gasses and higher pressure ranges.

In the design of the 3-to-1 fluid selector initially a high voltage amplifier with a small footprint (11,4 x 8,9 x 9,4 mm) was used. During testing, the high voltage amplifier was overloaded, while the high voltage amplifier wasn't able to deliver the required peak current during charging of the piezo stack. A new high voltage amplifier was bought at the same company that sold the piezo stack, this made sure that the overload problem wouldn't happen again. This new high voltage amplifier is especially designed for delivering high peak currents during charging of the piezo stack. Another benefit of the high voltage amplifier are the high charge and discharge characteristics.

To conclude, this thesis project had some disappointments concerning the unimorph designs and overloading of the initial high voltage amplifier, but also had some exiting results (and probably in future work) with the 3D printed microvalve using a piezo stack microactuator. The proposed microvalve can be manufactured relatively easily (compared to Si-Micromachining), has large actuation forces, zero leakage characteristics and a wide pressure control range for liquids and (potentially) gases.

Bibliography

[1] Wilkinson, M. (2019). The potential of organ on chip technology for replacing animal testing. In Animal Experimentation: Working Towards a Paradigm Change (pp. 639-653). Brill.

[2] Aziz, A. U. R., Geng, C., Fu, M., Yu, X., Qin, K., Liu, B. (2017). The role of microfluidics for organ on chip simulations. Bioengineering, 4(2), 39.

[3] Huh, D. (2015). A human breathing lung-on-a-chip. Annals of the American Thoracic Society, 12(Supplement 1), S42-S44.

[4] Beverung, S., Wu, J., Steward, R. (2020). Lab-on-a-chip for cardiovascular physiology and pathology. Micromachines, 11(10), 898.

[5] Dauth, S., Maoz, B. M., Sheehy, S. P., Hemphill, M. A., Murty, T., Macedonia, M. K., ... Parker, K. K. (2017). Neurons derived from different brain regions are inherently different in vitro: a novel multiregional brain-on-a-chip. Journal of neurophysiology, 117(3), 1320-1341.

[6] Bhise, N. S., Manoharan, V., Massa, S., Tamayol, A., Ghaderi, M., Miscuglio, M., ... Khademhosseini, A. (2016). A liver-on-a-chip platform with bioprinted hepatic spheroids. Biofabrication, 8(1), 014101.

[7] Zanetti, F. (2020). Kidney-on-a-chip. In Organ-on-a-chip (pp. 233-253). Academic Press.

[8] Shim, K. Y., Lee, D., Han, J., Nguyen, N. T., Park, S., Sung, J. H. (2017). Microfluidic gut-on-a-chip with three-dimensional villi structure. Biomedical microdevices, 19(2), 37.

[9] Sutterby, E., Thurgood, P., Baratchi, S., Khoshmanesh, K., Pirogova, E. (2020). Microfluidic Skin-on-a-Chip Models: Toward Biomimetic Artificial Skin. Small, 16(39), 2002515.

[10] Skardal, A., Murphy, S. V., Devarasetty, M., Mead, I., Kang, H. W., Seol, Y. J., ... Atala, A. (2017). Multi-tissue interactions in an integrated three-tissue organ-on-a-chip platform. Scientific reports, 7(1), 1-16.

[11] Lim, Y. C., Kouzani, A. Z., Duan, W. (2010). Lab-on-a-chip: a component view. Microsystem Technologies, 16(12), 1995-2015.

[12] Haeberle, S., Zengerle, R. (2007). Microfluidic platforms for lab-on-a-chip applications. Lab on a Chip, 7(9), 1094-1110.

[13] Weisgrab, G., Ovsianikov, A., Costa, P. F. (2019). Functional 3D printing for microfluidic chips. Advanced Materials Technologies, 4(10), 1900275.

[14] Zhu, H. (2020). Portable and Integrated Organ-On-Chip Platform Using Off-the-shelf Components.

[15] Zhong, J. F., Chen, Y., Marcus, J. S., Scherer, A., Quake, S. R., Taylor, C. R., Weiner, L. P. (2008). A microfluidic processor for gene expression profiling of single human embryonic stem cells. Lab on a Chip, 8(1), 68-74.

[16] Wang, J., Sui, G., Mocharla, V. P., Lin, R. J., Phelps, M. E., Kolb, H. C., Tseng, H. R. (2006). Integrated microfluidics for parallel screening of an in situ click chemistry library. Angewandte Chemie International Edition, 45(32), 5276-5281.

[17] Thorsen, T., Maerkl, S. J., Quake, S. R. (2002). Microfluidic large-scale integration. Science, 298(5593), 580-584.

[18] Melin, J., Quake, S. R. (2007). Microfluidic large-scale integration: the evolution of design rules for biological automation. Annu. Rev. Biophys. Biomol. Struct., 36, 213-231.

[19] Cole, M. C., Desai, A. V., Kenis, P. J. (2011). Two-layer multiplexed peristaltic pumps for high-density integrated microfluidics. Sensors and Actuators B: Chemical, 151(2), 384-393.

[20] Lee, C. C., Sui, G., Elizarov, A., Shu, C. J., Shin, Y. S., Dooley, A. N., ... Tseng, H. R. (2005). Multistep synthesis of a radiolabeled imaging probe using integrated microfluidics. Science, 310(5755), 1793-1796.

[21] Blazej, R. G., Kumaresan, P., Mathies, R. A. (2006). Microfabricated bioprocessor for integrated nanoliter-scale Sanger DNA sequencing. Proceedings of the National Academy of Sciences, 103(19), 7240-7245.

[22] Pal, R., Yang, M., Lin, R., Johnson, B. N., Srivastava, N., Razzacki, S. Z., ... Burns, M. A. (2005). An integrated microfluidic device for influenza and other genetic analyses. Lab on a Chip, 5(10), 1024-1032.

[23] Rohde, C. B., Zeng, F., Gonzalez-Rubio, R., Angel, M., Yanik, M. F. (2007). Microfluidic system for on-chip high-throughput whole-animal sorting and screening at subcellular resolution. Proceedings of the National Academy of Sciences, 104(35), 13891-13895.

[24] Lee, D. W., Cho, Y. H. (2009). High-radix microfluidic multiplexer with pressure valves of different thresholds. Lab on a Chip, 9(12), 1681-1686.

[25] Kawai, K., Shibata, Y., Kanai, M., Shoji, S. (2008, October). Multiplexed pneumatic valve control system for large scale integrated microfluidic circuit (LSIMC). In Twelfth International Conference on Miniaturized Systems for Chemistry and Life Sciences, San Diego, California, USA (pp. 683-685).

[26] Liu, C., Park, J. Y., Xu, Y., Lee, S. (2007). Arrayed pH-responsive microvalves controlled by multiphase laminar flow. Journal of Micromechanics and Microengineering, 17(10), 1985.

[27] Vyawahare, S., Sitaula, S., Martin, S., Adalian, D., Scherer, A. (2008). Electronic control of elastomeric microfluidic circuits with shape memory actuators. Lab on a Chip, 8(9), 1530-1535.

[28] Qian, J. Y., Hou, C. W., Li, X. J., Jin, Z. J. (2020). Actuation mechanism of microvalves: A review. Micromachines, 11(2), 172.

[29] Yang, Y. N., Hsiung, S. K., Lee, G. B. (2009). A pneumatic micropump incorporated with a normally closed valve capable of generating a high pumping rate and a high back pressure. Microfluidics and Nanofluidics, 6(6), 823-833.

[30] Pourmand, A., Shaegh, S. A. M., Ghavifekr, H. B., Aghdam, E. N., Dokmeci, M. R., Khademhosseini, A., Zhang, Y. S. (2018). Fabrication of whole-thermoplastic normally closed microvalve, micro check valve, and micropump. Sensors and Actuators B: Chemical, 262, 625-636.

[31] Araci, I. E., Quake, S. R. (2012). Microfluidic very large scale integration (mVLSI) with integrated micromechanical valves. Lab on a Chip, 12(16), 2803-2806.

[32] Mosadegh, B., Bersano-Begey, T., Park, J. Y., Burns, M. A., Takayama, S. (2011). Next-generation integrated microfluidic circuits. Lab on a Chip, 11(17), 2813-2818.

[33] Madou, M. J. (2002). Fundamentals of Microfabrication 2nd edn (Boca Raton: CRC).

[34] Anjewierden, D., Liddiard, G. A., Gale, B. K. (2012). An electrostatic microvalve for pneumatic control of microfluidic systems. Journal of Micromechanics and Microengineering, 22(2), 025019.

[35] Atik, A. C., Özkan, M. D., Özgür, E., Külah, H., Yıldırım, E. (2020). Modeling and fabrication of electrostatically actuated diaphragms for on-chip valving of MEMS-compatible microfluidic systems. Journal of Micromechanics and Microengineering, 30(11), 115001.

[36] Tice, J. D., Rosheck, J. B., Hamlin, C. D., Apblett, C. A., Kenis, P. J. (2013). Normally-closed electrostatic microvalve fabricated using exclusively soft-lithographic techniques and operated with portable electronics. Journal of microelectromechanical systems, 22(6), 1251-1253.

[37] Yıldırım, E., Arıkan, M. S., Külah, H. (2012). A normally closed electrostatic parylene microvalve for micro total analysis systems. Sensors and Actuators A: Physical, 181, 81-86.

[38] Oh, K. W., Ahn, C. H. (2006). A review of microvalves. Journal of micromechanics and microengineering, 16(5), R13.

[39] Gunda, A., Özkayar, G., Tichem, M. (2020). Proportional Microvalve Using a Unimorph Piezoelectric Microactuator. Micromachines, 11(2), 130.

[40] Zhang, D.; Lv, J.; Jiang, Y.; Chen, H.; Fu, J. A piezoelectric microvalve with a flexure-hinged driving frame and microfabricated silicon sealing pair. Mechatronics 2014, 24, 511–518.

[41] Hagstrom, N. P., Fikru, N., Hargus, A. M., Chase, T. R. (2019). A Novel Piezoelectrically Driven Miniature Proportional Pneumatic Control Valve Utilizing a Microfabricated Orifice Array. IEEE/ASME Transactions on Mechatronics, 24(5), 1931-1941.

[42] Lee, C., Yang, E. H., Saeidi, S. M., Khodadadi, J. M. (2006). Fabrication, characterization, and computational modeling of a piezoelectrically actuated microvalve for liquid flow control. Journal of microelectromechanical systems, 15(3), 686-696.

[43] Pradeep, A., Stanley, J., Nair, B. G., Babu, T. S. (2018). Automated and programmable electromagnetically actuated valves for microfluidic applications. Sensors and Actuators A: Physical, 283, 79-86.

[44] Liu, J., Liu, X., Li, S. (2016, October). Design and performance study on electromagnetic microvalve. In 2016 IEEE International Conference on Aircraft Utility Systems (AUS) (pp. 564-569). IEEE.

[45] Böhm, S., Burger, G. J., Korthorst, M. T., Roseboom, F. (2000). A micromachined silicon valve driven by a miniature bi-stable electro-magnetic actuator. Sensors and Actuators A: Physical, 80(1), 77-83.

[46] Sutanto, J., Hesketh, P. J., Berthelot, Y. H. (2006). Design, microfabrication and testing of a CMOS compatible bistable electromagnetic microvalve with latching/unlatching mechanism on a single wafer. Journal of Micromechanics and Microengineering, 16(2), 266.

[47] Jiang, X., Lillehoj, P. B. (2017, April). Pneumatic microvalves fabricated by multi-material 3D printing. In 2017 IEEE 12th International Conference on Nano/Micro Engineered and Molecular Systems (NEMS) (pp. 38-41). IEEE.

[48] Mohan, R., Schudel, B. R., Desai, A. V., Yearsley, J. D., Apblett, C. A., Kenis, P. J. (2011). Design considerations for elastomeric normally closed microfluidic valves. Sensors and Actuators B: Chemical, 160(1), 1216-1223.

[49] Liu, X., Li, S., Bao, G. (2016). Numerical simulation on the response characteristics of a pneumatic microactuator for microfluidic chips. Journal of laboratory automation, 21(3), 412-422.

[50] Tameson. Solenoid valve response time. https://tameson.com/solenoid-valve-response-time.html

[51] Schmidt, R. M., Schitter, G., Rankers, A. (2014). The design of high performance mechatronics-: high-Tech functionality by multidisciplinary system integration. Ios Press, 415-425.

[52] Amin, R., Joshi, A., Tasoglu, S. (2017). Commercialization of 3D-printed microfluidic devices. Journal of 3D printing in medicine, 1(2), 85-89.

[53] Low, Z. X., Chua, Y. T., Ray, B. M., Mattia, D., Metcalfe, I. S., Patterson, D. A. (2017). Perspective on 3D printing of separation membranes and comparison to related unconventional fabrication techniques. Journal of membrane science, 523, 596-613.

[54] "Envisiontec HTM 140 V2 Data sheet". Accessed on 18-05-22. https://envisiontec.com/material/htm-140/

[55] Dixon, P. G., Muth, J. T., Xiao, X., Skylar-Scott, M. A., Lewis, J. A., Gibson, L. J. (2018). 3D printed structures for modeling the Young's modulus of bamboo parenchyma. Acta biomaterialia, 68, 90-98.

[56] Greaves, G. N., Greer, A. L., Lakes, R. S., Rouxel, T. (2011). Poisson's ratio and modern materials. Nature materials, 10(11), 823-837.

[57] "Memetis Series09 Data sheet". Accessed on 20-07-22. https://www.memetis.com/assets/uploads/dateien/memetis-nc-datasheet.pdf

[58] "Bürkert type 6724B Data sheet". Accessed on 20-07-22. https://www.burkert.com/en/type/6724

[59] "Staiger VP204-50 Data sheet". Accessed on 20-07-22. https://www.staiger.de/en-us/products/online-catalogue/details?name=VP %20204-502

[60] "silQflo® Silicon Servo Valve Data sheet". Accessed on 20-07-22. https://www.dmq-us.com/wp-content/uploads/2018/07/SSV-Datasheet-1.003.pdf

Appendix A - Supplementary Material

In the following chapter the supplementary material is presented.

A.1 Piezoelectricity theory

A.1.1 Piezoelectricity

The microvalve presented in this work uses piezoelectric actuation. When a voltage is applied to a piezoelectric material the dipoles in the material gets aligned [51]. This causes a contraction or expansion of the material, which is dependent on the direction of the electric field. This behaviour is called the inverse piezoelectric effect. The piezoelectric effect is caused by charge asymmetries in the material called dipoles.

Piezoelectric characteristics are found in natural materials like quartz and Rochelle salt and in synthetic materials like Lead Zirconate Titanate (PZT) and Polyvinylidene Fluoride (PVDF). In synthetic materials poling is needed at the Curie temperature to align the Weiss domains. After this process the synthetic material gets its piezoelectric properties. Piezoelectric materials function as capacitors, while there are no free electrons moving in the material. The potential charge difference is a result of the accumulation of charge displacements in the molecules of the materials. Leakage current will happen in reality as a consequence of humidity, surface contamination or other potential charge paths.

For the inverse piezoelectric effect the following relation exists between strain, stress and applied electric field:

$$S = C^E T + dE \tag{4}$$

In the above equation S is the strain vector, C^E is the specific compliance matrix at constant electric field, T is the stress vector, d is the piezoelectric coefficient matrix and E is the electric field vector. Equation 4 shows a linear relation, however piezoelectric materials also show non linear phenomena like creep and hysteresis. Creep is observed as a slow expansion of the piezoelectric material. This effect is caused by the actuation voltage on the remnant polarization of the dipoles. Hysteresis manifest itself as a difference in the displacement of the piezoelectric material between the voltage-up path and voltage-down path.

A.1.2 DLP-printing

DLP-printing is a photo-polymerization manufacturing technique which can print 3D structures for microfluidic applications with high resolution bio-compatible polymers [52]. The 3D structures are made layer by layer, whereby the DLP printer projects an entire cross sectioned layer of the 3D model with UV light on a vat containing the resin. The projected sections get polymerized and the area which are not projected remains in liquid form. Once a layer is projected the platform (or printing head) is lifted so a new layer can be projected. Photo-polymerization is the most popular 3D printing method for fabricating finely machined structures, while this technique has the highest resolution compared to other 3D printing techniques like powder, extrusion and lamination techniques [53].

The available material resins with their layer thicknesses are shown in Table 13.

Table 13: Resin layer thicknesses

Resin	**Layer thickness**
E-Glass V2	50 μm, 100 μm
HTM 140 V2	25 μm, 35 μm, 50 μm
ABS tough	50 μm
3DM tough	35 μm, 50 μm

The properties of the HTM 140 V2 are presented in Table 14. HTM 140 V2 is a green bio-compatible resin. The Poisson ratio presented is an estimation using other polymer Poisson's ratios.

Table 14: HTM 140 V2 Properties

Property [54]	**Value**
Tensile strength	56 MPa
Young's modulus [55]	1855.3 MPa $\pm$ 62.1
Poisson's ratio [56]	0.33
Elongation at break	3.5%
Heat deflection temperature	140C
Density	1191 kg/m^3

A.2 Fabrication process

In this section first the 3D printing steps and post-processing of the microvalve base and frame are presented. Next to that the assembly steps of the microvalve are shown.

A.2.1 3D printing parts

The microvalve base and frame are fabricated using the EnvisionTec Micro-plus Hi-Res DLP-printer. The used resin is HTM 140 V2. It should be possible to fabricate the parts with any 3D printer that has a $\leq$35 m vertical resolution. In the next tables the 3D printing process for the microvalve base and frame are presented.

Step No.	Image	Description
1	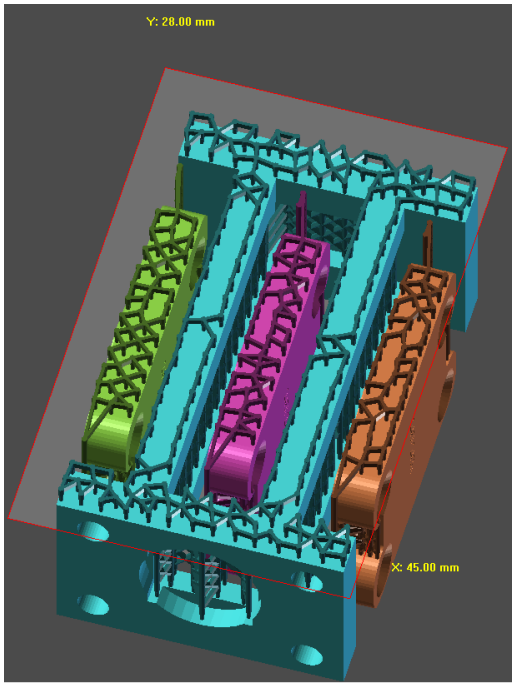	Create support pillars on the STL.files of the parts with a dedicated software package used for 3D printing. In the image three microvalve bases (green, purple and brown parts) and one frame (blue part) are shown. The support pillars are printed first, indicating the printing direction. The red outlined rectangle indicates the printing head dimension.
2	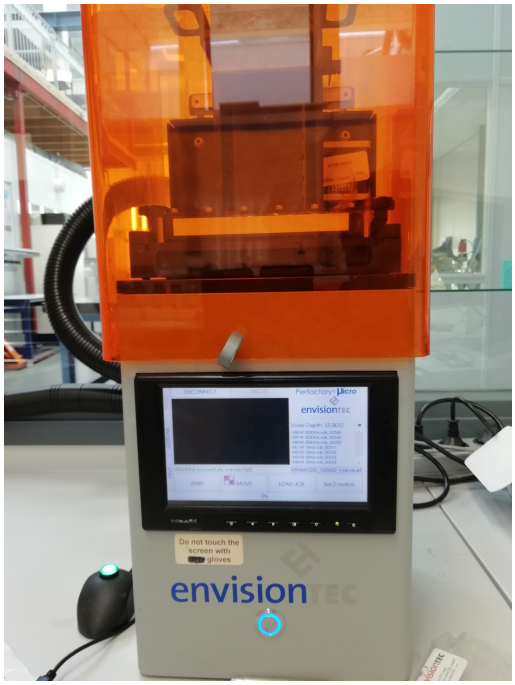	Upload the STL.files of the parts including the supports to the DLP-printer.

Step No.	Image	Description
3	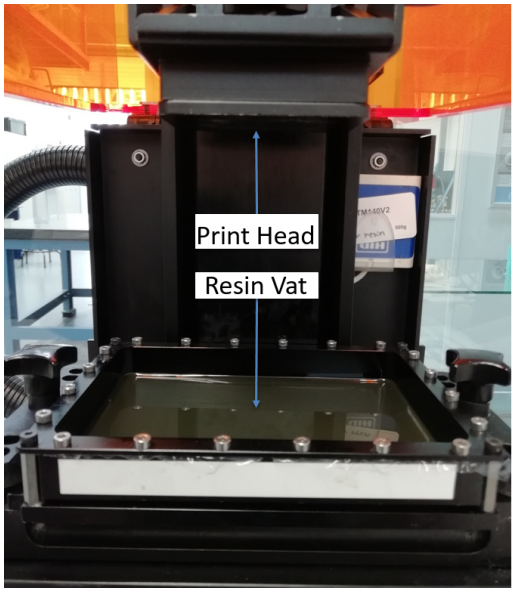	Fill the resin vat with HTM 140 V2. The printing head has to move to its home position, after which the printing can start.
4	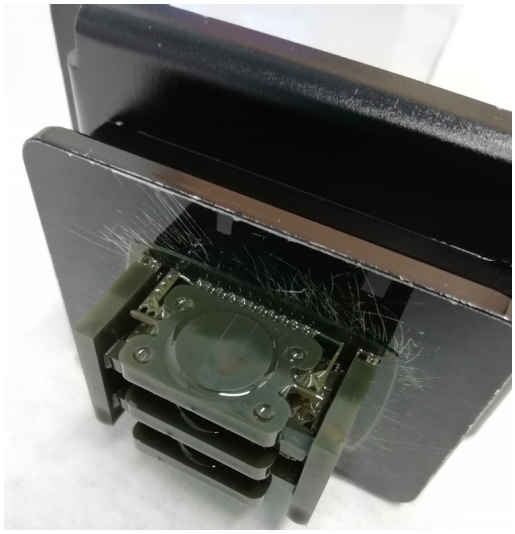	Three microvalve bases and one frame part after printing bonded to the printing head. Remove the 3D-printed parts using a scalpel.
5		Ultrasonicate the parts with IPA for 3 minutes.

Step No.	Image	Description
6	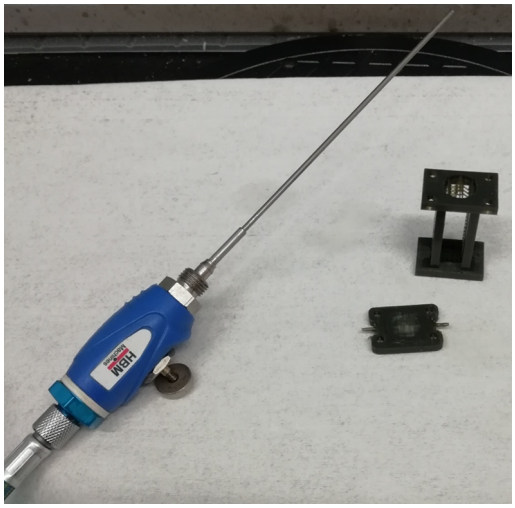	After ultrasonication use compressed air to remove remaining uncured resin, repeat the ultrasonication step if uncured resin is still visible.
7	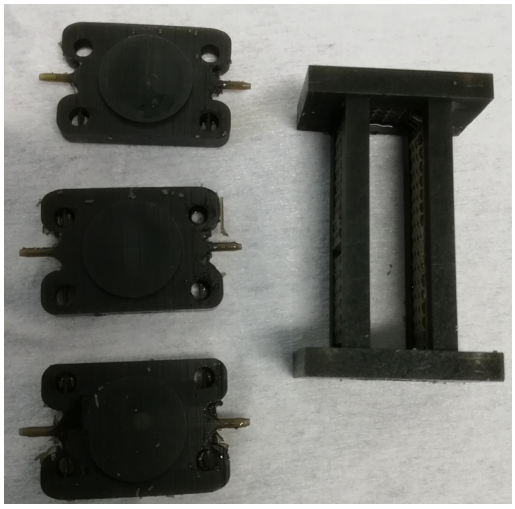	Remove the supports using a scalpel. In the Figure to the left three microvalve bases and one frame are shown without supports.
8	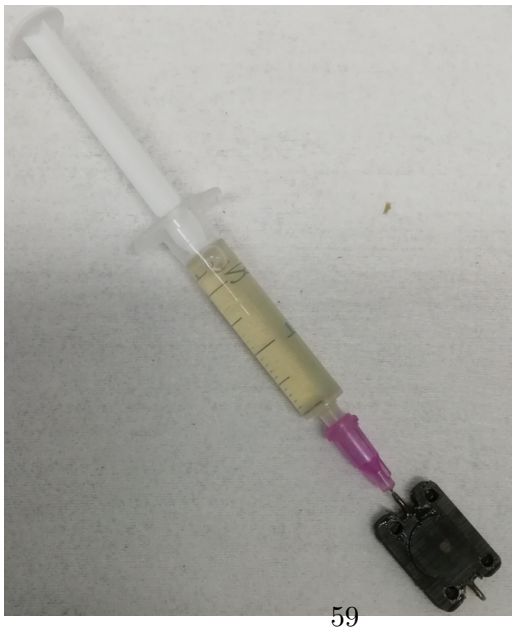	The frame is ready for further post-processing. The microvalve base is flushed by utilizing a syringe pressing IPA into the microchannels and valving chamber to remove all uncured resin.

Step No.	Image	Description
9		When all resin residue is removed the microvalve base is flushed again to clean the microchannels and valving chamber by utilizing a syringe with Di-water.
10	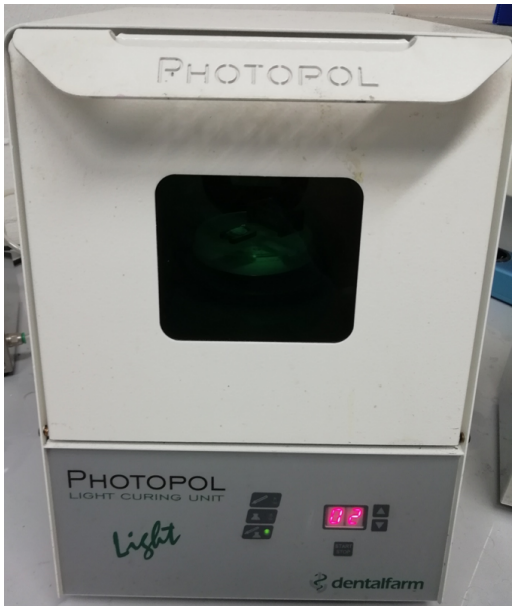	Post-cure the frame by using a UV curing device for 3 minutes.
11	**Finished 3D parts**	The parts are ready to be assembled.

A.2.2 Assembly

Step No.	Image	Description
1	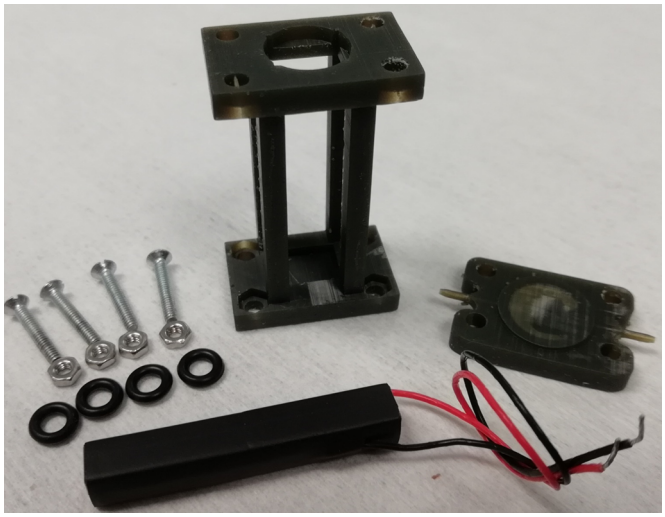	Collect all items used to assemble the microvalve. Shown in the Figure are the: Piezo stack, 4x O-rings, 4x M2 bolts and nuts, Microvalve base and Microvalve frame. Not shown is the double sided tape.
2	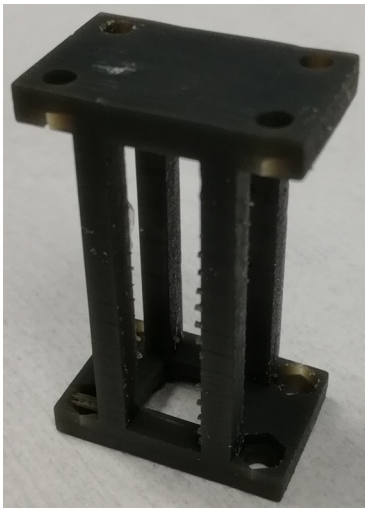	Assembly starts with positioning the frame as shown in the Figure.
3	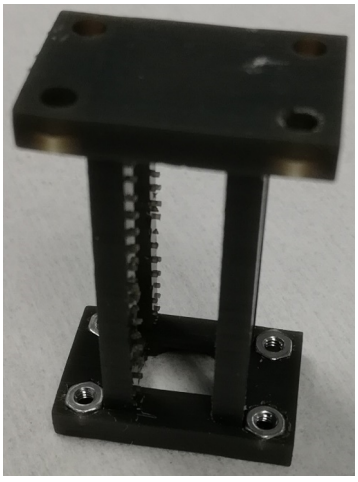	Place the four M2 nuts in the nuts locations as shown in the Figure and fix them with glue.

Step No.	Image	Description
4	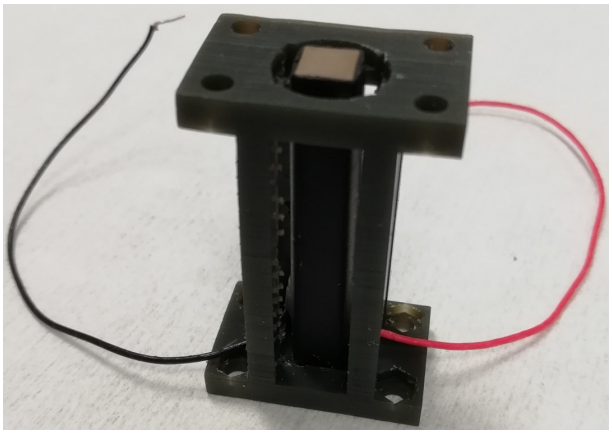	Turn the microvalve frame (including the four M2 nuts 180 degrees) and place the piezo stack as shown in the Figure. Fix the piezo stack to the frame with double sided tape.
5	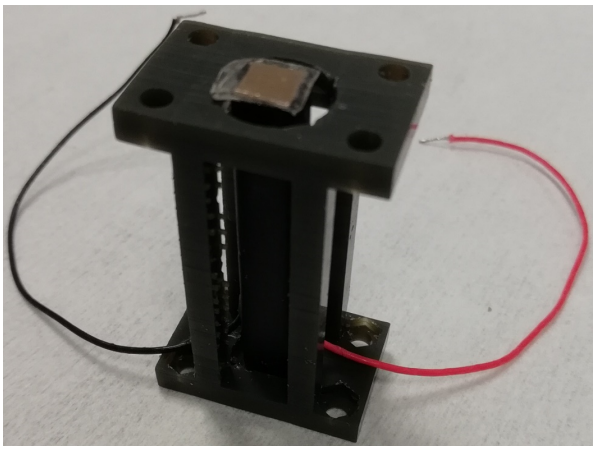	Put double sided tape on the piezo stack.
6	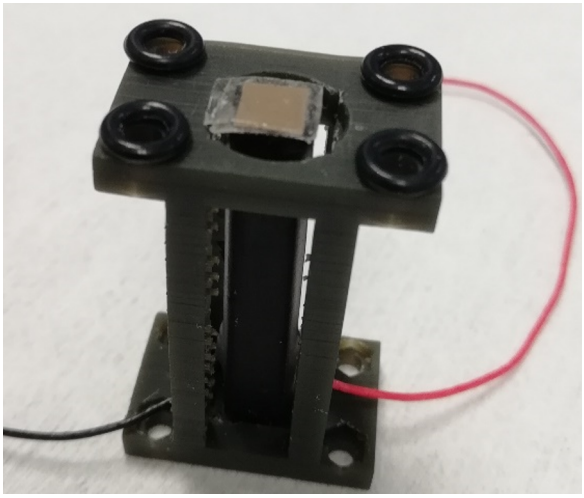	Position and align the four O-rings with the M2 openings as shown in the Figure.

Step No.	Image	Description
7	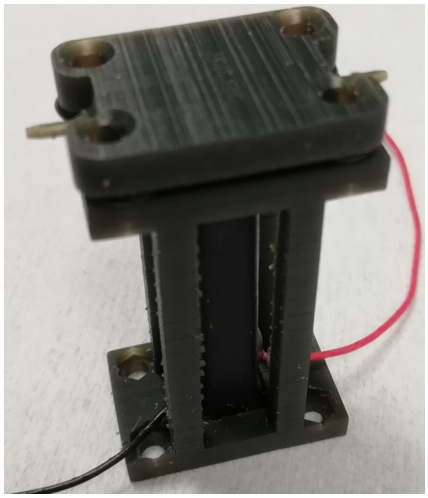	Place the microvalve base on top of the frame and align them with the M2 openings. The piezo stack is bonded with double sided tape to the membrane of the microvalve base.
8	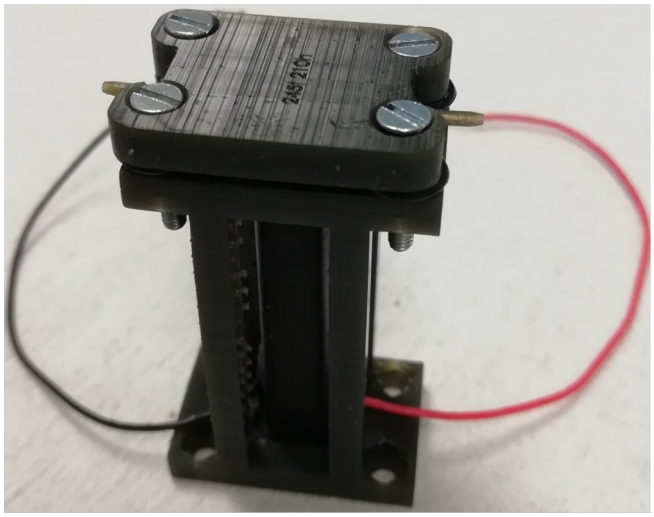	Align the M2 bolts with the M2 openings and O-rings and screw them into the M2 nuts. The maximum torque on the bolts to clamp the microvalve base is ∼0.7 Nm, measured using a torque screw driver. After assembly the set up process starts.

A.3 FEM model Microvalve flow-rate

A FEM model is build using COMSOL Multiphysics Version 5.6 to predict the flow-rate at various chamber heights and pressure levels.

A.3.1 Building the model

In the following figure the flow path of the microvalve is shown.

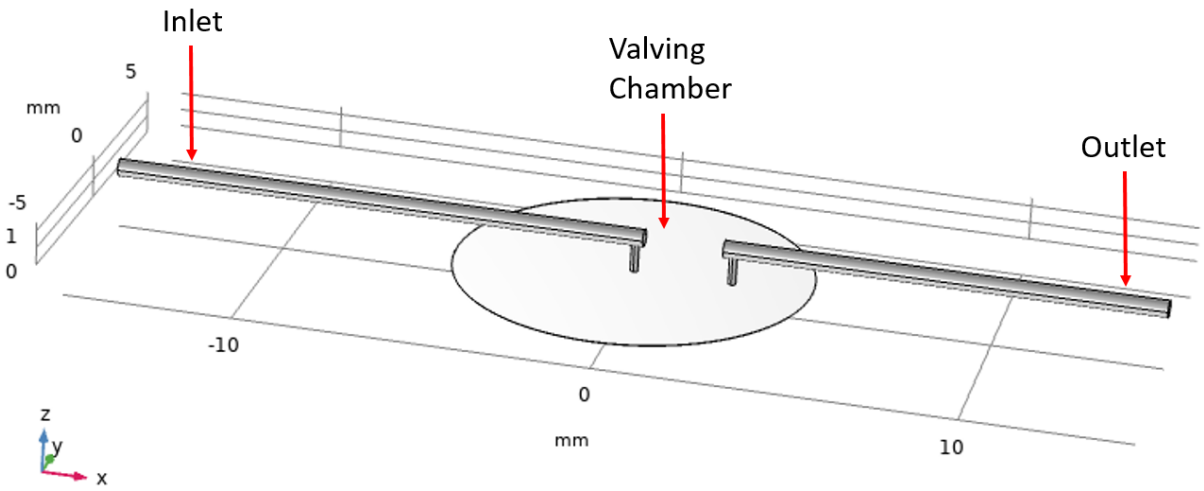

Building Material = Water

The smallest feature is the valving chamber height which varies between $0 - 34$ μm.

A.3.2 Setting up the study

A stationary study is conducted and the volume flow-rate is estimated using:

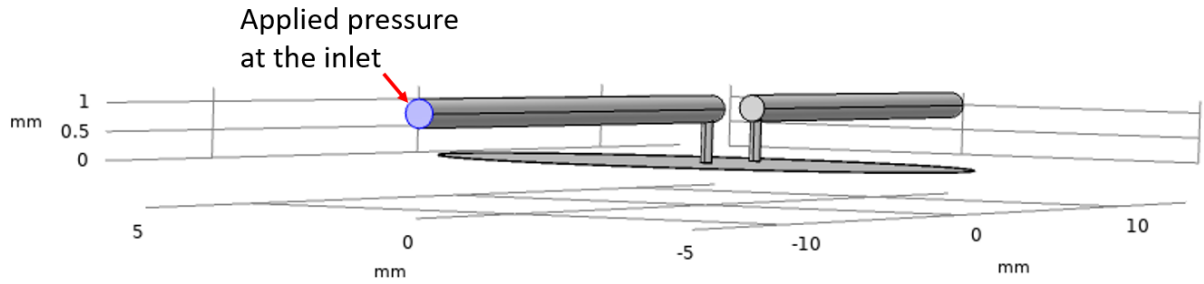

Physics = Creeping flow

Mesh = Physics controlled mesh

Pressure Range = -600 mbar unto 600 mbar

A.4 Fabrication results

In this section the fabrication results are shown. First of all the different produced microvalve bases are presented. Secondly the valving seat surface roughness is estimated and lastly the microfluidic connections are shown in more detail.

A.4.1 Intact membranes

In a conducted experimental study different microvalve bases were printed with varying chamber heights and membrane thicknesses. Every membrane has a diameter of 10 mm. The following fabrication results are obtained:

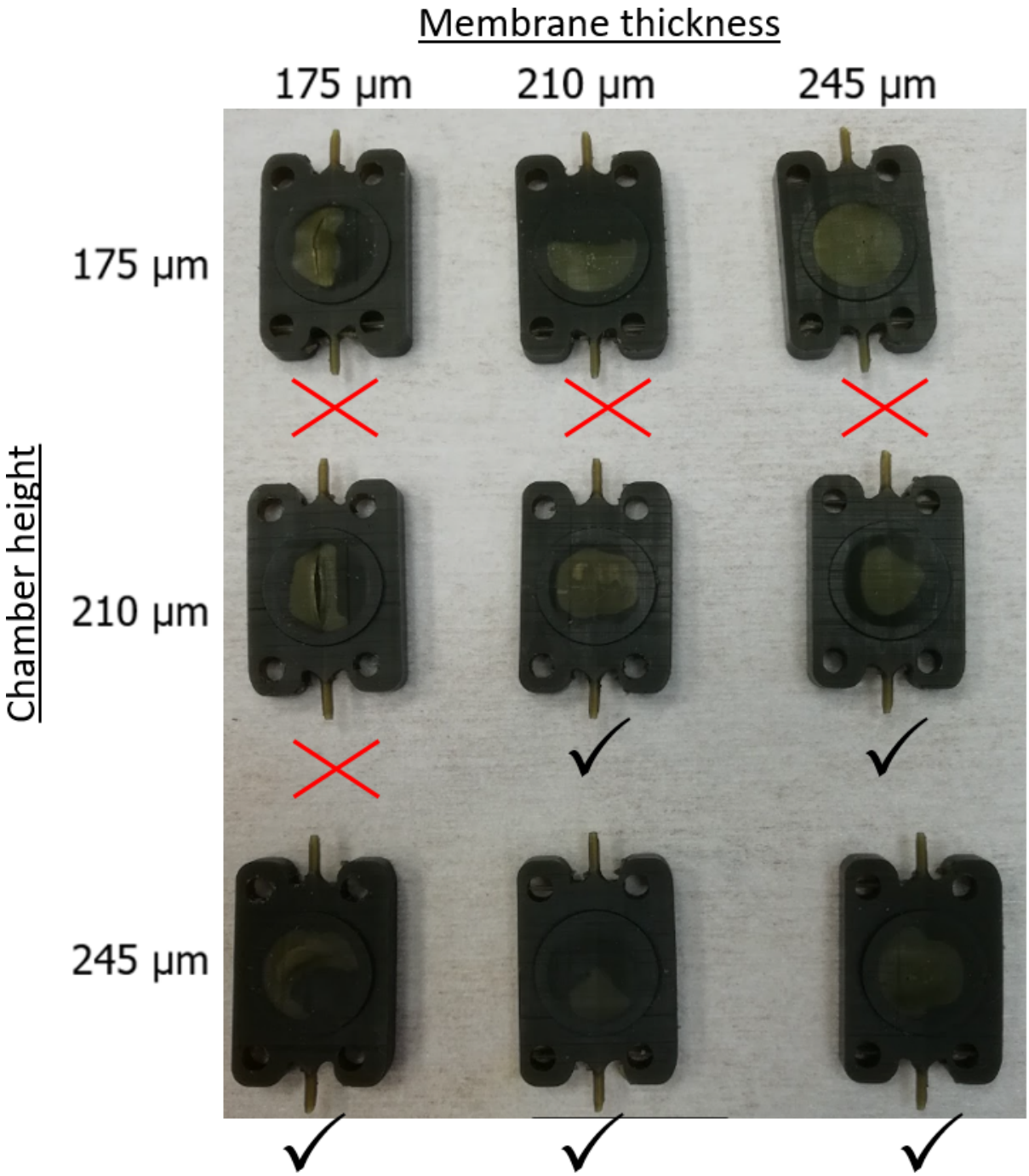

As can be seen in the figure above the damaged/not intact membranes are marked with a red cross, while the intact membranes are marked with a check mark. An intact membrane is printed when at least a chamber height of 210 μm and a membrane thickness of 210 μm is used. During testing a chamber height of 245 μm and a membrane thickness of 245 μm is used to guarantee a robust membrane.

A.4.2 Surface roughness

The surface roughness of the valving seat is meausured using a Keyence VHX-6000. The color bar in the top left sub-figure indicates the surface roughness distribution of the particular valve seat. The following (sub)-figures are obtained:

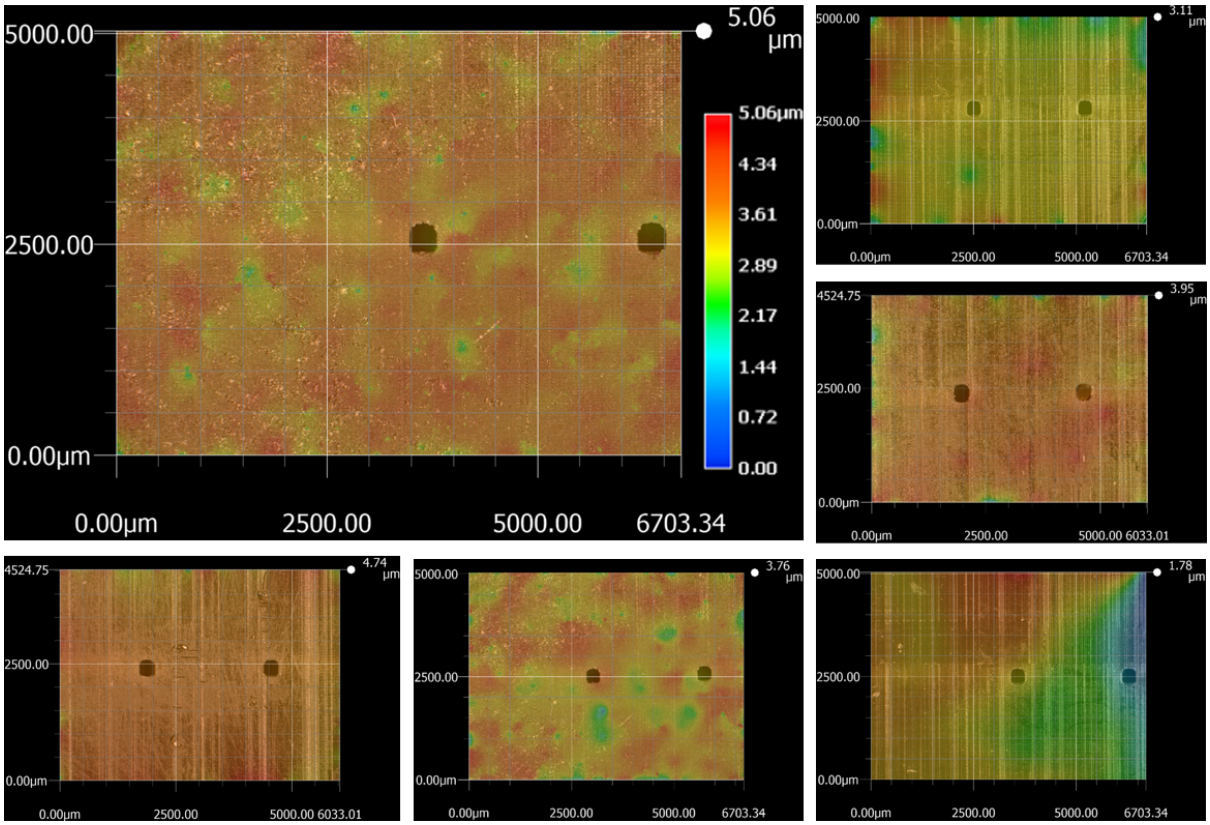

In the right top corner of every sub-figure the maximum surface roughness of the valve seat of that particular microvalve base is shown. The estimated surface roughness is $3.69 \pm 1.32 \mu m$.

A.4.3 Microfluidic connections

In the following Figure the microfluidic connection dimensions (in mm) of the microvalve are shown.

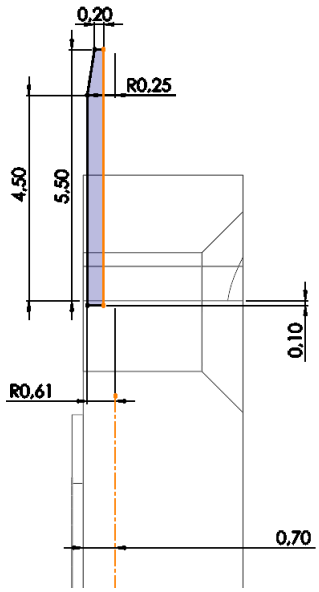

In the following Figure the microfluidic connection procedure is shown.

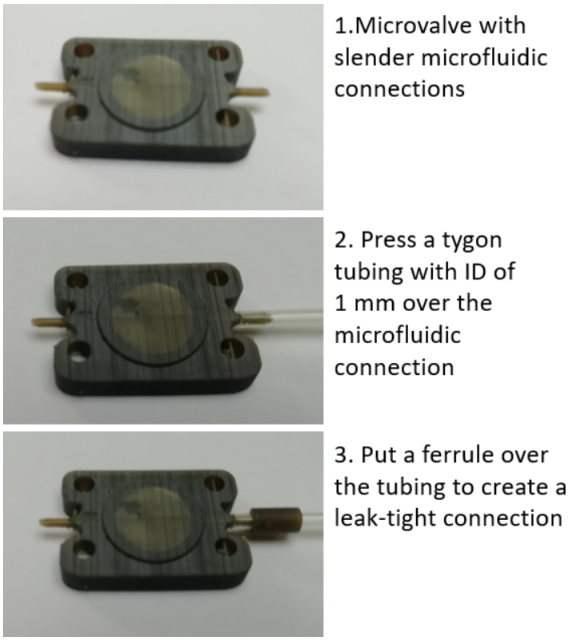

A.5 Fluid selector

A.5.1 3-to-1 fluid selector

A portable 3-to-1 fluid selector is produced by placing three microvalves in parallel. The piezo stacks are actuated by a high voltage amplifier which can proportionally control the output voltages to the piezo stacks. A close-up of the high voltage amplifier (Piezo Drive, PDu150) connected to three microvalves in parallel is shown in the left Figure below.

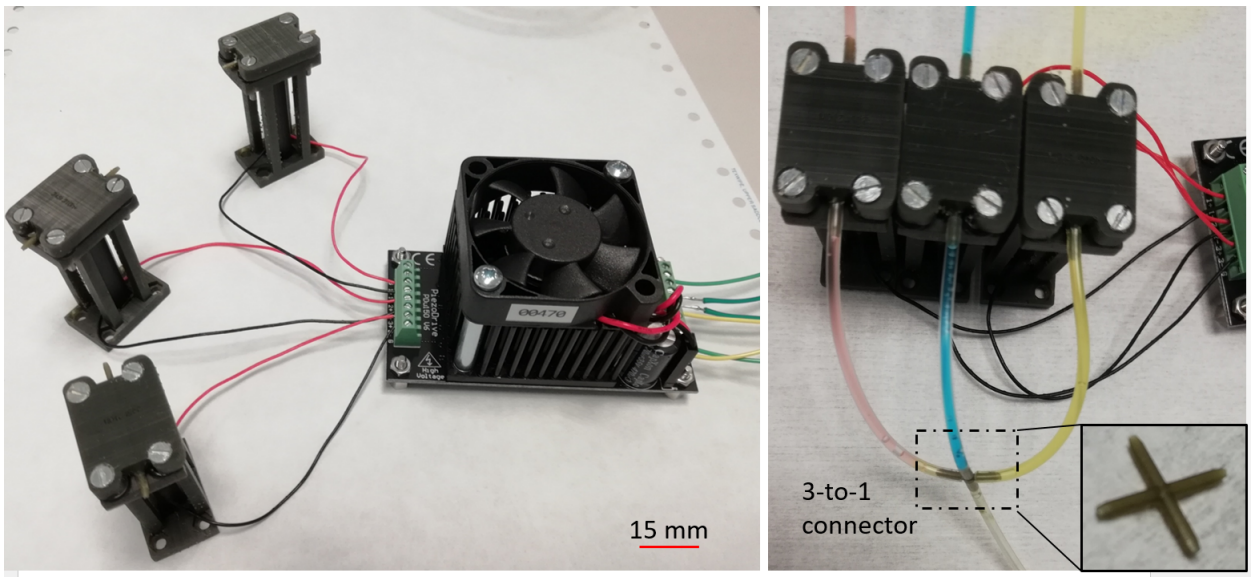

To create a 3-to-1 fluid selector the outputs of the three microvalves are connected by tubings to a 3-to-1 connector. The 3-to-1 connector has 1 output in which the selected fluid is channeled forward. A detailed view of the 3-to-1 selector is shown in the right Figure above.

A.5.2 Failed high voltage amplifier

In the first instance a small high voltage amplifier (NHV0502) would be used. In the following schematic the proposed implementation for a 2-to-1 fluid selector is presented. An Arduino is used to control the high voltage amplifier and to provide the needed energy.

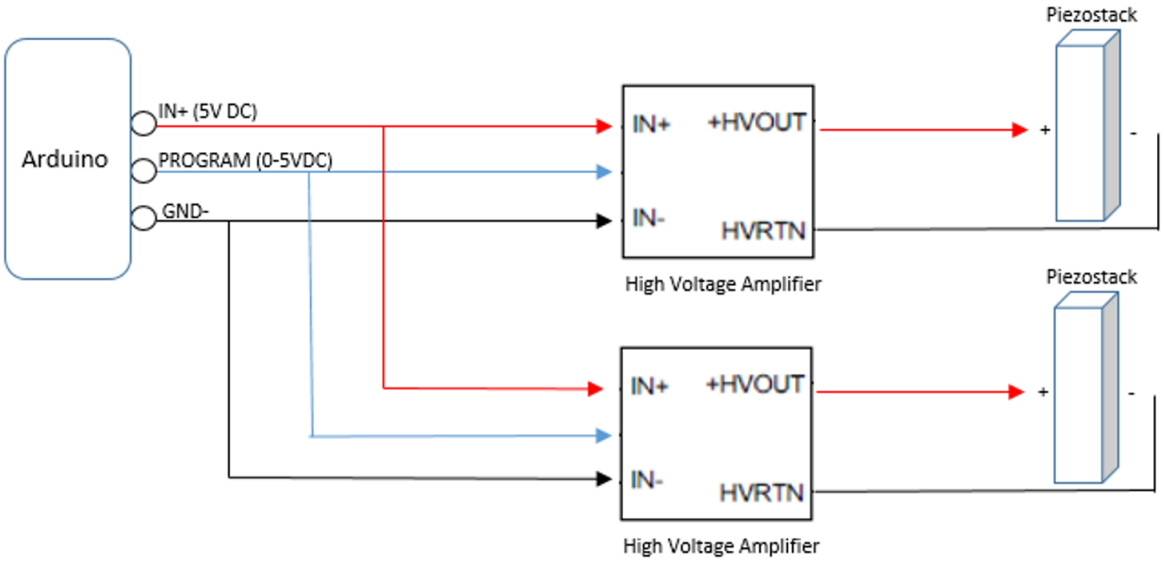

In the following Figure the high voltage amplifier NHV0502 is shown on a print board. It failed during testing while it couldn't provide the peak current when charging the piezo stack

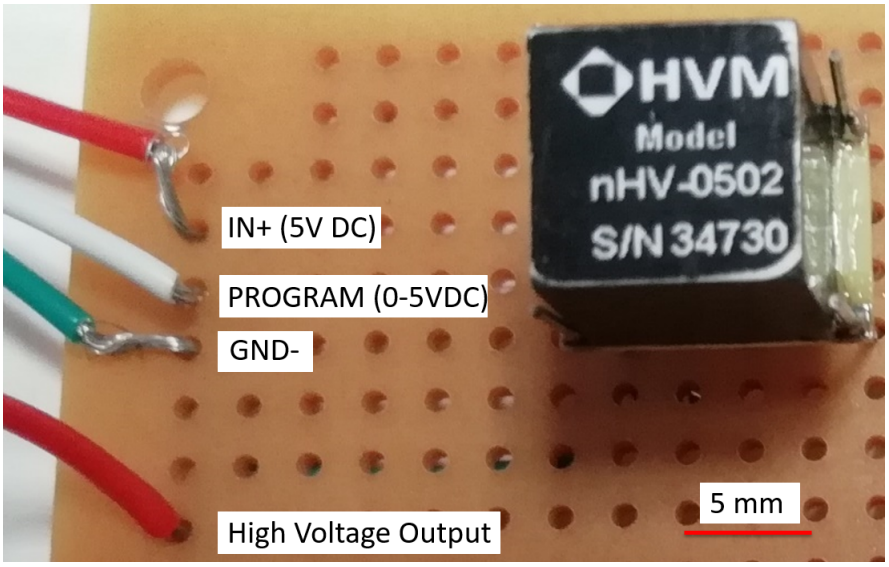

Appendix B - Piezoelectric Unimorph Microvalve designs

The initial approach was to fabricate a unimorph microvalve, using a PZT-5H disk bonded with conductive epoxy to a membrane. Two types of microvalves were initially proposed as improvements of the microvalve designed by Gunda et al. [39]. The first microvalve has a 3D-printed spacer. A spacer is the gap height between the membrane and the valve seat of a microvalve. The microvalve designed by Gunda et al. used a laser cut stainless steel spacer of 5 μm thickness. To get rid of this fabrication step a 3D-printed spacer was proposed which is directly printed together with the micro-channels. On top of the 3D-printed spacer the stainless steel membrane and PZT-5H where clamped. The monolithic microvalve goes one step further in minimizing the fabrication steps by not only 3d-printing the spacer, but also the membrane. This means that it is not needed to laser cut a stainless steel membrane, while the membrane is monolithically printed on top of the 3D-printed spacer and micro-channels. This reduces the misalignment and leakages while no separate membrane is used. The schematics of the proposed designs are shown in the following figure.

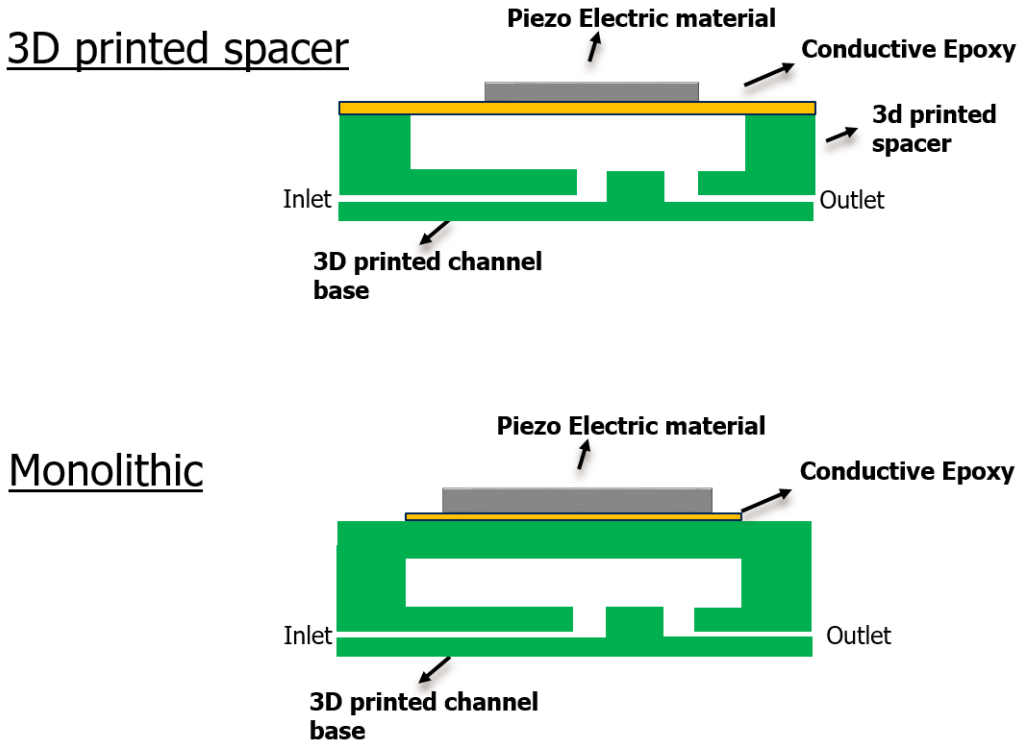

The proposed unimorph designs faced some problems.

Problems 3D-printed spacer microvalve: During clamping of the membrane on the 3D-printed spacer buckling of the membrane was occurring. This lead to bad closing behaviour in the case were upward buckling with respect to the valve seat took place. Due to upward buckling the unimorph actuator wasn't able anymore to overcome the displacement needed to fully close the microvalve. Another problem was the leakage, especially using vacuum, at the contact between the 3D-printed spacer and membrane. The smallest openings between the surfaces led to leakage problems, as a result of which pressure couldn't built up.

Problems Monolithic: The monolithically 3D-printed microvalve faced problems when bond-

ing the PZT-5H disk to the 3D-printed membrane using conductive epoxy. It is impractical to equally spread the conductive epoxy on the membrane, while the membrane is flexible and offers little resistance. Also when the disk is placed on the membrane (after conductive epoxy is spread on the membrane surface) the membrane deforms and no flat contact can be achieved. Another problem was the large spacer height >210 μm. The microactuator could only achieve such large displacements when a large PZT-5H disk diameter was used, but this also resulted in less stiffness of the membrane. This was a problem when using vacuum, whereby a downward displacement was created in the initial state due to vacuum resulting in smaller open flow-rates. The monolithic concept was promising, while during experiments a monolithically microvalve was printed. By replacing the PZT-5H disk with a piezo stack the bonding problem and the low stiffness were no longer an issue. The monolithic microvalve is the basis of the paper.

In the following Figures the fabricated 3D-printed spacer microvalve and monolithic microvalve are shown.